Charles University in Prague

Faculty of Mathematics and Physics

DOCTORAL THESIS

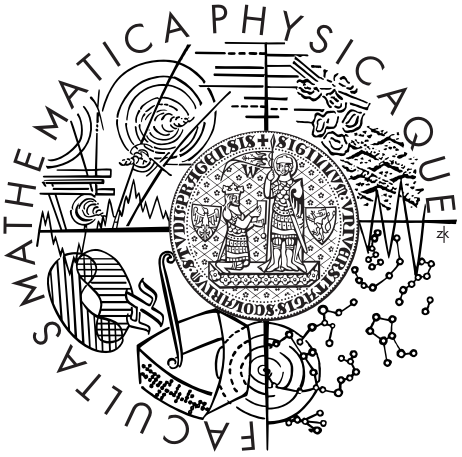

Jan Olšina

Theory of Relaxation and Energy Transfer in Open Quantum Systems

Institute of Physics of Charles University

Supervisor of the doctoral thesis: RNDr. Tomáš Mančal, Ph. D.

Study programme: Physics

Specialization: Biophysics and Chemical Physics

Prague 2014

First and foremost, I would like to thank my advisor Tomáš Mančal, who was the best guide to the world of science I could wish for. I would also like to thank my parents and my wife Marie for their love, support and encouragement during my whole doctoral studies.

The work was supported by the Czech Science Foundation (GACR) grant no. 205/10/0989, by the Ministry of Education, Youth and Sports of the Czech Republic via grant KONTAKT ME899 and the research plan MSM0021620835, and by the Charles University in Prague via grant GAUK 416311.

I declare that I carried out this doctoral thesis independently, and only with the cited sources, literature and other professional sources.

I understand that my work relates to the rights and obligations under the Act No. 121/2000 Coll., the Copyright Act, as amended, in particular the fact that the Charles University in Prague has the right to conclude a license agreement on the use of this work as a school work pursuant to Section 60 paragraph 1 of the Copyright Act.

In Prague, January 9, 2014

Název práce: Teorie relaxace a přenosu energie v otevřených kvantových systémech

Autor: Jan Olšina

Katedra: Fyzikální ústav Univerzity Karlovy

Vedoucí disertační práce: RNDr. Tomáš Mančal, Ph. D.

Abstrakt: Práce shrnuje základy teorie relaxace, přenosu energie a dekoherence ve fotosyntetických molekulárních agregátech popsaných jako otevřené kvantové systémy a základy teorie koherentní nelineární spektroskopie třetího řádu. Práce prezentuje dvě metody pro výpočet fotoindukované dynamiky molekulárních agregátů. Tyto metody odstraňují jisté aproximace běžně užívané při popisu relaxace a přenosu energie v molekulárních systémech na sub-pikosekundové časové škále. První metoda, odvozená ve formalismu parametrických projekčních operátorů, zahrnuje vliv korelací mezi prvním a druhým intervalem nelineární funkce odezvy druhého řádu běžně zanedbávaných ve formalismu řídících rovnic. Druhá metoda představuje stochastický model přesné dynamiky založený na kumulantním rozvoji. Práce také prezentuje analýzu vlivu sekulární a markovské aproximace v popisu dynamiky odvozeném v druhém řádu poruchové teorie v systém-lázňové vazbě s důrazem na dobu života excitonové koherence.

Klíčová slova: otevřené kvantové systémy, nelineární spektroskopie, agregáty molekul, přenos energie, dekoherence

Title: Theory of Relaxation and Energy Transfer in Open Quantum Systems

Author: Jan Olšina

Department: Institute of Physics of Charles University

Supervisor: RNDr. Tomáš Mančal, Ph. D.

Abstract: The work summarizes basic theory of relaxation, energy transfer and decoherence in photosynthetic molecular aggregates described as open quantum systems and basic theory of third order coherent non-linear spectroscopy. The work presents two methods for calculation of photo-induced dynamics of molecular aggregates. The methods relax certain approximations of the theories commonly used to model the relaxation and energy transfer in the molecular systems on the sub-picosecond time scale. The first theory derived in the formalism of parametric projection operators accounts for correlations in a second-order non-linear response-function that are usually neglected in the formalism of master equations. The second theory represents stochastic model of exact dynamics via the cumulant expansion. The work also presents an analysis of importance of the secular and the Markov approximations in the description of dynamics derived in the second-order perturbation theory in the system-bath coupling with emphasis on the excitonic coherence lifetime.

Keywords: open quantum systems, non-linear spectroscopy, molecular aggregates, energy transfer, decoherence

CONTENTS

INTRODUCTION

When discovered, the quantum theory turned our understanding of how the nature works upside down. We were forced to accept that, unlike in the classical physics, our measurement often necessarily and significantly affects the system investigated. We also had to accept the fundamental indeterminism present in the core of the theory and many other important changes. The most important change, however, was probably the change in our understanding of what the physical state of the system is. In the quantum theory, it is represented by the Hilbert space wave-vector or the wave-function that contain all characteristics of the system. This approach is very well developed now and it has led to many far reaching discoveries with many applications. However, being defined on the system Hilbert space that is a direct product of the Hilbert spaces of the subsystems present, the wave-vector quickly becomes incredibly complex object for bigger systems. Moreover, the bigger the system is, the harder it is to separate it from its surrounding. Such imperfect isolation leads to quick entanglement of such system with the rest of the universe, which prevents further usage of the wave-vector approach on the system. Theory of open quantum systems faces these problems by separation of the total Hilbert space into few degrees of freedom of interest which are described explicitly in detail, and which are called *system*, and the rest of the universe that is described implicitly and it is usually called *bath*. The so-called reduced density matrix defined as trace of the total density matrix over the bath degrees of freedom is used for the system description. It is a very good tool capable of describing all possible measurements performed on the system part.

One field where the open quantum systems play a very important role is the theory of spectroscopy. Interaction with light specifies the particular set of degrees of freedom that we can directly measure – the system. Rather than defined by the spatial separation in the real space, it is characterized by the structure of the Hilbert space. In optical spectroscopy, the system is constituted by the electronic degrees of freedom (DOF) that manifest transitions coupled to the radiation by their transition dipole moments. The system DOF constantly interact with nuclear

and other DOF that constitute the bath. Only in presence of such interaction, one can observe effects such as energy transfer, relaxation, thermalization and decoherence.

This thesis focuses on the problems of relaxation, energy transfer and decoherence in the photosynthetic molecular aggregates – one of many fields where the methods of spectroscopy represent a vital source of information. Many molecular systems that ensure functions necessary in primary processes of the photosynthesis have form of molecular aggregates composed of Chlorophyll molecules [Bla02]. They are often embedded into a protein matrix and other molecules, e. g. carotenoids, may be present. Theory of Frenkel excitons is used for a description of the aggregates. The main area of interest is the energy transfer from the light-absorbing molecules (LH2 and LH1 photosynthetic antennae and others) to the so-called reaction center, where the first steps of the photosynthetic chemistry take place.

Advances recently achieved in non-linear spectroscopy opened many new ways to investigate ultrafast photo-induced dynamics of molecules and molecular aggregates. Particularly the two-dimensional (2D) coherent spectroscopy [Jon03, Cow04, Bri04b, Bri04a], both in the infra-red and visible regions, allowed us to obtain an unprecedented amount of information about the third-order non-linear response of systems with a femtosecond time resolution by analysis of the third order non-linear signal. 2D electronic spectra (2DES) [Jon03, Bri04a] resulting from a four-wave mixing (FWM) experiment have many advantages over other methods. Unlike in the case of the pump-probe experiments, their time-resolution is not limited by their frequency resolution, they can reveal the homogeneous line-width, which is otherwise often obscured by the inhomogeneous broadening, and they generally contain more information about the system. More importantly, they also allow us to distinguish between incoherent mixture of the Frenkel exciton populations and their coherent quantum superposition. The latter is characterized by a presence of the off-diagonal elements of the reduced density matrix also called coherences. The presence of the coherences was predicted to manifest as certain oscillations of the peaks of the 2DES [Pis06, Kje06]. Experiments on the photosynthetic Fenna-Matthews-Olson (FMO) pigment-protein complex [Eng07] confirmed these predictions with a surprising result – the coherence manifests unexpectedly long lifetime compared to predictions of the the standard theories used in the field [Ish09c, Hei12]. Since then, similar oscillations were observed in many other photosynthetic systems [Lee07, Cal09, Mer09, Col10, Har12] and conjugated polymers [Col09], as was also reviewed in detail in [Che13b]. It was argued that the coherent quantum superposition of the molecular excitons could significantly contribute to the efficiency of energy transfer in photosynthesis and

the debate about the nature of the long coherence lifetime and their significance to the energy transfer still continues [Ish10, Wu10, Ish11, Car12, Chr12, Che13a, Che13b, Man13a, Tiw13].

All these exciting new results are connected by a common feature: Before the advances in the 2D coherent non-linear spectroscopy, the theories for prediction of the molecular systems dynamics could be based on a host of approximations that turned out to be insufficient for a precise description of the new experiments. Depending on the strength of the coupling between the electronic degrees of freedom and the bath degrees of freedom, the Förster [Foe48] or the Redfield [Red65] rate equations are used. The first works best if the system-bath coupling is weak and the second if it is strong. Master equation theories going beyond the rate theories often use the so-called *secular approximation* that decouples coherences of the reduced density matrix from each other and from the populations, thus significantly lowering the computational cost. Even at the very short time-scale, the experiments focused on the population dynamics (pump probe) are not sensitive to the non-secular effects. Their impact in the 2DES is therefore subject to particular interest and it is an important issue to analyze [Zha98, Yan02, Jan04, Olš10].

Another class of approximations is closely connected to the way how the master equations are used in calculation of the non-linear response functions. Although it was shown that it is possible to obtain an exact result for the linear response function with the use of master equations [Dol08], the same approach cannot include the bath correlations between the different periods of the photo-induced system evolution in higher orders of the response [Ish08]. In some cases, i. e. in presence of the vibrational modulation of the 2DES, such approximation can lead to a complete loss of information about the experimentally observed signal [Nem08]. It was suggested to solve the problem by taking the previous system time evolution explicitly into the equations of motion [Ric10], or by including it into projection operators that are used to reduce the equations of motion to the system DOF [Man12]. The latter technique was later used to develop a correction to the master equations for the second-order response functions [Olš12]. Although the second-order response functions cannot be directly used to model the 2DES, it can be readily applied in the models of excitation of a molecular system by a general quantized light [Man10, Olš11]. This became a matter of general interest in the investigation of the impact of the long-living quantum coherence on the energy transfer in photosynthetic systems. It was argued that although the quantum coherence can be prepared in laboratory by a ultrashort-pulsed laser light, it does not appear under excitation by a natural sunlight [Bru12], which is strongly incoherent. Consequently, theories that include the quantum nature of the natural light were sought [Man10, Olš11, Fas12].

General lack of theories able to describe all observed effects also aroused interest in exact methods in the field. This includes many path integral techniques [Sto02, Shi03, Xu05, Huo10], Monte Carlo methods [Hub59, Sha04, Zho05, Mo05, Lac05, Sha06], and also the stochastic wave-function method [Dal92], quantum state diffusion method [Aha93] and some other approaches [Sch07, Moh08]. Nowadays, probably the most popular exact method are the Hierarchical Equations of Motion (HEOM) developed by Kubo and Tanimura [Tan89, Ish05, Tan09]. It was introduced by Ishizaki [Ish09b] into the field, and recently, it was successfully implemented on the massively parallel graphics processing units [Kre11, Kre12, Kre13].

New exact theory was proposed also in [Olš13] – a stochastic method that covers the resonance coupling term in the Hamiltonian by a stochastic unraveling. Here, the evolution of the system's state is modeled by an ensemble of trajectories in the space of the projectors on the states in the system's Hilbert space. This projector space is known in the theory of non-linear spectroscopy as the *Liouville space* (see Chapter 1 or Ref. [Muk95]). Each trajectory from the ensemble can be assigned a sequence of resonance coupling-free evolution operators that remains after the unraveling. The resulting expression is related to the high order non-linear response functions. With a proper application of the cumulant expansion, it can be evaluated analytically in terms of the so-called lineshape functions commonly used in theory of nonlinear spectroscopy. The properly weighted sum over trajectories gives a result for the system's reduced dynamics, which is exact assuming the Gaussian property for the higher order bath correlation functions.

The techniques of non-linear optical spectroscopy are still developing and they have big potential for future applications. The connection of theory and experiment is very close in this field, since it is generally difficult to understand the experimental results without a detailed theoretical modeling. This thesis follows the line of research developing methods for calculation of the dynamics of molecular aggregates as open quantum systems with focus on the relaxation and energy transfer. These methods may help us to improve our understanding of the sub-picosecond electronic photo-induced processes not only in the photosynthetic systems, but also a in large molecular aggregates, polymers, quantum dots, carbon nanotubes and other systems accessible by the non-linear spectroscopy.

The thesis is based on two articles [Olš10, Olš12] and an arXiv e-print [Olš13] of the author and coworkers. It is organized as follows. Chapter 1 briefly reviews formalism of open quantum systems applied to molecular aggregates and the basic theories that are further used or elaborated in the rest of the work. Chapter 2 serves as a reference to the non-linear spectroscopy, explains the pump probe and the 2DES experiments and provides background that connects the models of the dynamics of open quantum systems with experiment. Chapter 3 is based on the

article [Olš10] and presents a discussion of the relevance of the non-secular effects and application of the Markov approximation to the models of 2DES. Chapter 4 is based on the article [Olš12] and presents a derivation of a correction term to a Redfield-type time-local master equations in the calculation of the second-order response function with the use of parametric projectors [Man12]. Chapter 5, based on the article [Olš13], presents the aforementioned method of stochastic unraveling of resonance-coupling by the cumulant expansion and its application to a problem of interaction between excitonic state and a charge-transfer state. In this problem, the exact theory is required since the bath relaxation effects are large and the effects of approximations based on perturbation expansion in the system-bath coupling are pronounced.

CHAPTER

ONE

OPEN QUANTUM SYSTEMS

This chapter aims to provide basics of the theory of open quantum systems (OQS). We introduce the density matrix, the concept of separation of the total physical system into the so-called system degrees of freedom that are described in full detail, and the so-called bath DOF that are described implicitly and enter the equations of motion through secondary bath-averaged quantities. We also introduce basic models of the bath and the most commonly used theories for calculation of the dynamics of the OQS. Main sources, where an interested reader can obtain more detailed information, are the following books [Fai00, Gre98, Ken82, May01, Muk95, Val13].

1.1 Density Matrix and Basic Terminology and Notation Overview

The fundamental object of the Quantum Theory is the wave-vector $|\Psi\rangle$ (or the wave-function $\Psi(x_1, \ldots, x_n)$) from a Hilbert space $\mathscr{H}$ of the system, which uniquely defines the system state. In order to study the open quantum systems, however, it is very useful to introduce the so-called density operator or density matrix that holds full information about all possible measurements performed on the system. We can, for example, use the density matrix to describe a statistical ensemble of systems in states $|\Psi_i\rangle$ with probabilities p_i. The density matrix of an ensemble is defined as

$$\rho = \sum_i p_i |\Psi_i\rangle\langle\Psi_i| \,. \tag{1.1}$$

The probabilities p_i then simply represent our lack of knowledge about the ensemble. In other cases, we are interested only in a subsystem with Hilbert space $\mathscr{H}_{\text{sub}} \subset \mathscr{H}$. Here, the wave-vectors belong to the total Hilbert space and the cases where the

individual wave-vectors of the subsystems are well-defined and the quantum state is separable are a very special case. However, one can still define the so-called reduced density matrix (RDM) of the subsystem as a trace over all other degrees of freedom

$$\rho = \mathrm{Tr}_{\mathscr{H}\setminus\mathscr{H}_{\mathrm{sub}}} |\Psi\rangle\langle\Psi| \ . \tag{1.2}$$

The distinction between our lack of knowledge and the uncertainty arising purely from the quantum nature of the system or its entanglement with a larger system is still not very well understood, and various interpretations of the Quantum Theory would offer different answers to the question. The density matrix, however, represents extremely practical tool in the theory of open quantum systems.

The density matrix is a hermitian operator and its matrix elements are thus basis-dependent objects. The diagonal elements are called *populations* (of the basis states) and they always have real values between 0 and 1 that represent the probabilities of measuring the respective basis state. The density matrix that has all eigenvalues equal to zero with exception of a single eigenvalue that is equal to 1, corresponds to a quantum state representable by a single wave-vector. Such states are referred as *pure state*s, while all other states are called *mixed states* [Fai00]. The off-diagonal elements of the density matrix are called *coherences*. They serve as an indicator of the quantum superposition between the basis states.

We use standard notation for basic operations with Hilbert space operators. We define the commutator and anti-commutator of operators A and B as

$$[A, B]_- = AB - BA \ , \tag{1.3}$$

$$[A, B]_+ = AB + BA \ . \tag{1.4}$$

We also use a notation in which we explicitly write matrix elements of operators in some basis. The operator matrix elements are then denoted by indices as

$$A_{ab} = \langle a|A|b\rangle \ . \tag{1.5}$$

1.1.1 Interaction Picture

In Quantum Theory, there are two fundamental ways how to hold the information about the system dynamics. In the so-called Schrödinger picture, all information about the system is held by the time-dependent wave-vector $|\Psi(t)\rangle$, and all operators corresponding to physical quantities are constant (unless they express a time-dependent external classical field). Another possible description is the so-called Heisenberg picture, where we remove the dynamics induced by the total Hamiltonian H of the system from the wave-vector and we define the Heisenberg-

picture wave-vector $|\Psi^{(H)}\rangle = \exp(iHt/\hbar)|\Psi(t)\rangle$ and Heisenberg-picture operators $A^{(H)}(t) = \exp(iHt/\hbar)\, A\, \exp(-iHt/\hbar)$. After this transformation, the information about the system dynamics is completely held by the time-dependent Heisenberg-picture operators and the wave-vector is time independent. It is also possible to perform a partial transformation usually called an *interaction picture*. Here, we transform only the parts of the Hamiltonian that are easy to describe in order to simplify the resulting equation of motion. For example, for a Hamiltonian $H = H_0 + H'$ composed of two parts described by Hamiltonians H_0 and H', we define interaction picture with respect to the Hamiltonian H_0 for a wave-vector

$$|\Psi^{(I)}(t)\rangle = \exp(iH_0t/\hbar)|\Psi(t)\rangle \tag{1.6}$$

and for the operators

$$A^{(I)}(t) = \exp(iH_0t/\hbar)\, A\, \exp(-iH_0t/\hbar)\ . \tag{1.7}$$

We denote the operators in the interaction picture by a superscript (I). For operators that are time-independent in the Schrödinger picture, we sometimes omit the superscript and use the time-dependence of the operators alone to indicate they are in the interaction picture. For example, if an operator A is time-independent, we will use a symbol $A(t)$ in place of the symbol $A^{(I)}(t)$ when no ambiguity can arise.

In the Section (1.2), we introduce splitting of the total system into system and bath parts. If not stated otherwise, the interaction picture is always taken with respect to both the system and the bath parts of the total Hamiltonian.

1.2 Model of Molecular Aggregate in Contact with a Phonon Bath

Many molecular systems of interest can be characterized only by a small number of relevant DOF that have to be described in detail. We call these DOF a *system* and a full quantum description is used to model their dynamics. All other DOF also play an important role in a host of effects, particularly they govern the relaxation towards the thermal equilibrium and the decoherence, but a less detailed description can be used for them. We call these DOF a *bath*. We denote the system and bath Hilbert spaces $\mathscr{H}_S$ and $\mathscr{H}_B$ respectively.

Further, we focus our interest towards photosynthesis. Among the photosynthetic complexes, there are many systems composed of Chlorophyll molecules embedded in a protein matrix with different organization (LH1, LH2, FMO and

other systems). Such aggregates can be modeled as groups of N molecules which have two states: the ground state $|g_i^{\mathrm{m}}\rangle$ and the excited state $|e_i^{\mathrm{m}}\rangle$. These DOF are chosen to be the system, while all other DOF constitute the bath. The global aggregate electronic states have a form

$$|g\rangle = \prod_{i=1}^{N} |g_i^{\mathrm{m}}\rangle \ , \tag{1.8a}$$

$$|e_n\rangle = \prod_{i=1}^{n-1} |g_i^{\mathrm{m}}\rangle |e_n^{\mathrm{m}}\rangle \prod_{i=n+1}^{N} |g_i^{\mathrm{m}}\rangle \ , \tag{1.8b}$$

$$|f_{mn}\rangle = \prod_{i=1}^{m-1} |g_i^{\mathrm{m}}\rangle |e_m^{\mathrm{m}}\rangle \prod_{i=m+1}^{n-1} |g_i^{\mathrm{m}}\rangle |e_n^{\mathrm{m}}\rangle \prod_{i=n+1}^{N} |g_i^{\mathrm{m}}\rangle \ . \tag{1.8c}$$

Due to the fact that the relaxation to the ground state in the Chlorophyll molecules is much slower than the typical timescale of energy transfer, it is possible to neglect the relaxation and divide the molecular electronic states into four groups: states of a ground-state manifold (GSM) $|g_n\rangle$, states of a manifold of single-excited states $|e_n\rangle$, states of a manifold of double-excited states $|f_n\rangle$ and higher excited states. If we are interested only in modeling non-linear spectroscopic experiments up to third order in the electric field intensity, the higher excited states can usually be completely neglected. The separation between these manifolds is comparable to the optical frequency of the laser Ω. On the ultrafast time scale, the relaxation between the manifolds can be neglected and the transition between them thus happens only via interaction with the laser field. The blocks of the density matrix corresponding to different state manifolds are thus independent of each other during the dynamics. Elements of the density matrix that belong to different density matrix blocks on their bra- and ket-sides oscillate with frequencies close to the optical radiation and they are called *optical coherences*.

The total Hamiltonian for the photosynthetic molecular aggregate can be written as

$$\begin{aligned} H = & (\epsilon_g^{'} + T + V_g(\{Q\}))|g\rangle\langle g| \\ & + \sum_{n=1}^{N_e} (\epsilon_n^{'} + T + V_n(\{Q\}))|e_n\rangle\langle e_n| \\ & + \sum_{n=1}^{N_e} \sum_{m=1}^{n-1} J_{mn}(|e_m\rangle\langle e_n| + |e_n\rangle\langle e_m|) \\ & + \sum_{n=1}^{N_f} (\epsilon_n^{'f} + T + V_n^f(\{Q\}))|f_n\rangle\langle f_n| \\ & + \sum_{n=1}^{N_f} \sum_{m=1}^{n-1} J_{mn}^f(|f_m\rangle\langle f_n| + |f_n\rangle\langle f_m|) \ . \end{aligned} \tag{1.9}$$

Apart from electronic energies of states $|g\rangle$, $|e_i\rangle$ and $|f_i\rangle$ denoted $\epsilon_g^{'}$, $\epsilon_i^{'}$ or $\epsilon_i^{'f}$, there are also energy contributions from the bath. The kinetic operator of the bath T is assumed to be independent of the electronic state. The bath potential energy operators $V_g(\{Q\})$, $V_n(\{Q\})$, $V_n^f(\{Q\})$ depend on some set of coordinates $\{Q\}$. The total Hamiltonian (1.9) can be decomposed into a system part H_S, a bath part H_B and a system-bath interaction part H_{S-B} by rearranging its terms

$$H = H_S + H_{S-B} + H_B \ , \tag{1.10}$$

$$\begin{aligned} H_S = &\epsilon_g|g\rangle\langle g| + \sum_{n=1}^{N_e} \epsilon_n|e_n\rangle\langle e_n| + \sum_{n=1}^{N_f} \epsilon_n^f|f_n\rangle\langle f_n| \\ &+ \sum_{n=1}^{N_e}\sum_{m=1}^{n-1} J_{mn}(|e_m\rangle\langle e_n| + |e_n\rangle\langle e_m|) \\ &+ \sum_{n=1}^{N_f}\sum_{m=1}^{n-1} J_{mn}^f(|f_m\rangle\langle f_n| + |f_n\rangle\langle f_m|) \ , \end{aligned} \tag{1.11}$$

$$H_{S-B} = \sum_{n=1}^{N_e} \Delta V_n|e_n\rangle\langle e_n| + \sum_{n=1}^{N_f} \Delta V_n^f|f_n\rangle\langle f_n| \ , \tag{1.12}$$

$$H_B = T + V_g(\{Q\}) \ . \tag{1.13}$$

The symbol N_e denotes number of states in the manifold of single excited states and the symbol N_f denotes the number of states in the manifold of double-excited states. We added and subtracted the kinetic and potential terms of the ground state by introducing the energy gap potential operators

$$\Delta V_i = V_i(\{Q\}) - V_g(\{Q\}) - \lambda_i \ , \tag{1.14a}$$

$$\Delta V_i^f = V_i^f(\{Q\}) - V_g(\{Q\}) - \lambda_i^f \ , \tag{1.14b}$$

and the reorganization energies λ_i and λ_i^f. The H_B is independent of the system DOF and it represents the bath part of the Hamiltonian. The rest of the bath operators constitute the system-bath interaction, which enters via two bi-linear terms (1.12). The reorganization energies

$$\lambda_i = \langle V_i(\{Q\}) - V_g(\{Q\})\rangle \ , \tag{1.15a}$$

$$\lambda_i^f = \langle V_i^f(\{Q\}) - V_g(\{Q\})\rangle \tag{1.15b}$$

are defined as an average of the energy-gap difference over the bath DOF. This averaging, defined as trace over bath DOF

$$\langle \bullet \rangle = \mathrm{Tr}_B \bullet w_{\mathrm{eq}} \tag{1.16}$$

for arbitrary operator $\bullet$, assumes that the bath is in the Boltzmann canonical thermal equilibrium

$$w_{\mathrm{eq}} = \frac{e^{-H_B/k_BT}}{\mathrm{Tr}\ e^{-H_B/k_BT}} \ . \tag{1.17}$$

Finally, we introduced energies

$$\epsilon_g = \epsilon_g^{'} \ , \tag{1.18a}$$

$$\epsilon_i = \epsilon_i^{'} + \lambda_i \ , \tag{1.18b}$$

$$\epsilon_i^f = \epsilon_i^{'f} + \lambda_i^f \ . \tag{1.18c}$$

There are two reasons for this definition: Firstly, the mean value of the energy-gap operators $\langle \Delta V_i \rangle$ and $\langle \Delta V_i^f \rangle$ is zero with such a definition, and this significantly simplifies the models based on a perturbation expansion in the system-bath coupling. Secondly, the new energies (1.18) correspond to the optical transitions directly probed by the spectroscopy. In contrast, the old energies $\epsilon_g^{'}$, $\epsilon_i^{'}$ and $\epsilon_i^{'f}$ are the energies in which the thermal equilibrium has the form of canonical distribution

$$\rho_{\mathrm{eq}} = \frac{e^{-H_S/k_BT}}{\mathrm{Tr}\ e^{-H_S/k_BT}} \ . \tag{1.19}$$

The resonance couplings J_{mn} are free parameters of the model, but the double-excited state manifold resonance couplings can be approximately derived from them using the so-called Bethe ansatz [Mei97]

$$J^f_{mn,rs} \approx \delta_{ns} J_{mr} + \delta_{nr} J_{ms} + \delta_{ms} J_{nr} + \delta_{mr} J_{ns} \ . \tag{1.20}$$

The double-excited potential bath operators are constructed from assumption

$$\Delta V^f_{mn} \approx \Delta V_m + \Delta V_n \ . \tag{1.21}$$

In the chapters that follow, we denote total, system and bath evolution operators

$$U(t) = \exp\left(-\frac{i}{\hbar} H t\right) \ , \tag{1.22a}$$

$$U_S(t) = \exp\left(-\frac{i}{\hbar} H_S t\right) \ , \tag{1.22b}$$

$$U^g(t) = \exp\left(-\frac{i}{\hbar} H_B t\right) \ , \tag{1.22c}$$

$$U^e_n(t) = \exp\left(-\frac{i}{\hbar} (H_B + \Delta V_n) t\right) \ . \tag{1.22d}$$

The evolution operator (1.22c) corresponds to the evolution of the bath in presence of the electronic ground state, while the evolution operator (1.22d) corresponds

to the evolution of the bath in the presence of the electronic excited state $|n\rangle$.

1.3 Interaction with the Electromagnetic Field

Apart from the interaction of the system with the phonon bath through the Hamiltonian H_{S-B}, Eq. (1.12), one also has to describe its interaction with the electromagnetic radiation in order to model the spectroscopic experiments. For molecular systems, where the individual transition dipole moments are much smaller than the optical wavelength, one can use the dipole approximation, which corresponds to an interaction Hamiltonian[1]

$$H_{S-R} = -\sum_{i\in\{x,y,z\}} \mu_i E_i(\mathbf{r}) \,. \tag{1.23}$$

In this description, the system DOF interact with the radiation through the total dipole moment operator μ_i composed of the dipole moment operators of the individual transitions

$$\mu_i = \sum_{n=1}^{N_e} \mu_i^{e,n}(|g\rangle\langle e_n| + |e_n\rangle\langle g|) + \sum_{n=1}^{N_f}\sum_{m=1}^{n-1} \mu_i^{f,mn}(|f_m\rangle\langle e_n| + |e_n\rangle\langle f_m|) \,. \tag{1.24}$$

The electric field is described by operators E_m from the Hilbert space of the radiation $\mathscr{H}_R$. They can be defined by decomposition into modes with wave-vectors $\mathbf{k}$, polarization vectors $\boldsymbol{\varepsilon}^{\mathbf{k}m}$ and creation and annihilation operators $a^\dagger_{m\mathbf{k}}$, $a_{m\mathbf{k}}$ as

$$E_m(\mathbf{r}) = \frac{i}{c}\sum_{\mathbf{k}} N_{\mathbf{k}}\omega_{\mathbf{k}}\boldsymbol{\varepsilon}^{\mathbf{k}m}\left(a_{m\mathbf{k}}e^{i\mathbf{k}\cdot\mathbf{r}} - a^\dagger_{m\mathbf{k}}e^{-i\mathbf{k}\cdot\mathbf{r}}\right) \,. \tag{1.25}$$

The polarization vectors $\boldsymbol{\varepsilon}^{\mathbf{k}m}$ are orthogonal to $\mathbf{k}$ and to each other. The speed of light is denoted c. The radiation field is quantized in a box of a size L and the limit $L \to \infty$ is to be performed at the end of our calculations [Gre98]. This procedure leads to normalization constants

$$N_{\mathbf{k}} = \sqrt{\frac{2\pi\hbar c^2}{L^3\omega_{\mathbf{k}}}} \,. \tag{1.26}$$

[1]The full form of light-matter interaction Hamiltonian is $H_{S-R} = -\frac{e}{mc}\mathbf{p}\cdot\mathbf{A}(\mathbf{r}) + \frac{e^2}{2mc^2}\mathbf{A}^2(\mathbf{r})$, where e denotes the elementary charge, c denotes the speed of light, m denotes the electron mass, $\mathbf{p}$ denotes the electron momentum operator and $\mathbf{A}(\mathbf{r})$ denotes the vector potential known from the Maxwell theory of electromagnetism. The Hamiltonian (1.23) assumes $\mathbf{A}^2(\mathbf{r}) \approx 0$. Also, the usage of the dipole moment operator μ requires that we neglects the space-dependence of the vector potential across the individual molecules.

The radiation field is a quantum bath governed by a Hamiltonian

$$H_R = \sum_{\sigma \mathbf{k}} \hbar \omega_{\mathbf{k}} \left(a^\dagger_{\sigma \mathbf{k}} a_{\sigma \mathbf{k}} + \frac{1}{2} \right) . \tag{1.27}$$

Apart from special cases where the details of quantum nature of the radiation field might play role [Man10, Olš11, Bru12, Fas12], much simpler semi-classical approach can be used to describe the radiation. Eq. (1.23) can be replaced by semi-classical system-radiation interaction Hamiltonian in the dipole approximation

$$H_{S-R} = - \sum_{i \in \{x,y,z\}} \mu_i E_i(\mathbf{r}, t) . \tag{1.28}$$

Here, $E_i(\mathbf{r}, t)$ are not operators, but time-dependent functions representing the time-dependent electric field. The Hamiltonian (1.28) does not contain the description of spontaneous emission, which we do not require here. The Hamiltonian (1.28), however, does not directly enter the equations of motion. We treat it in the formalism of response theory instead. It is briefly explained in the Chapter 2.1.

The experiments we aim to describe are based on a sequence of femtosecond pulses. Pulses this short can be well represented by a δ-pulse. The electric field in a form

$$E(\mathbf{r}, t) = e^{-\mathbf{k}\cdot\mathbf{r}} \delta(t - t_0) E_0 \tag{1.29}$$

is used. In this case, the excitation in time t_0 simply corresponds to a jump in the RDM written as

$$\rho(t_0 + \varepsilon) = [\mu E_0, \rho(t_0 - \varepsilon)]_- . \tag{1.30}$$

Symbol ε denotes infinitesimally small positive quantity here.

1.4 Local and Excitonic Basis

According to the Quantum Theory, we are, of course, free to choose any basis of states for our calculation. There are, however, two bases of special importance. It is the *exciton basis* defined as a basis in which the system Hamiltonian H_S, Eq. (1.11), is diagonal and the *local basis* defined by Eqs. (1.8).

In the local basis, every excited basis state is localized on particular molecule. It is therefore the basis in which the couplings, the transition dipole moments or the correlations of the energy gap fluctuations directly relate to the geometrical arrangement of the molecules. The exciton basis is natural choice in the case of a weak system-bath coupling, because then the populations of the eigenstates of H_S, the so-called *excitons*, change only slowly due to the interaction with the bath, compared to the oscillations caused by the H_S in other bases. In the excitonic

basis, the dynamics of populations and coherences is only very weakly coupled and the separation into populations and coherences is more physical, as will be discussed in the Section 1.7.5 in more detail. Also, for the weak system-bath coupling, the thermalization drives the system towards the canonical distribution (1.19).

The excitonic states from the excited-state and double-excited state manifolds are denoted by tilde, as $|\tilde{e}_i\rangle$ and $|\tilde{f}_i\rangle$. Sometimes we want to stress that summation over indices of operator $\bullet$ is performed in the exciton basis. In such case, we use indices with tilde, e. g. $\bullet_{\tilde{a}\tilde{b}}$. General operator A is transformed from the local basis to the exciton basis as

$$A_{\tilde{m}\tilde{n}} = \sum_{ij} A_{ij} \langle i|\tilde{m}\rangle\langle\tilde{n}|j\rangle \ . \tag{1.31}$$

We also define the potential energy bath operators for the excited eigenstates $|\tilde{m}\rangle$, $|\tilde{n}\rangle$

$$V_{\tilde{m}\tilde{n}}(\{Q\}) = \sum_{ij} \delta_{ij} V_i(\{Q\}) \langle i|\tilde{m}\rangle\langle\tilde{n}|j\rangle \tag{1.32}$$

here. It will be useful in the Chapter 4.

1.5 Energy Gap Correlation Function and Its Properties

The system-bath interaction in the second-order of the perturbation expansion in the system-bath coupling can be completely characterized with help of the a correlation function of the potential energy difference bath operators (1.14) reduced over the bath DOF. It is called *energy gap correlation function* (EGCF) and it is defined as

$$C_{mn}(t) = \mathrm{Tr}_B \left\{ U^{g\dagger}(t) \Delta V_m U^g(t) \Delta V_n w_{\mathrm{eq}} \right\} \ , \tag{1.33}$$

where ΔV_m was introduced in Eq. (1.14a) and w_{eq} was introduced in Eq. (1.17). The bath dynamics is included by the interaction picture with respect to the bath. The EGCF is highly relevant also in the non-perturbative approaches. They can be for example derived from assumption that the bath has the Gaussian property, i. e. that the higher-order correlation functions can be expressed in terms of the second-order EGCF (1.33) through the Wick's theorem. In general case, higher order correlation functions are necessary.

Before specifying the particular form of the EGCF, it is useful to define related

quantities – the so-called lineshape functions

$$g_{mn}(t) = \frac{1}{\hbar^2} \int_0^t d\tau \int_0^\tau d\tau' C_{mn}(\tau') \ . \tag{1.34}$$

In Chapter 4, we will also need EGCF and the lineshape functions transformed into the exciton basis in one or both of their indices

$$C_{a\tilde{b}}(t) = \langle \Delta V_a(t) \Delta V_{\tilde{b}\tilde{b}} \rangle \ , \tag{1.35a}$$

$$g_{a\tilde{b}}(t) = \frac{1}{\hbar^2} \int_0^t d\tau \int_0^\tau \tau' C_{a\tilde{b}}(\tau') \ , \tag{1.35b}$$

$$C_{\tilde{a}\tilde{b}}(t) = \langle \Delta V_{\tilde{a}\tilde{a}}(t) \Delta V_{\tilde{b}\tilde{b}} \rangle \ , \tag{1.35c}$$

$$g_{\tilde{a}\tilde{b}}(t) = \frac{1}{\hbar^2} \int_0^t d\tau \int_0^\tau \tau' C_{\tilde{a}\tilde{b}}(\tau') \ . \tag{1.35d}$$

1.5.1 Energy Gap Correlation Function of Quantum Harmonic Oscillator

In application of nonlinear spectroscopy to the molecular aggregates in photosynthesis, we are particularly interested in bath represented by nuclear degrees of freedom. If we assume that these DOF can be described as a set of infinitely many harmonic oscillators, we get both very powerful and simple model of a quantum bath. The harmonic modes are independent, since the most natural set of harmonic modes would be obtained through the normal mode analysis. The modes are often referred as to phonons, although they have different properties than the phonons in crystallography or solid-state physics. They lack the long-distance spatial coherence and locally manifest higher reorganization energy as well as slower response time.

To get a fully quantum EGCF for such a harmonic bath, we must derive the EGCF for a single harmonic mode connected to a transition between the ground and the excited electronic states. There is a single harmonic oscillator with different potential energy operator in the ground state and in the excited state, see Fig. 1.1. We are particularly interested in the energy gap potential operator (1.14a)

$$\Delta V(Q) = \underbrace{\frac{1}{2} m\omega^2 (Q+d)^2}_{V_e} - \underbrace{\frac{1}{2} m\omega^2 Q^2}_{V_g} - \underbrace{\frac{1}{2} m\omega^2 d^2}_{\langle V_e - V_g \rangle} \ , \tag{1.36}$$

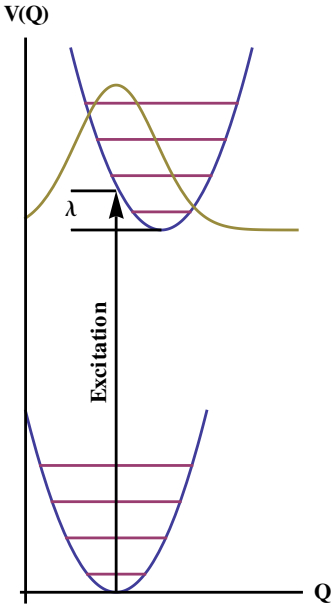

Figure 1.1: A bath of harmonic oscillators: Nuclear degrees of freedom are modeled as a bath of infinitely many harmonic oscillators with different coupling strengths given by a spectral density $J(\omega)$. The model for a transition between states $|a\rangle$ and $|b\rangle$ assumes two harmonic surfaces for both states which are shifted by a separation d in a single common coordinate Q. According to the Condon principle, an excitation from the ground state of the lower harmonic oscillator vertically excites a set of states of the upper harmonic oscillator, which results in a coherent dynamics. In presence of many oscillators, the system dissipates reorganization energy λ, which has classical analogy of a difference between the energy at which the higher harmonic oscillator is excited and minimum of its potential energy surface. The precise quantum definition is given by Eqs. (1.15).

where we indicated the terms corresponding to the general expression V_e, V_g and $\langle V_e - V_g \rangle$. The potential energy surface parabolas are shifted by distance d. This allows for the description of the Stokes shift. We write all the important quantities in terms of the ladder operators

$$Q = \sqrt{\frac{\hbar}{2m\omega}}(a + a^\dagger) \,, \tag{1.37a}$$

$$H = \hbar\omega a^\dagger a \,, \tag{1.37b}$$

$$U(t) = \exp(-i\omega a^\dagger a t) \,. \tag{1.37c}$$

The zero-mode energy was excluded from the harmonic oscillator Hamiltonian (1.37b). We assume that the energy levels of the oscillator are initially in the Boltzmann thermal equilibrium

$$W_{\text{eq}} = \frac{1}{Z} \exp(-H\beta) \,, \tag{1.38}$$

where

$$Z = \sum_{k=0}^{\infty} \langle k|e^{-a^\dagger a\hbar\omega\beta}|k\rangle = \frac{e^{\hbar\omega\beta}}{e^{\hbar\omega\beta}-1} \tag{1.39}$$

is the Bose-Einstein normalization factor. Now, one can write down the energy gap correlation function

$$\langle U^\dagger(t)\Delta V U(t)\Delta V\rangle = \sum_{k=0}^{\infty}(\frac{1}{2}m\omega^2)^2\frac{1}{Z}\left[\langle k|e^{i\omega a^\dagger at}2Qde^{-i\omega a^\dagger at}2Qde^{-a^\dagger a\hbar\omega\beta}|k\rangle\right] . \tag{1.40}$$

After evaluating the sum (1.40), we obtain

$$\langle U^\dagger(t)\Delta V U(t)\Delta V\rangle = \omega^2\hbar^2 S\left[\cos\omega t\ \coth\hbar\beta\omega/2 - i\sin\omega t\right] . \tag{1.41}$$

We defined

$$S = \frac{1}{2}\frac{d^2 m\omega}{\hbar} , \tag{1.42}$$

a dimension-less quantity called a Huang-Rhys factor, in order to reduce the number of parameters. The Eq. (1.41) is the EGCF of a single harmonic oscillator. It is also referenced as an EGCF of an undamped harmonic oscillator.

1.5.2 Multi-Mode Harmonic Bath

There are many DOF in the bath. In the harmonic approximation, one can always perform a normal mode decomposition, which results in many uncoupled harmonic oscillators coupled only with the system of interest. Only in the limit of infinitely many harmonic oscillators, one gets important features, such as irreversibility [Fai00]. The EGCF of such multi-mode harmonic bath can be defined as an integral of harmonic oscillator EGCF (1.41) weighted by the so-called spectral density $J(\omega)$

$$C(t) = \int_0^\infty d\omega\ J(\omega)\omega^2\left(\cos\omega t\ \coth\hbar\beta\omega/2 - i\sin\omega t\right) . \tag{1.43}$$

Further, we assume generally different spectral density $J_m(\omega)$ for every molecule m of the molecular aggregate and no correlation between the baths of individual molecules, i. e. $C_{mn}(t) = \delta_{mn}C_{mn}(t)$.

There are two important properties of a general bosonic EGCF: Firstly, it hermite-conjugates on time reversal

$$C_{mn}(-t) = C^*_{nm}(t) \tag{1.44}$$

as can be seen directly from its definition $C^*_{mn}(t) = \mathrm{Tr}\{\Delta V_m(t)\Delta V_n w_{\mathrm{eq}}\}^* =$

$\mathrm{Tr}\{\Delta V_n \Delta V_m(t) w_{\mathrm{eq}}\} = \mathrm{Tr}\{\Delta V_n(-t) \Delta V_m w_{\mathrm{eq}}\} = C_{nm}(-t)$. The last step is possible because the bath evolution operators in the interaction picture of $\Delta V_m(t)$ commute with the stationary bath density matrix w_{eq}. Secondly, the Fourier-transformed EGCF

$$C_{mn}(\omega) = \int_{-\infty}^{\infty} dt\ e^{i\omega t} C_{mn}(t) \tag{1.45}$$

has a property

$$C_{mn}(\omega) = e^{\hbar\omega\beta} C_{nm}(-\omega)\ . \tag{1.46}$$

It is a special case of the Fluctuation-Dissipation Theorem and it ensures that in the limit of weak (but non-zero) system-bath coupling, the Boltzmann thermal equilibrium is reached between the energy levels (1.18). In the multi-mode harmonic bath model, it is satisfied because we assumed the Boltzmann equilibrium (1.38) for every harmonic oscillator present in the bath.

An important special case of the multi-mode harmonic bath is EGCF of an overdamped harmonic oscillator [Muk95]

$$\begin{aligned} C_{mn}(t) =& \hbar\lambda\Lambda\delta_{mn} \left[\cot(\Lambda\hbar\beta/2) - i\right] \exp(-\Lambda t) \\ &+ \frac{4\lambda\Lambda\delta_{mn}}{\beta} \sum_{n=1}^{\infty} \frac{\nu_n \exp\left(-\nu_n t\right)}{\nu_n^2 - \Lambda^2}\ . \end{aligned} \tag{1.47}$$

The parameter $\beta = 1/k_B T_B$ relates to the bath temperature T_B and the parameter $\Lambda = 1/\tau_c$ is given by the characteristic time of damping of the oscillators τ_c. The so-called Matsubara frequencies are defined as $\nu_n = 2\pi n/\beta\hbar$. The EGCF (1.47) is derived from the Lorentz-Drude spectral density

$$\omega^2 J(\omega) = \frac{2\hbar}{\pi} \frac{\lambda\omega\Lambda}{\omega^2 + \Lambda^2}\ , \tag{1.48}$$

where the parameter Λ is called cutoff frequency. Both the EGCFs (1.41) and (1.47) are special cases of the EGCF of the general harmonic oscillator [Muk95] with frequency ω and damping rate γ

$$\begin{aligned} C_{mn}(t) =& \frac{\hbar\lambda\omega^2}{2\zeta}\delta_{mn} \left[\coth(i\phi\hbar\beta/2)\ \exp(-\phi t) - \coth(i\phi'\hbar\beta/2)\ \exp(-\phi' t)\right] \\ &- \frac{4\lambda\omega^2\gamma}{\beta} \sum_{n=1}^{\infty} \frac{\nu_n \exp(-\nu_n t)}{(\omega^2 + \nu_n^2)^2 - \gamma^2\nu_n^2} - \frac{i\hbar\lambda\omega^2}{\zeta} \exp(-\gamma t/2) \sin(\zeta t)\ , \end{aligned} \tag{1.49}$$

where

$$\phi = \frac{\gamma}{2} + i\zeta \ , \tag{1.50}$$

$$\phi' = \frac{\gamma_i}{2} - i\zeta_i \ , \tag{1.51}$$

$$\zeta = \sqrt{\omega^2 - \gamma^2/4} \ . \tag{1.52}$$

1.6 Superoperator Formalism

For a closed system described by a density matrix, the role of the Schrödinger equation is taken by the Liouville-von Neumann equation

$$\frac{d}{dt}\rho(t) = -\frac{i}{\hbar}[H, \rho(t)]_- \ . \tag{1.53}$$

For open quantum systems, the equations of motion is typically much more complicated. It is therefore convenient to adopt more compact formalism. Linear operators on a Hilbert space of the system constitute a vector space. It is called *Liouville space* and the operators on it are called *superoperators.* We introduce the Liouville superoperator, or shortly Liouivillian

$$\mathcal{L}\bullet \equiv \frac{1}{\hbar}[H, \bullet]_- \ . \tag{1.54}$$

Now, we can write the Eq. (1.53) in more compact form

$$\frac{d}{dt}\rho(t) = -i\mathcal{L}\rho(t) \ . \tag{1.55}$$

We also define Liouvillians of the system, the bath and the system-bath interaction

$$\mathcal{L}_S \equiv \frac{1}{\hbar}[H_S, \bullet]_- \ , \tag{1.56a}$$

$$\mathcal{L}_B \equiv \frac{1}{\hbar}[H_B, \bullet]_- \ , \tag{1.56b}$$

$$\mathcal{L}_{S-B} \equiv \frac{1}{\hbar}[H_{S-B}, \bullet]_- \ , \tag{1.56c}$$

and the corresponding evolution superoperators

$$\mathcal{U}(t) = \exp\left(-i\mathcal{L}t\right) \ , \tag{1.57a}$$

$$\mathcal{U}_S(t) = \exp\left(-i\mathcal{L}_S t\right) \ , \tag{1.57b}$$

$$\mathcal{U}_B(t) = \exp\left(-i\mathcal{L}_B t\right) \ . \tag{1.57c}$$

It is also useful to introduce a superoperator notation for the interaction with

the electromagnetic field through the Hamiltonian (1.28). We define

$$\mathcal{V}_i \bullet = \frac{1}{\hbar}[\mu_i, \bullet]_- \ , \tag{1.58a}$$

$$\mathcal{V}_i^{(R)} \bullet = -\frac{1}{\hbar} \bullet \mu_i \ , \tag{1.58b}$$

$$\mathcal{V}_i^{(L)} \bullet = \frac{1}{\hbar} \mu_i \bullet \ . \tag{1.58c}$$

Even more general notation is often used: Given operator A on a Hilbert space, we define related superoperators

$$A^{\times} = \frac{1}{\hbar}[\mu, \bullet]_- \ , \tag{1.59a}$$

$$A^{\circ} = \frac{1}{\hbar}[\mu, \bullet]_+ \ . \tag{1.59b}$$

In the context of separation of the system into the system and bath parts, we also introduce the reduced evolution superoperators

$$\tilde{\mathcal{U}}(t) = \mathrm{Tr}_B\{\mathcal{U}(t) W_0\} \ , \tag{1.60}$$

that are result of the full dynamics traced over the bath DOF. We denote them by tilde. The exact definition always depends on the initial state W_0 specified later in the work.

A general superoperator $\mathcal{A}$ has four indices and its action on an operator B can be written as

$$A_{ab} = \sum_{cd} \mathcal{A}_{abcd} B_{cd} \ . \tag{1.61}$$

We also introduce a notation to stress the block structure of the density matrix described in the Section 1.2 for each of the indices. We add a superscript index with a value g, e or f for every subscript index, depending if it belongs to the ground state manifold, the manifold of the single-excited states or the manifold of the double-excited states. These auxiliary superscript indices are given in brackets not to be confused with the regular indices. For example the reduced evolution superoperator acting on the optical coherence block of density matrix $\rho_{ab}^{(eg)}(0)$ is written as

$$\rho_{ab}^{(eg)}(t) = \sum_{cd} \tilde{\mathcal{U}}_{abcd}^{(egeg)}(t) \rho_{cd}^{(eg)}(0) \ . \tag{1.62}$$

1.7 Projector Approach to System-Bath Separation

1.7.1 Nakajima-Zwanzig Identity

For molecular systems embedded in a bath it is necessary to derive equations of motion dealing only with the DOF of interest. It can be done by separation of the total system into system and bath parts. The system-bath separation yields the so-called reduced density matrix, which contains detailed information only about the system DOF and couples with the bath DOF through the EGCF. A very straightforward and useful way of system-bath separation is the so-called projector approach [Fai00], which was introduced by Nakajima and Zwanzig [Nak58, Zwa60] to obtain a general equation of motion for the RDM.

As a starting point, one defines projector that preserves the system DOF and traces over the bath DOF. The most common choice is the so-called Argyres-Kelly (AK) projector [Arg64]

$$\mathcal{P}^{AK}\bullet = w_0 \,\mathrm{Tr}_B \bullet \,, \tag{1.63}$$

where w_0 is bath density matrix for which $\mathrm{Tr}\, w_0 = 1$. The most common choice is $w_0 = w_{\mathrm{eq}}$ according to definition (1.17), which is equivalent to an assumption that the bath can be approximated by the canonical equilibrium state. For the rest of this chapter, we will however use general projector on the system DOF $\mathcal{P}$. We only require that the projector property $\mathcal{P}^2 = \mathcal{P}$ holds. Further, we define the projector on the bath DOF as

$$\mathcal{Q} = 1 - \mathcal{P} \,. \tag{1.64}$$

Now, we introduce reduced system density matrix $\rho(t)$ and reduced bath density matrix $w(t)$ as

$$\rho(t) = \mathrm{Tr}_B \, W(t) \,, \tag{1.65a}$$

$$w(t) = \mathrm{Tr}_S \, W(t) \,, \tag{1.65b}$$

where the trace Tr_B traces over the bath DOF and the trace Tr_S traces over the system DOF. The system RDM (1.65a) is very closely related with projection $\mathcal{P}W(t) = \rho(t)\, w_0$. It differs only by the presence of the bath RDM w_0. Important property of the projector $\mathcal{P}$ is that is does not influence the system RDM, $\mathrm{Tr}_B \mathcal{P} W(t) = \mathrm{Tr}_B W(t) = \rho(t)$. We hold to the convention of using symbols ρ, w and W for the density matrices of the system, the bath and the total density matrix respectively in the whole work. Starting from the Liouville equation (1.55),

we include the identity $\mathcal{P}+\mathcal{Q}$ into proper places

$$\frac{d}{dt}(\mathcal{P}+\mathcal{Q})W(t) = -i(\mathcal{P}+\mathcal{Q})\mathcal{L}(\mathcal{P}+\mathcal{Q})W(t)\ . \tag{1.66}$$

Due to the properties of the projectors $\mathcal{P}$, $\mathcal{Q}$, we can divide the Eq. (1.66) into two parts

$$\frac{d}{dt}\mathcal{P}W(t) = -i\mathcal{P}\mathcal{L}\mathcal{P}W(t) - i\mathcal{P}\mathcal{L}\mathcal{Q}W(t)\ , \tag{1.67a}$$

$$\frac{d}{dt}\mathcal{Q}W(t) = -i\mathcal{Q}\mathcal{L}\mathcal{P}W(t) - i\mathcal{Q}\mathcal{L}\mathcal{Q}W(t)\ . \tag{1.67b}$$

We can formally solve the Eq. (1.67b) and obtain

$$\mathcal{Q}W(t) = -ie^{-i\mathcal{Q}\mathcal{L}(t-t_0)}\mathcal{Q}W(t_0) - i\int_{t_0}^{t} d\tau\ e^{-i\mathcal{Q}\mathcal{L}(t-\tau)}\mathcal{Q}\mathcal{L}\mathcal{P}W(\tau)\ . \tag{1.68}$$

Plugging the Eq. (1.68) back into the Eq. (1.67a) yields

$$\begin{aligned}\frac{d}{dt}\mathcal{P}W(t) =& -i\mathcal{P}\mathcal{L}\mathcal{P}W(t) - \mathcal{P}\mathcal{L}e^{-i\mathcal{Q}\mathcal{L}(t-t_0)}\mathcal{Q}W(t_0)\\ &- \mathcal{P}\mathcal{L}\int_{0}^{t-t_0} ds\ e^{-i\mathcal{Q}\mathcal{L}s}\mathcal{Q}\mathcal{L}\mathcal{P}W(t-s)\ ,\end{aligned} \tag{1.69}$$

which is the so-called Nakajima-Zwanzig identity in the Schrödinger picture. We can repeat the same procedure, but this time in the interaction picture with respect to the Hamiltonians of the system and the bath. The resulting Nakajima-Zwanzig identity yields

$$\begin{aligned}\frac{d}{dt}\mathcal{P}W^{(I)}(t) =& -i\mathcal{P}\mathcal{L}^{(I)}(t)\mathcal{P}W^{(I)}(t)\\ &- \mathcal{P}\mathcal{L}^{(I)}(t)\exp\left(-i\int_{t_0}^{t} d\tau\ \mathcal{Q}\mathcal{L}^{(I)}(\tau)\right)\mathcal{Q}W^{(I)}(t_0)\\ &- \mathcal{P}\mathcal{L}^{(I)}(t)\int_{0}^{t-t_0} ds\ \exp\left(-i\int_{t_0}^{s} d\tau'\ \mathcal{Q}\mathcal{L}^{(I)}(\tau')\right)\mathcal{Q}\mathcal{L}^{(I)}(t-s)\mathcal{P}W^{(I)}(t-s)\ .\end{aligned} \tag{1.70}$$

1.7.2 Convolutionless Equation of Motion

Before we introduce approximations into the Eq. (1.70), we can make one more formal step, which allows us to overcome its time non-local character. Let us

assume an evolution superoperator $\mathcal{U}'(t)$, which satisfies

$$\mathcal{P}W(t) = \mathcal{U}'(t - t_0)\mathcal{P}W(t_0). \tag{1.71}$$

This superoperator is of course unknown, but it allows us to turn a time non-local differential equation (1.70) formally into a time-local one. We can write

$$\begin{aligned}\frac{d}{dt}\mathcal{P}W(t) = &- i\mathcal{P}\mathcal{L}_I(t)\mathcal{P}W(t) - \mathcal{P}\mathcal{L}_I(t)\exp\left\{-i\int_{t_0}^{t} d\tau \mathcal{Q}\mathcal{L}_I(\tau)\mathcal{Q}\right\}\mathcal{Q}W(t_0) \\ &- \Big[\int_0^{t-t_0} d\tau' \mathcal{P}\mathcal{L}_I(t)\exp\left\{-i\int_{t_0}^{\tau'} d\tau'' \mathcal{Q}\mathcal{L}_I(\tau'')\mathcal{Q}\right\} \\ &\times \mathcal{Q}\mathcal{L}_I(t-\tau')\mathcal{U}'(-\tau')\Big]\mathcal{P}W(t)\ .\end{aligned} \tag{1.72}$$

We do not develop the convolutionless (or time local) theory any further here, because we will be interested only in terms up to the second order in $\mathcal{L}_I$. In such case $\mathcal{U}'(-\tau)$ can be approximated as $\mathcal{U}'(-\tau) \approx \mathcal{U}_S(-\tau)\mathcal{U}_B(-\tau)$, where $\mathcal{U}_S(-\tau)$ and $\mathcal{U}_B(-\tau)$ are evolution superoperators with respect to $\mathcal{L}_S$ and $\mathcal{L}_B$. Interested reader can refer e. g. to Refs. [Has77, Shi77, Muk78, Muk79, Fai00] for further details.

1.7.3 Time-Nonlocal Quantum Master Equation

Quantum Master Equation (QME) is an equation of motion derived in second-order perturbation theory in system-bath coupling (SBC) [May01]. One possible derivation starts with the Nakajima-Zwanzig identity (1.70), where we use the Argyres-Kelly projector $\mathcal{P}^{AK}$, Eq. (1.63), with $w_0 = w_{\mathrm{eq}}$. The second term of Eq. (1.70) is often assumed to be zero, $\mathcal{L}^{(I)}(t)\mathcal{Q}W^{(I)}(t_0) = 0$, which is ensured by a proper choice of the initial condition

$$W^{(I)}(t_0) = w_{\mathrm{eq}}\rho_0\ , \tag{1.73}$$

where the system and the bath are not entangled initially. Here, w_{eq} is the bath density matrix in the canonical equilibrium (1.17). The system-part initial condition ρ_0 is not restricted by this assumption. The first term of the Eq. (1.70) is also zero, since the interaction terms (1.14a, 1.15b) contained in $\mathcal{L}^{(I)}(t)$ in the first order vanish after the bath-averaging, i. e. after the action of $\mathcal{P}^{AK}$. The

remaining term simplifies to

$$\frac{d}{dt}\mathcal{P}^{AK}W^{(I)}(t) = -\,\mathcal{P}^{AK}\mathcal{L}^{(I)}(t)\int_0^{t-t_0} ds\;\mathcal{Q}^{AK}\mathcal{L}^{(I)}(t-s)\mathcal{P}^{AK}W^{(I)}(t-s) \tag{1.74}$$

in the second-order in SBC. If we define the reduced density matrix in the interaction picture with respect to the H_S and H_B as

$$\rho^{(I)}(t) = \mathrm{Tr}_B W^{(I)}(t)\;, \tag{1.75}$$

we can write the Eq. (1.74) as well-known Quantum Master Equation

$$\frac{d}{dt}\rho^{(I)}(t) = -\,\mathrm{Tr}_B\mathcal{L}^{(I)}(t)\int_0^{t-t_0} ds\;\mathcal{L}^{(I)}(t-s)\rho^{(I)}(t-s)\;, \tag{1.76}$$

which, written in Hilbert space representation, yields

$$\begin{aligned}\frac{d}{dt}\rho^{(I)}(t) = -\frac{1}{\hbar^2}\sum_{i,j}\int_0^{t-t_0} ds\\ \langle[\Delta V_j(t)K_j^{(I)}(t),[\Delta V_i(t-s)K_i^{(I)}(t-s),\rho^{(I)}(t-s)]_-]_-\rangle\;.\end{aligned} \tag{1.77}$$

We can also write it in terms of EGCF as

$$\begin{aligned}\frac{d}{dt}\rho^{(I)}(t) = -\,\frac{1}{\hbar^2}\sum_{i,j}\int_0^{t-t_0} ds\\ \Big(C_{ji}(s)[K_j^{(I)}(t),K_i^{(I)}(t-s)\rho^{(I)}(t-s)]_-\\ -\,C_{ij}(-s)[K_j^{(I)}(t),\rho^{(I)}(t-s)K_i^{(I)}(t-s)]_-\Big)\end{aligned} \tag{1.78}$$

in the interaction picture, or as

$$\begin{aligned}\frac{d}{dt}\rho(t) = -\,\frac{i}{\hbar}[H_S,\rho(t)]_- - \frac{1}{\hbar^2}\sum_{i,j}\int_0^{t-t_0} ds\\ \Big(C_{ji}(s)[K_j,U_S^\dagger(-s)K_i\rho(t-s)U_S(-s)]_-\\ -\,C_{ij}(-s)[K_j,U_S^\dagger(-s)\rho(t-s)K_iU_S(-s)]_-\Big)\end{aligned} \tag{1.79}$$

in the Schödinger picture. We will call this equation of motion Time-Nonlocal Quantum Master Equation (TNL-QME). The Eq. (1.79) can be rewritten into

the superoperator formalism as

$$\frac{d}{dt}\rho_{ab}(t) = \sum_{cd} -i\mathcal{L}_{abcd}\rho_{cd}(t) - \int_{t_0}^{t} ds\ \mathcal{M}_{abcd}(s)\rho_{cd}(t-s)\ . \tag{1.80}$$

The superoperator $\mathcal{M}(t)$ defined by the matrix structure of Eq. (1.79) is defined as

$$\begin{aligned}\mathcal{M}(t)\bullet = -\frac{1}{\hbar^2}\sum_{i,j}\ \Big(&C_{ji}(t)[K_j, U_S^\dagger(-t)K_i \bullet U_S(-t)]_- \\ &- C_{ij}(-t)[K_j, U_S^\dagger(-t)\bullet K_i U_S(-t)]_-\Big)\ .\end{aligned} \tag{1.81}$$

1.7.4 Time-Local Quantum Master Equation

The TNL-QME (1.79) is an equation with convolution, which often makes its solution numerically difficult. In various practical applications, the bath can be considered to be only weakly coupled to the system so the system RDM does not significantly change in the interaction picture with respect to the system and bath Hamiltonians. Following this argument, we assume relation

$$\rho^{(I)}(t-\tau) \approx \rho^{(I)}(t) \tag{1.82}$$

known as the *Markov approximation* [May01]. In all orders of expansion, the Markov approximation can be used to transform the time non-local equation of motion into a certain time-local form. This has to be regarded as an additional approximation which simplifies the numerical treatment of the time non-local equations. Interestingly, in the second order the time-local equations and the time non-local equations with the Markov approximation have exactly the same form [Val13].

Under condition (1.82), the Eq. (1.79) simplifies to the ordinary differential equation

$$\begin{aligned}\frac{d}{dt}\rho^{(I)}(t) = -\frac{1}{\hbar^2}\sum_{i,j}\Big(&[K_j^{(I)}(t), U_S^\dagger(t)\int_0^{t-t_0} ds\ C_{ji}(s)K_i^{(I)}(-s)U_S(t)\rho^{(I)}(t)]_- \\ &- [K_j^{(I)}(t), \rho^{(I)}(t)U_S^\dagger(t)\int_0^{t-t_0} ds\ C_{ij}(-s)K_i^{(I)}(-s)U_S(t)]_-\Big)\end{aligned} \tag{1.83}$$

or in the Schrödinger picture

$$\begin{aligned}\frac{d}{dt}\rho(t) =& -\frac{i}{\hbar}[H_S, \rho(t)]_- \\ &-\frac{1}{\hbar^2}\sum_{i,j}\Big([K_j, \int_0^{t-t_0} ds\; C_{ji}(s)K_i^{(I)}(-s)\rho(t)]_- \\ &\qquad - [K_j, \rho(t)\int_0^{t-t_0} ds\; C_{ij}(-s)K_i^{(I)}(-s)]_-\Big)\;. \end{aligned} \tag{1.84}$$

We will refer to this equation of motion as to Time-Local Quantum Master Equation (TL-QME). The matrix structure of the last two lines on the right hand side defines a superoperator

$$\begin{aligned}\mathcal{R}(t)\bullet = -\frac{1}{\hbar^2}\sum_{i,j}\Big([K_j, \int_0^{t-t_0} ds\; C_{ji}(s)K_i^{(I)}(-s)\bullet]_- \\ - [K_j, \bullet\int_0^{t-t_0} ds\; C_{ij}(-s)K_i^{(I)}(-s)]_-\Big)\;, \end{aligned} \tag{1.85}$$

which we will call time-dependent Redfield tensor. The Eq. (1.84) then takes a form

$$\frac{d}{dt}\rho_{ab}(t) = \sum_{cd} -i\mathcal{L}_{abcd}\rho_{cd}(t) + \mathcal{R}_{abcd}(t)\rho_{cd}(t)\;. \tag{1.86}$$

The famous Redfield equation, originally derived for use in the nuclear magnetic resonance [Red65]), is obtained from the Eq. (1.86), if the time-dependent Redfield tensor is integrated to infinity,

$$\mathcal{R} = \lim_{t\to\infty}\mathcal{R}(t)\;. \tag{1.87}$$

The Redfield equation can then be written as

$$\frac{d}{dt}\rho_{ab}(t) = \sum_{cd} -i\mathcal{L}_{abcd}\rho_{cd}(t) + \mathcal{R}_{abcd}\rho_{cd}(t)\;. \tag{1.88}$$

The TL-QME is works well in the limit of weak system-bath coupling. For stronger SBC, it is known to break the positivity of the density matrix, which leads to negative probabilities and unphysical results.

1.7.5 Secular Approximation

Unlike the coherent electronic spectroscopy, which will be introduced in Chapter 2, most experiments are not sensitive to coherence between electronic levels. Even

the short time-scale experiments (e. g. pump probe) mostly focus on studying population dynamics and they do not require description of the coherences dynamics. This allows many further approximations to simplify the equations of motion. Most notably, the *secular approximation*, which decouples the RDM elements oscillating on different frequencies from each other and thus limits the energy transfer phenomena to separate dynamics of population transfer and coherence dephasing [May01].

Technically, the secular approximation is performed in the exciton basis, where the system Hamiltonian H_S is diagonal, by ignoring all terms of the $\mathcal{R}(t)$ in the Eq. (1.86) and $\mathcal{M}(t)$ in the Eq. (1.80) that couple populations to coherences and the coherences to each other. We refer to the resulting equations as to secular TL-QME and secular TNL-QME. Contrary, the models without the secular approximation are referred as full TL-QME and full TNL-QME.

The justification for the secular approximation is following: the system Liouville operator $\mathcal{L}$ leads to a dynamics in which the excitonic populations remain constant and the coherences oscillate with the transition frequency between the two energy levels to which the coherence belongs. In the limit of weak SBC, the relaxation dynamics caused by the time-dependent Redfield tensor $\mathcal{R}(t)$ is much slower than the oscillations caused by $\mathcal{L}$. All elements of $\mathcal{R}(t)$ containing such oscillations are suppressed by the integration of the quickly oscillating function. For example, if a population $p(t)$ is coupled with a coherence $c(t)$ via equation

$$\frac{d}{dt}p(t) = kc(t) \ , \tag{1.89}$$

where rate k is caused by the presence of the bath, and the coherence oscillates with the frequency ω corresponding to the energy-gap as

$$c(t) = c_0 \cos(\omega t + \varphi_0) \ , \tag{1.90}$$

the integrated effect of the coherence on the population will be

$$p(t) \approx \frac{kc_0}{\omega} \sin(\omega t + \varphi_0) \ . \tag{1.91}$$

We can see that the presence of the coherence causes population oscillations shifted in phase by $\pi/2$ with respect to the coherence and suppressed by the factor k/ω. Secular approximation assumes the ratio k/ω is small and that the effect of coherences to populations can be neglected.

Numerically, the secular approximation brings many advantages. Instead of the full Eq. (1.86), which has complexity comparable with the dimension of the system Liouville space ($O((\dim \mathscr{H}_S)^4)$), one gets equations with complexity comparable

to the rate equations between the populations ($O((\dim \mathscr{H}_S)^2)$). Furthermore, it can be shown that the long time equilibrium between the populations has form of the canonical equilibrium in the secular theories, provided the system is ergodic and only baths with one temperature are present [May01]. For these reasons, the secular approximation is a very common method of choice in spectroscopy, unless we are forced to choose more sophisticated methods.

CHAPTER

TWO

NON-LINEAR SPECTROSCOPY

2.1 Basic Framework

In the semi-classical approximation, the radiation field is described by the macroscopic Maxwell theory. The electric field intensity $\mathbf{E}(\mathbf{r}, t)$ inside a sample obeys the wave equation

$$\Delta\mathbf{E}(\mathbf{r}, t) - \frac{1}{c^2}\frac{\partial^2}{\partial t^2}\mathbf{E}(\mathbf{r}, t) = \mu_0 \frac{\partial^2}{\partial t^2}\mathbf{P}(\mathbf{r}, t) \ , \tag{2.1}$$

where the material effects of the sample are described by the polarization $\mathbf{P}(\mathbf{r}, t)$. The symbol μ_0 denotes the vacuum permeability and c denotes the speed of light. For now, we drop the position dependence. The polarization can be expanded into a Taylor series in orders of the electric field intensity

$$\mathbf{P}(t) = \mathbf{P}^{(1)}(t) + \mathbf{P}^{(2)}(t) + \mathbf{P}^{(3)}(t) + \dots \ . \tag{2.2}$$

The n-th order polarization $\mathbf{P}^{(n)}(t)$ is proportional to n-th order of the external electric field applied to the sample. The first order describes the linear absorption spectrum. Second order gives zero contribution in homogeneous samples [Muk95] and it is therefore not directly interesting for us, although the second order response is important in precise description of molecule excitation [Man10, Olš11]. The third order in the polarization expansion describes a host of interesting effects, such as Raman scattering, fluorescence[1] or the photon echo. It can be used to

[1]The reader might be surprised by including the fluorescence and the Raman scattering into third order of the expansion (2.2). Both fluorescence and Raman scattering are linear in the laser intensity! More precisely, the expansion (2.2) is not always given by the polarization dependence on the *external* electric field, but it is defined by the orders of the response function analogous to Eqs. (2.3a) and (2.3c). In the formalism of the non-linear spectroscopy developed by Mukamel, the fluorescence and the Raman scattering are described by two modes of the electric field: the external electric field in which the effects are quadratic (and hence linear in the laser intensity), and the virtual electric field composed of single photon leaving the sample in

completely characterize the pump-probe, the four-wave mixing or the coherent Raman scattering experiments. The relevant terms of the expansion (2.2) can be written using the response theory as

$$P_i^{(1)}(t) = \int_0^\infty dt_1\, S_{ij}^{(1)}(t_1) E_j(t-t_1)\ , \tag{2.3a}$$

$$P_i^{(2)}(t) = \int_0^\infty dt_2 \int_0^\infty dt_1\, S_{ijk}^{(2)}(t_2,t_1) E_j(t-t_2) E_k(t-t_2-t_1)\ , \tag{2.3b}$$

$$\begin{aligned} P_i^{(3)}(t) = &\int_0^\infty dt_3 \int_0^\infty dt_2 \int_0^\infty dt_1\, S_{ijkl}^{(3)}(t_3,t_2,t_1)\times \\ &E_j(t-t_3) E_k(t-t_3-t_2) E_l(t-t_3-t_2-t_1)\ , \end{aligned} \tag{2.3c}$$

where the $S_{ij}^{(1)}(t_1)$, $S_{ijk}^{(2)}(t_2,t_1)$ and $S_{ijkl}^{(3)}(t_3,t_2,t_1)$ are the first-, the second- and the third- order response functions (RF) of the polarization. The Einstein summation convention is applied.

To make a connection to the microscopic theory of the OQS, we employ the Liouville equation of the total system (1.53) in the interaction picture with respect to all parts of total Hamiltonian except of the system-radiation interaction (1.28)

$$\frac{d}{dt} W^{(I)}(t) = i\mathcal{V}^{(I)}(t) W^{(I)}(t) E(t)\ , \tag{2.4}$$

where

$$\mathcal{V}^{(I)}(t) = \mathcal{U}^\dagger(t-t_0)\mathcal{V}\mathcal{U}(t-t_0)\ , \tag{2.5a}$$

$$W^{(I)}(t) = \mathcal{U}^\dagger(t-t_0) W(t)\ . \tag{2.5b}$$

an arbitrary direction. Both effects belong to the third-order response function of polarization, which is also the reason why Raman scattering and fluorescence contain more information that the absorption spectrum. For more information, see Chapter 9 of [Muk95].

One can expand this equation into a perturbation series to obtain a formal solution

$$\begin{aligned} W^{(I)}(t) = W_0 &+ i \int_{t_0}^{t} dt_1 \, \mathcal{V}_i^{(I)}(t_1) W_0 E_i(t_1) \\ &- \int_{t_0}^{t} dt_1 \int_{t_0}^{t_1} dt_2 \, \mathcal{V}_i^{(I)}(t_1) \mathcal{V}_j^{(I)}(t_2) W_0 E_i(t_1) E_j(t_2) \\ &- i \int_{t_0}^{t} dt_1 \int_{t_0}^{t_1} dt_2 \int_{t_0}^{t_2} dt_3 \, \mathcal{V}_i^{(I)}(t_1) \mathcal{V}_j^{(I)}(t_2) \mathcal{V}_k^{(I)}(t_3) W_0 \\ &\times E_i(t_1) E_j(t_2) E_k(t_3) \ , \end{aligned} \tag{2.6}$$

with initial condition

$$W(t_0) = W^{(I)}(t_0) = W_0 \ . \tag{2.7}$$

We apply the Einstein summation convention over the indices i, j and k. We are interested in the mean value of polarization. The polarization is a macroscopic quantity that corresponds to a mean value of the polarization operator

$$\hat{P}_i = \sum_{j \in \text{molecules}} \delta(\mathbf{r} - \mathbf{r}_j) \mu_i^j \ , \tag{2.8}$$

$$P_i(t) = \text{Tr} \ \hat{P}_i W(t) \ . \tag{2.9}$$

Index i is a vector index and runs through values $i \in \{x, y, z\}$. If we employ substitutions

$$t_1 = t - \tau_1 \ , \tag{2.10a}$$

$$t_2 = t - \tau_1 - \tau_2 \ , \tag{2.10b}$$

$$t_3 = t - \tau_1 - \tau_2 - \tau_3 \tag{2.10c}$$

to the Eq. (2.6), use the assumption that the initial state of system is stationary, i. e.

$$\mathcal{U}(t) W_0 = W_0 \ , \tag{2.11}$$

and apply limit $t_0 \to -\infty$, we obtain

$$\begin{aligned} W(t) = W_0 &+ i \int_0^\infty d\tau_1 \mathcal{U}(\tau_1)\mathcal{V}_i W_0 E_i(t-\tau_1) \\ &- \int_0^\infty d\tau_1 \int_0^\infty d\tau_2 \mathcal{U}(\tau_1)\mathcal{V}_i\mathcal{U}(\tau_2)\mathcal{V}_j W_0 E_i(t-\tau_1)E_j(t-\tau_1-\tau_2) \\ &- i\int_0^\infty d\tau_1 \int_0^\infty d\tau_2 \int_0^\infty d\tau_3 \mathcal{U}(\tau_1)\mathcal{V}_i\mathcal{U}(\tau_2)\mathcal{V}_j\mathcal{U}(\tau_3)\mathcal{V}_k W_0 \\ &\qquad \times E_i(t-\tau_1)E_j(t-\tau_1-\tau_2)E_k(t-\tau_1-\tau_2-\tau_3)\ . \end{aligned} \tag{2.12}$$

If we plug this result into Eqs. (2.8), (2.9) and compare it with the definitions of the response functions (2.3), we see that we can calculate the RF from the formalism of the quantum theory as

$$S^{(1)}_{ij}(t_1) = i\theta(t_1)\mathrm{Tr}\left\{\mu_i \mathcal{U}(t_1)\mathcal{V}_j W_0\right\}\ , \tag{2.13a}$$

$$S^{(2)}_{ijk}(t_2,t_1) = i^2\theta(t_1)\theta(t_2)\ \mathrm{Tr}\left\{\mu_i \mathcal{U}(t_2)\mathcal{V}_j\mathcal{U}(t_1)\mathcal{V}_k W_0\right\}\ , \tag{2.13b}$$

$$S^{(3)}_{ijkl}(t_3,t_2,t_1) = i^3\theta(t_1)\theta(t_2)\theta(t_3)\ \mathrm{Tr}\left\{\mu_i \mathcal{U}(t_3)\mathcal{V}_j\mathcal{U}(t_2)\mathcal{V}_k\mathcal{U}(t_1)\mathcal{V}_l W_0\right\}\ . \tag{2.13c}$$

Here, $\theta(x)$ denotes the Heaviside step-function that has value 1 for positive values of x and value 0 for negative values of x. The response functions (2.13) are composed of many additive terms, the so-called Liouville pathways [Muk95]. Particularly for third-order response, it is convenient do define the so-called response operators

$$R_{1g}(t,T,\tau) = \mathrm{Tr}_B\{\mathcal{U}^{(egeg)}(t)\mathcal{V}^{(R)}_{(eg)}\mathcal{U}^{(eeee)}(T)\mathcal{V}^{(R)}_{(ge)}\mathcal{U}^{(egeg)}(\tau)\mathcal{V}^{(L)}_{(eg)}W_0\}\ , \tag{2.14a}$$

$$R_{2g}(t,T,\tau) = \mathrm{Tr}_B\{\mathcal{U}^{(egeg)}(t)\mathcal{V}^{(R)}_{(eg)}\mathcal{U}^{(eeee)}(T)\mathcal{V}^{(L)}_{(eg)}\mathcal{U}^{(gege)}(\tau)\mathcal{V}^{(R)}_{(ge)}W_0\}\ , \tag{2.14b}$$

$$R_{3g}(t,T,\tau) = \mathrm{Tr}_B\{\mathcal{U}^{(egeg)}(t)\mathcal{V}^{(L)}_{(eg)}\mathcal{U}^{(gggg)}(T)\mathcal{V}^{(R)}_{(eg)}\mathcal{U}^{(gege)}(\tau)\mathcal{V}^{(R)}_{(ge)}W_0\}\ , \tag{2.14c}$$

$$R_{4g}(t,T,\tau) = \mathrm{Tr}_B\{\mathcal{U}^{(egeg)}(t)\mathcal{V}^{(L)}_{(eg)}\mathcal{U}^{(gggg)}(T)\mathcal{V}^{(L)}_{(ge)}\mathcal{U}^{(egeg)}(\tau)\mathcal{V}^{(L)}_{(eg)}W_0\}\ , \tag{2.14d}$$

$$R_{1f}(t,T,\tau) = \mathrm{Tr}_B\{\mathcal{U}^{(efef)}(t)\mathcal{V}^{(R)}_{(ef)}\mathcal{U}^{(eeee)}(T)\mathcal{V}^{(R)}_{(ge)}\mathcal{U}^{(egeg)}(\tau)\mathcal{V}^{(L)}_{(eg)}W_0\}\ , \tag{2.14e}$$

$$R_{2f}(t,T,\tau) = \mathrm{Tr}_B\{\mathcal{U}^{(efef)}(t)\mathcal{V}^{(R)}_{(ef)}\mathcal{U}^{(eeee)}(T)\mathcal{V}^{(L)}_{(eg)}\mathcal{U}^{(gege)}(\tau)\mathcal{V}^{(R)}_{(ge)}W_0\} \tag{2.14f}$$

and their complex conjugates for the Liouville pathways. The response operators (2.14) have a tensor structure identical with the RF (2.13c). We omit it in further text for the sake of brevity.

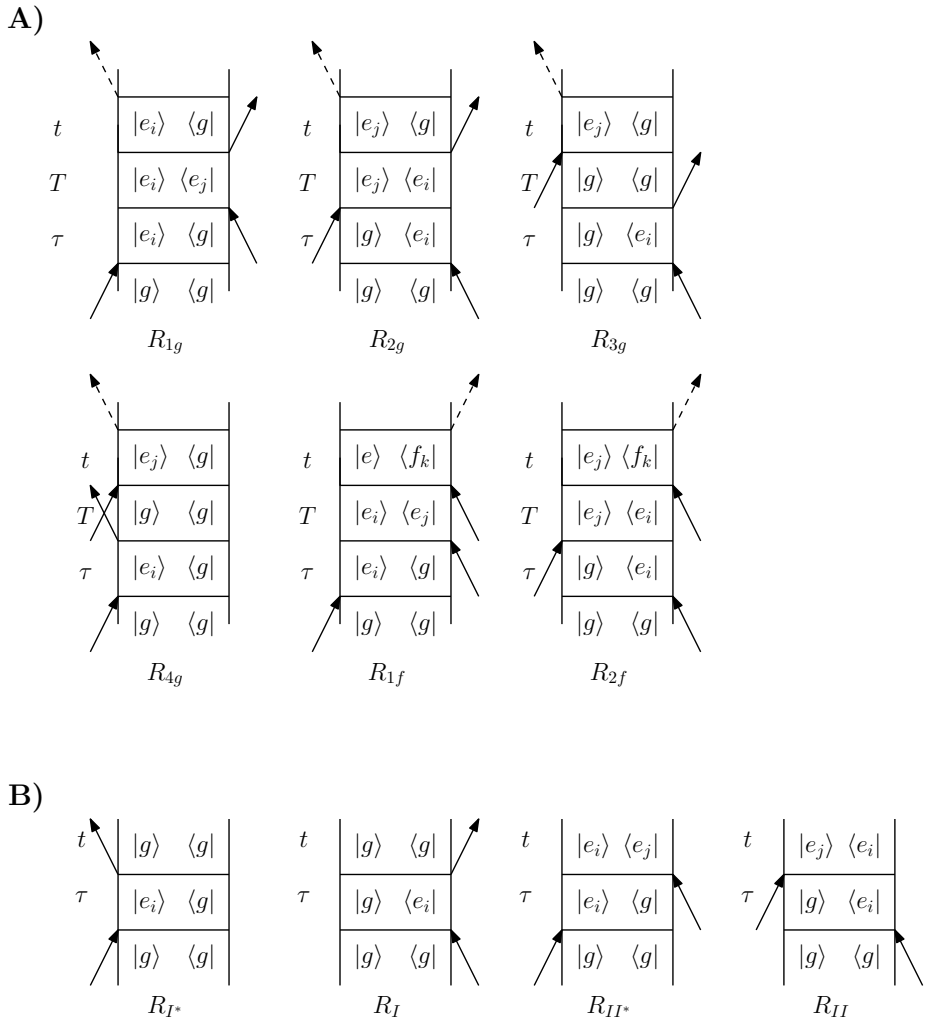

Figure 2.1: Double-sided Feynman diagrams representing the Liouville pathways A) of the third order response function (2.14) and B) of the second-order response operators (2.17).

The RF (2.13c) can then be written as

$$S^{(3)}(t,T,\tau) = i^3\theta(t_1)\theta(t_2)\theta(t_3)\sum_{i=1}^{4}(R_i(t,T,\tau) - R_i^*(t,T,\tau)) \,, \tag{2.15}$$

where

$$R_1(t,T,\tau) = \mathrm{Tr}\,(\mu_{(ge)}R_{1g}(t,T,\tau) - \mu_{(fe)}R_{1f}^\dagger(t,T,\tau)) \,, \tag{2.16a}$$
$$R_2(t,T,\tau) = \mathrm{Tr}\,(\mu_{(ge)}R_{2g}(t,T,\tau) - \mu_{(fe)}R_{2f}^\dagger(t,T,\tau)) \,, \tag{2.16b}$$
$$R_3(t,T,\tau) = \mathrm{Tr}\,\mu_{(ge)}R_{3g}(t,T,\tau) \,, \tag{2.16c}$$
$$R_4(t,T,\tau) = \mathrm{Tr}\,\mu_{(ge)}R_{4g}(t,T,\tau) \tag{2.16d}$$

are RFs of the non-linear signal according to the standard notation of [Muk95]. A diagrammatic graphical representation shown on the Fig. 2.1 is often used for

the terms (2.14). In the Chapter 4, we will be interested in a correct description of the correlations in the second interval of the RFs (2.3). For the second-order response (2.13b), we define quantities

$$R_I(t,\tau) = \mathrm{Tr}_B\{\mathcal{U}^{(gggg)}(t)\mathcal{V}^{(R)}_{(eg)}\mathcal{U}^{(gege)}(\tau)\mathcal{V}^{(R)}_{(ge)}W_0\}\ , \tag{2.17a}$$

$$R_{II}(t,\tau) = \mathrm{Tr}_B\{\mathcal{U}^{(eeee)}(t)\mathcal{V}^{(L)}_{(eg)}\mathcal{U}^{(gege)}(\tau)\mathcal{V}^{(R)}_{(ge)}W_0\}\ , \tag{2.17b}$$

similar to Eqs. (2.14) and their Hermite conjugates $R_{I^*} = R_I^\dagger$, $R_{II^*} = R_{II}^\dagger$.

2.2 Orientational Averaging

The total response functions (2.13) and the related response operators (2.14), (2.17) and functions (2.16) representing the Liouville pathways have a tensor structure in the real space originating from the dipole-moment operators μ_i. The orientations of the dipole moments depend on the orientation of the molecule. The measurements are performed in liquid phase in most cases, and an orientational averaging has to be taken. One possible approach is to calculate the reduced evolution superoperators (1.60) for all involved blocks of the RDM and to perform the tensor orientational averaging analytically [Dre03, Abr06]. All 2DES in this work are calculated by this method. Another commonly used approach is to directly average over an ensemble of molecules with different orientations, or by symmetric positioning of the different orientations of the molecules on the unit sphere to reduce the computational cost [Hei12].

2.3 Pump-Probe Experiments

The basic experiment of the ultra-fast non-linear spectroscopy is the pump-probe experiment. Two pulses are sent to the sample from different directions separated by time τ. The first pulse is called a *pump*. Its purpose is to excite the molecules in the sample and initiate their dynamics. The second pulse is called a *probe*, because it probes changes in the absorption caused by the pump pulse. The pump-probe spectrum $I^\tau_{PP}(\omega)$ is defined as a difference between the absorption at given frequency after time τ, $I^\tau(\omega)$, from the absorption spectrum without the pump-pulse $I(\omega)$

$$I^\tau_{PP}(\omega) = I^\tau(\omega) - I(\omega)\ . \tag{2.18}$$

The pump-probe experiment has, however, certain limitations. The most important is probably the trade-off between the time resolution and the frequency resolution. The frequency spectrum of the electric field is defined by its Fourier

transform as

$$E(\omega) = \int_{-\infty}^{\infty} dt\, e^{i\omega t} E(t) \; . \tag{2.19}$$

From the properties of the Fourier transformation follows that in order to get a good frequency resolution, long pulses have to be used, which decreases the time resolution. On the other hand, a good time resolution requires short pulses broad in frequency and we therefore lose the frequency resolution.

2.4 Four-Wave Mixing Experiments

The four-wave mixing experiment is a non-linear spectroscopic experiment that allows us to overcome limitations of the pump-probe experiment to achieve resolution either in time or in frequency, but not in both. It can unravel much information about the sample, for example reveal the homogeneous linewidth, which is often hidden by the inhomogeneous broadening. These properties will be demonstrated in the following two sections.

The experimental setup, illustrated on Fig. 2.2, is following: Three phase-locked very short laser pulses are sent into sample from different directions given by vectors $\mathbf{k}_1$, $\mathbf{k}_2$ and $\mathbf{k}_3$. They reach the sample at times t_1, t_2 and t_3 respectively. The resulting third order signal is directional and appears only in the so-called phase-matching directions [Muk95] given by linear combination $\pm\mathbf{k}_1 \pm \mathbf{k}_2 \pm \mathbf{k}_3$ of the directions of the incident pulses. We are particularly interested in the so-called photon echo effect, which appears in the signal propagating in the direction

$$\mathbf{k}_S = -\mathbf{k}_1 + \mathbf{k}_2 + \mathbf{k}_3 \; . \tag{2.20}$$

The signal is mixed with the so-called local oscillator pulse in direction $\mathbf{k}_{LO} = \mathbf{k}_S$. This is experimental technique known as the heterodyne detection. Since the measured intensity is given by the square of the electric field, for weak signal field $\mathbf{E}_S$, it is easier to measure the difference intensity $|\mathbf{E}_{LO}+\mathbf{E}_S|^2 - |\mathbf{E}_{LO}|^2 \approx 2\mathbf{E}_{LO}\cdot\mathbf{E}_S$ than directly the signal intensity $|\mathbf{E}_S|^2$. The known relative phase of the local oscillator is also necessary for the reconstruction of the phase of the other pulses.

The electric field can be written as

$$\begin{aligned} E_i(t) = {} & A_{1,i}(t+T+\tau)e^{i\mathbf{k}_1\cdot\mathbf{r}-i\Omega(t+T+\tau)} + c.c. \\ & + A_{2,i}(t+T)e^{i\mathbf{k}_2\cdot\mathbf{r}-i\Omega(t+T)} + c.c. \\ & + A_{3,i}(t)e^{i\mathbf{k}_3\cdot\mathbf{r}-i\Omega t} + c.c. \end{aligned} \tag{2.21}$$

where the Ω is the fast laser frequency, which for optical 2DES experiments on

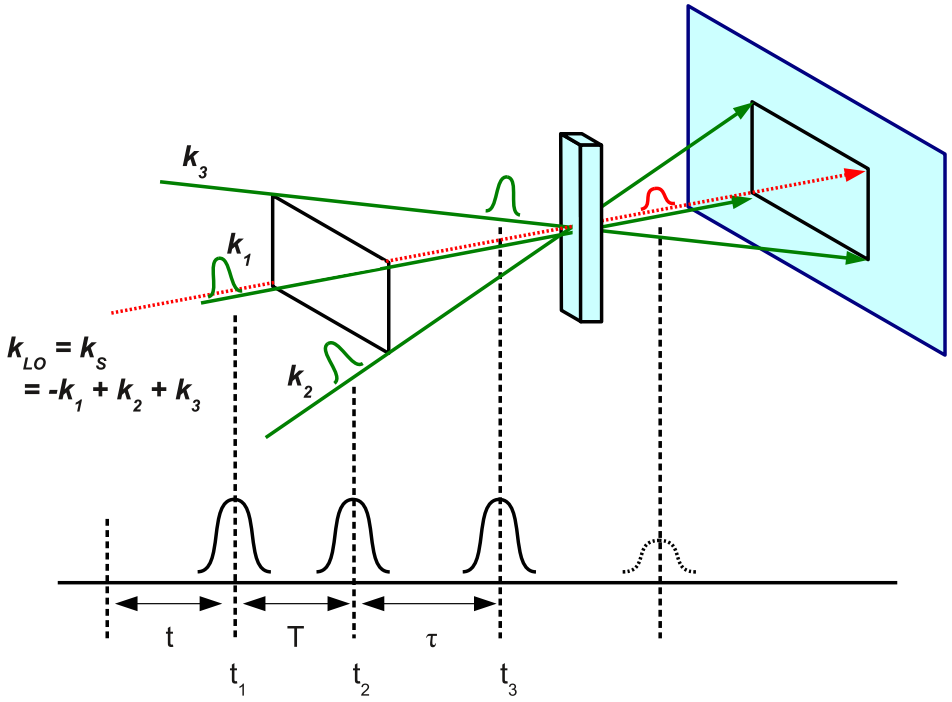

Figure 2.2: The experimental setup of four-wave mixing experiment. Three short phase-locked laser pulses are sent into the sample from different directions $\mathbf{k}_1$, $\mathbf{k}_2$ and $\mathbf{k}_3$ reaching the sample in times t_1, t_2 and t_3. The third-order signal is directed into the so-called phase-matching directions. The photon echo signal appears in the direction $\mathbf{k}_S = -\mathbf{k}_1 + \mathbf{k}_2 + \mathbf{k}_3$. The signal is mixed with the local oscillator pulse with known phase relation to the other pulses to gain advantages of the intensity enhancement via the heterodyne detection technique.

photosynthetic molecular aggregates typically has values between $10,000$ cm^{-1} and $20,000$ cm^{-1}. The functions $A_i(t)$ are slowly varying envelopes of the pulses centered around zero of their argument. The first ($\mathbf{k}_1$) and the second ($\mathbf{k}_2$) pulses are separated by time τ, while the second and the third ($\mathbf{k}_3$) pulses are separated by time T, which is often referred as a waiting time. Plugging the Eq. (2.21) into

the Eq. (2.3c) yields the following rather long expression

$$
\begin{aligned}
P_i^{(3)}(t) = \int_0^\infty dt_3 \int_0^\infty dt_2 \int_0^\infty dt_1 \, S_{ijkl}^{(3)}(t_3,t_2,t_1)\times \\
&(A_{1,j}^*(t+T+\tau-t_3)e^{-i\mathbf{k}_1\cdot\mathbf{r}+i\Omega(t+T+\tau-t_3)} \\
&\quad + A_{2,j}(t+T-t_3)e^{i\mathbf{k}_2\cdot\mathbf{r}-i\Omega(t+T-t_3)} \\
&\quad + A_{3,j}(t-t_3)e^{i\mathbf{k}_3\cdot\mathbf{r}-i\Omega(t-t_3)} + c.c.) \\
&(A_{1,k}^*(t+T+\tau-t_3-t_2)e^{-i\mathbf{k}_1\cdot\mathbf{r}+i\Omega(t+T+\tau-t_3-t_2)} \\
&\quad + A_{2,k}(t+T-t_3-t_2)e^{i\mathbf{k}_2\cdot\mathbf{r}-i\Omega(t+T-t_3-t_2)} \\
&\quad + A_{3,k}(t-t_3-t_2)e^{i\mathbf{k}_3\cdot\mathbf{r}-i\Omega(t-t_3-t_2)} + c.c.) \\
&(A_{1,l}^*(t+T+\tau-t_3-t_2-t_1)e^{-i\mathbf{k}_1\cdot\mathbf{r}+i\Omega(t+T+\tau-t_3-t_2-t_1)} \\
&\quad + A_{2,l}(t+T-t_3-t_2-t_1)e^{i\mathbf{k}_2\cdot\mathbf{r}-i\Omega(t+T-t_3-t_2-t_1)} \\
&\quad + A_{3,l}(t-t_3-t_2-t_1)e^{i\mathbf{k}_3\cdot\mathbf{r}-i\Omega(t-t_3-t_2-t_1)} + c.c.) \, .
\end{aligned}
\tag{2.22}
$$

If we collect only the terms that produce signal in the direction (2.20), we can construct the total polarization from three components that differ from each other by the frequency-dependent part under the integral (2.22),

$$
P_i^{(3)}(t) = P_{R,i}^{(3)}(t) + P_{NR,i}^{(3)}(t) + P_{DC,i}^{(3)}(t) \, . \tag{2.23}
$$

The part

$$
\begin{aligned}
P_{DC,i}^{(3)}(t) = \int_0^\infty dt_3 \int_0^\infty dt_2 \int_0^\infty dt_1 \, S_{ijkl}^{(3)}(t_3,t_2,t_1)e^{i(-\mathbf{k}_1+\mathbf{k}_2+\mathbf{k}_3)\cdot\mathbf{r}}\times \\
&\Big(A_{1,j}^*(t+T+\tau-t_3)A_{2,k}(t+T-t_3-t_2)A_{3,l}(t-t_3-t_2-t_1) \\
&+ A_{1,j}^*(t+T+\tau-t_3)A_{2,k}(t+T-t_3-t_2-t_1)A_{3,l}(t-t_3-t_2) \\
&+ c.c.\Big)e^{i\Omega(\tau-t+t_3+2t_2+t_1)}
\end{aligned}
\tag{2.24}
$$

is called double coherence. It contributes to the experimentally relevant polarization that produces the signal in the direction (2.20) only if the laser pulses overlap, i. e. for $T \approx 0$. Since the pulses are usually very short, it is not necessary to

include it into the theoretical description. The remaining two parts, the rephasing

$$P^{(3)}_{R,i}(t) = \int_0^\infty dt_3 \int_0^\infty dt_2 \int_0^\infty dt_1 \, S^{(3)}_{ijkl}(t_3,t_2,t_1) e^{i(-\mathbf{k}_1+\mathbf{k}_2+\mathbf{k}_3)\cdot\mathbf{r}} \times \\ + A^*_{1,j}(t+T+\tau-t_3-t_2-t_1) A_{2,k}(t+T-t_3) A_{3,l}(t-t_3-t_2) \\ + A^*_{1,j}(t+T+\tau-t_3-t_2-t_1) A_{2,k}(t+T-t_3-t_2) A_{3,l}(t-t_3) \\ + c.c.\Big) e^{i\Omega(\tau-t+t_3-t_1)} \, . \tag{2.25}$$

and the non-rephasing

$$P^{(3)}_{NR,i}(t) = \int_0^\infty dt_3 \int_0^\infty dt_2 \int_0^\infty dt_1 \, S^{(3)}_{ijkl}(t_3,t_2,t_1) e^{i(-\mathbf{k}_1+\mathbf{k}_2+\mathbf{k}_3)\cdot\mathbf{r}} \times \\ + A^*_{1,j}(t+T+\tau-t_3-t_2) A_{2,k}(t+T-t_3) A_{3,l}(t-t_3-t_2-t_1) \\ + A^*_{1,j}(t+T+\tau-t_3-t_2) A_{2,k}(t+T-t_3-t_2-t_1) A_{3,l}(t-t_3) \\ + c.c.\Big) e^{i\Omega(\tau-t+t_3+t_1)} \, . \tag{2.26}$$

both contribute to the signal. Since the pulses envelope functions $A_i(t)$ are all zero if their argument is far from zero and since the third-order RF $S^{(3)}_{ijkl}(t_3,t_2,t_1)$ is non-zero only if all of its arguments are positive, we obtain a set of inequalities that have to be satisfied for the signal to be non-zero. The rephasing part of the signal is non-zero only if $\tau > 0$, while the non-rephasing part of the signal is non-zero only for $\tau < 0$. This corresponds to two different experimental arrangements with different orderings of the first and second pulses. As a result, the rephasing and the non-rephasing parts can be measured separately.

2.5 Two-Dimensional Electronic Spectrum

The measured electric field $E_S(t,T,\tau)$ in the direction $\mathbf{k}_S$ depends on times t, T and τ. If we assume a simple box geometry of the (thin) sample, it can be shown that the measured field is connected with the polarization induced in the sample by relation [Val13]

$$E_{S,i}(t,T,\tau) \approx i\frac{h\Omega}{n(\Omega)\varepsilon_0 c} P^{(3)}_i(t,T,\tau) \, , \tag{2.27}$$

where h is the sample thickness, $n(\Omega)$ is the sample refractive index and ε_0 is the vacuum permittivity. From this relation follows that in the limit of ultrashort pulses, the measured electric field is proportional to the third-order response

function[2]

$$E_S(t,T,\tau) \sim iS^{(3)}(t,T,\tau)\ .$$

Experimentally, the so-called two-dimensional electronic spectrum

$$\Xi(\omega_t,T,\omega_\tau) = \int_{-\infty}^{\infty} dt \int_{-\infty}^{\infty} d\tau\ E_S(t,T,\tau)e^{i\omega_t t - i\omega_\tau \tau} \tag{2.28}$$

is constructed from the measured field [Jon03, Bri04a]. It serves as a direct visualization of the third-order non-linear response function. Since the response-function oscillates with the optical frequency in its first and third interval, the Fourier transform is performed over these times. The Fourier transform in τ yields an ω_τ dependence that is formally similar to linear absorption spectrum, while the Fourier transform in t yields generalized absorption and stimulated emission from a non-equilibrium state created by the first two laser pulses. As can be shown by proper mathematical analysis [Man13b], the real part of the 2D spectrum (2.28) can be interpreted as a correlation plot between the system absorption spectrum $I(\omega_\tau)$ and the absorption spectrum $I^T(\omega_t)$ after time T from the excitation. The imaginary part represents correlation between the system absorption spectrum and the dispersion after time T and it is rarely used for practical analysis. The Liouville pathways (2.14) contributing to the 2D spectrum can be interpreted in the following way: In the trajectories R_{1g} and R_{2g}, the molecule is in its excited state during the waiting time T and they thus represents a stimulated emission (SE). Unlike in the pump-probe spectrum, these trajectories have positive sign in the most commonly used convention. The trajectories R_{3g} and R_{4g} also have a positive sign and the molecule is in the ground state during the waiting time T. They can therefore be interpreted as the ground state bleach (GSB). The trajectories $R_{1f}^\dagger$ and $R_{2f}^\dagger$ contribute to the 2DES conjugated, which results in negative sign of the generated signal. They represent an excited state absorption (ESA).

We illustrate some of the properties of the 2DES spectrum on an excitonic molecular dimer with transition energies $e_1 = 14,000$ cm^{-1} and $e_2 = 16,000$ cm^{-1}, and with equal parallel transition dipole moments. The bath is described by the EGCF (1.47) with reorganization energy $\lambda = 250$ cm^{-1}, coherence time $\tau_c = 100$ fs and temperature $T_B = 300$ K. Fig. 2.3 presents a 2DES of the dimer in case no interaction between the two molecules is present ($J = 0$ cm^{-1}) in waiting times $T = 0$ ps and $T = 10$ ps. The only visible features in the spectrum are

[2]More precisely, the three unpaired tensor indices of $S^{(3)}_{ijkl}(t,T,\tau)$ are taken away by dot-products with unit polarization vectors of the laser pulses according to the same scheme as in Eq. (2.22).

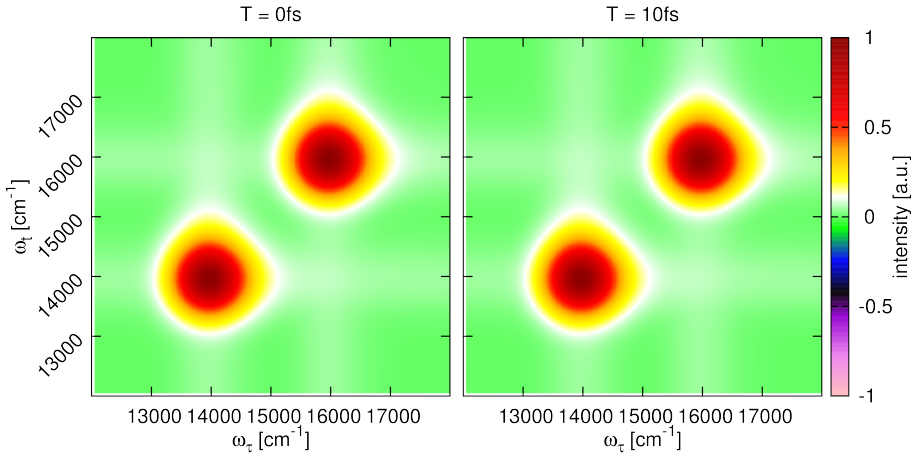

Figure 2.3: Total 2D electronic spectrum of a non-interacting dimer with energies $e_1 = 14,000$ cm^{-1} and $e_2 = 16,000$ cm^{-1}, and with equal parallel transition dipole moments. The bath is described by the EGCF (1.47) with parameters $\lambda = 250$ cm^{-1}, $\tau_c = 100$ fs and $T_B = 300$ K. Spectrum is plotted for waiting times $T = 0$ ps and $T = 40$ ps.

two diagonal peaks on the transition frequencies. The diagonal of the 2DES can be interpreted as a square of an absorption spectrum. The absence of off-diagonal features, the so-called cross-peaks, is result of cancellation between the excited state absorption pathways on one hand and the ground state bleach and stimulated emission pathways on the other hand. Reason behind this cancellation is the perfect symmetry between transitions $|g\rangle \rightarrow |e_1\rangle$ and $|e_2\rangle \rightarrow |f_{12}\rangle$ that both represent excitation of the first molecule and between transitions $|g\rangle \rightarrow |e_2\rangle$ and $|e_2\rangle \rightarrow |f_{12}\rangle$ with the same symmetry, representing the excitation of the second molecule. Contributions of the individual pathways is shown on Fig. 2.4. According to the model of photosynthetic molecular aggregates, described in Section 1.2, we assume there is no relaxation to the ground state. In absence of relaxation and coupling, the peaks do not disappear with increasing waiting time T and the 2DES has no dynamics.

The same dimer with resonance coupling $J = 200$ cm^{-1} between the states already manifests cross-peaks in the 2DES, as shown on Fig. 2.5. The excitonic mixing of states $|e_1\rangle$ and $|e_2\rangle$, originally with equal transition dipole moments, leads to enhancement of the transient dipole moment of one state and decrease of the other. This makes the analysis less clear and it is not practical for this demonstration. We compensate this effect by setting $\langle g|\mu|e_1\rangle = 1.22\langle g|\mu|e_2\rangle$ so that the excitonic transient dipole moments are equal. Cross-peaks appearing at $T = 0$ ps are a signature of excitonic origin of the observed excited states[3].

[3]The coherence between the vibrational states of weakly-coupled electronic states would manifest as a cross-peak only in later T.

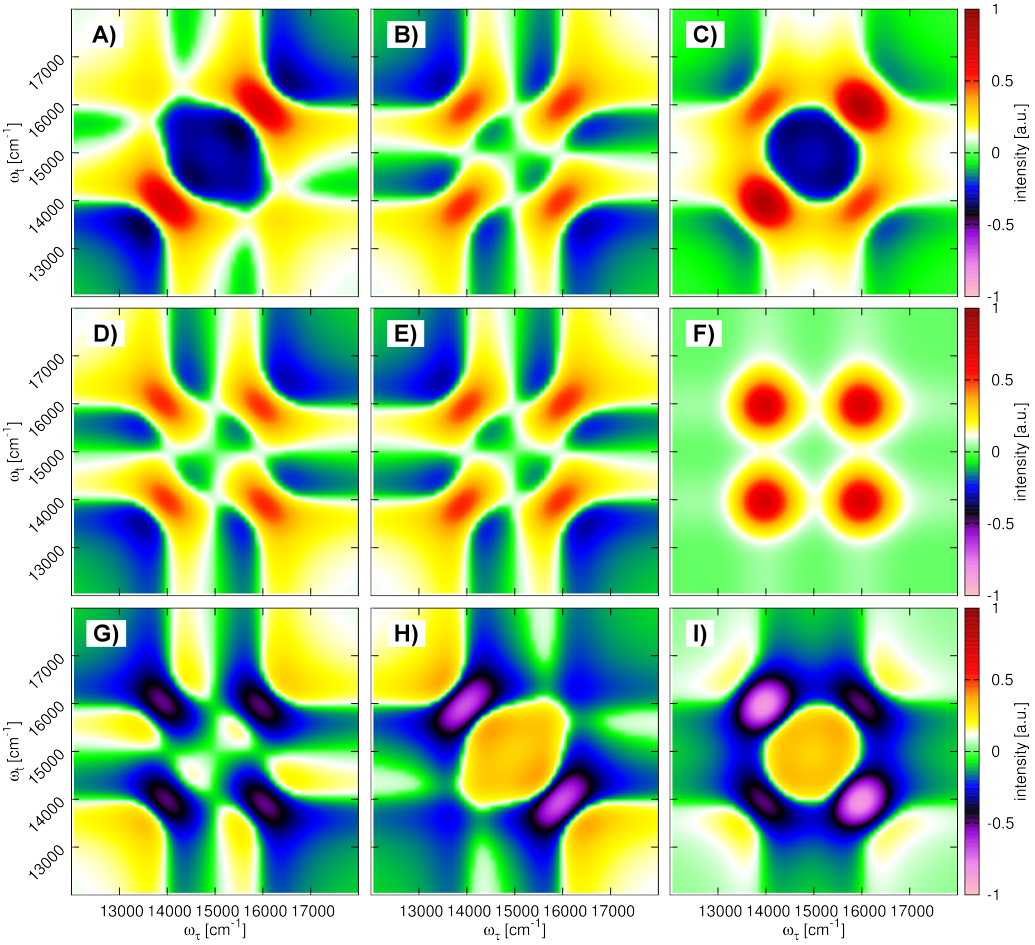

Figure 2.4: 2D electronic spectra in $T = 0$ ps resulting from individual Liouville pathways (2.14). The system investigated is a non-interacting dimer with energies $e_1 = 14,000$ cm^{-1} and $e_1 = 16,000$ cm^{-1}, and with parallel transition dipole moments equal in the excitonic basis. The bath is described by the EGCF (1.47) with parameters $\lambda = 250$ cm^{-1}, $\tau_c = 100$ fs and $T_B = 300$ K. The subfigures A), B), D), E), G) and H) represent pathways R_{1g}, R_{2g}, R_{4g}, R_{3g}, $R^{\dagger}_{1f}$ and $R^{\dagger}_{2f}$ respectively. In this arrangement, the rephasing trajectories are in the middle column, while the non-rephasing ones are in the left column. The subfigures C), F) and I) in the right column represent sum of the two spectra on the left. Unlike the individual pathways, they do have direct physical interpretation of total stimulated emission, ground state bleach and excited state absorption respectively.

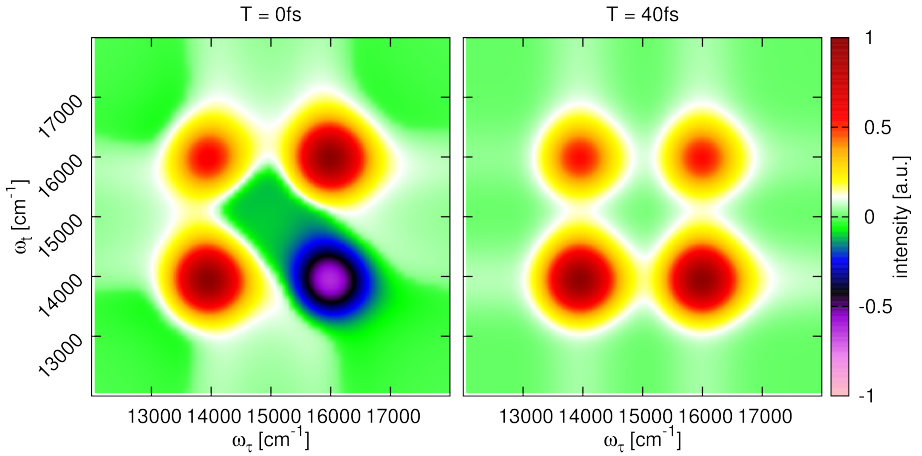

Figure 2.5: Total 2D electronic spectrum of a dimer with energies $e_1 = 14,000$ cm^{-1} and $e_2 = 16,000$ cm^{-1}, with resonance coupling $J = 200$ cm^{-1} and with equal parallel transition dipole moments. The bath is described by the EGCF (1.47) with parameters $\lambda = 500$ cm^{-1}, $\tau_c = 100$ fs and $T_B = 300$ K. Spectrum is plotted for waiting times $T = 0$ ps and $T = 40$ ps.

They emerge because the aforementioned symmetry between the transitions from ground state to the block of single excited states and from the block of single excited states to the block of double-excited states, is broken. Contribution of the individual pathways at $T = 0$ ps is shown on Fig. 2.6. The main difference from the non-interacting case, Fig. 2.4, is in the ESA pathway. It differs, because while the excitonic dipole moments of transitions from the ground state are equal, the dipole moments of transitions to the double-excited states are different. The 2D cross-peaks oscillate in T as long as the corresponding electronic coherence elements of the reduced density matrix are oscillating. The peak is elongated along the diagonal or the anti-diagonal in different phases of the oscillation and its shape is similar the shape of peaks in spectra of the the rephasing and non-rephasing pathways. (Figs. 2.4, 2.6 and 2.7.) The lifetime of the electronic coherences can thus be estimated directly from the T dependent sequence of 2D spectra [Pis06, Eng07]. More detailed analysis of the electronic-coherence related cross-peak oscillations can be found in the Chapter 3, particularly on Fig. 3.7.

During the time evolution, ESA and SE pathways rearrange according to the relaxation between the excitonic states. Once the electronic coherence is dephased, the peaks in the total ESA, GSB and SE spectra become round-shaped. On Fig. 2.7, the 2DES corresponding to different pathways are plotted for time $T = 40$ ps. (The total spectrum is on Fig. 2.5.) In this time, the system already reached the canonical thermal equilibrium between the excited states. The energy difference between the excited levels is chosen high here, and the upper excited state is consequently almost entirely depopulated. During the depopulation, the

ESA peaks shift towards the higher frequency and the SE peaks shift towards the lower frequency. The GSB does not change with T, since the single ground state in the GSM provides no dynamics. In presence of relaxation to the ground state, contributions from all pathways would gradually vanish.

In the experiment, the static disorder in transition energies often plays an important role. The disorder shifts the transition peaks along the 2DES diagonal. As a result, the observed peaks are elongated along the diagonal, but keep their homogeneous linewidth in the anti-diagonal direction. This is one of the important advantages the 2D electronic spectra have over the pump-probe experiment.

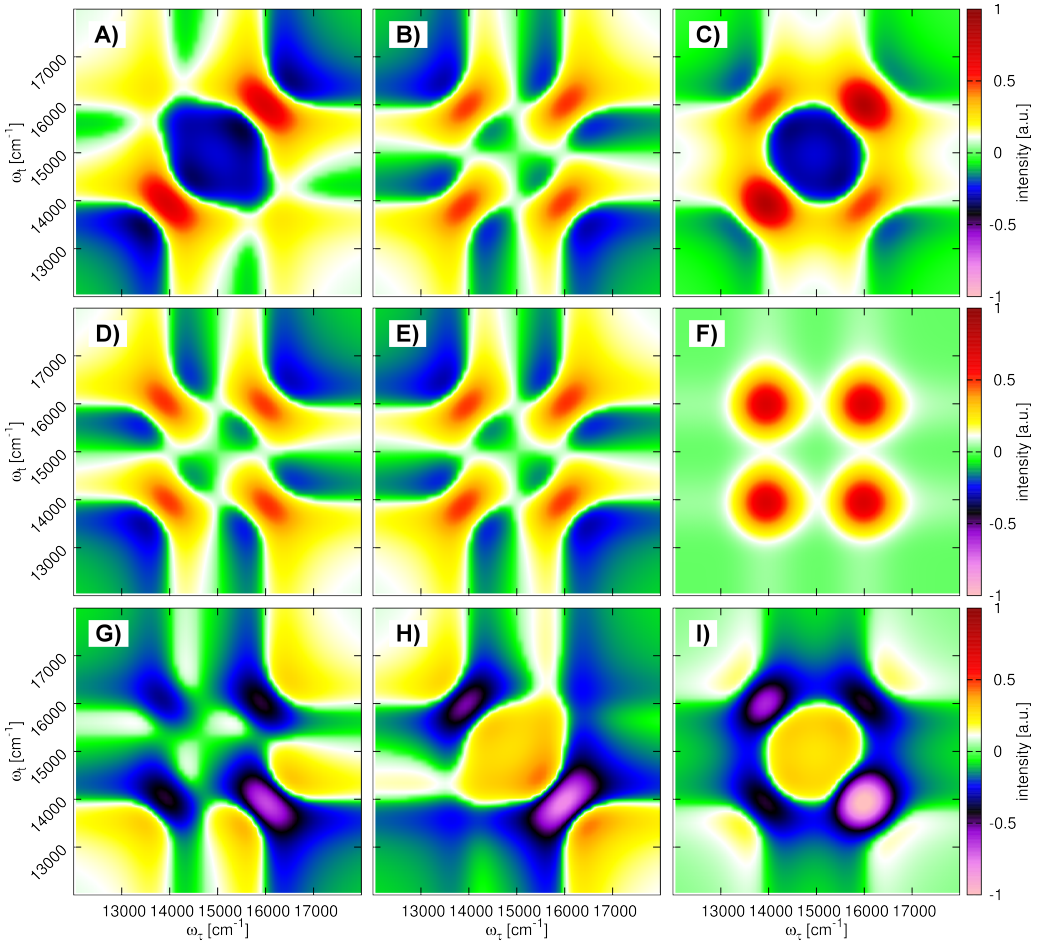

Figure 2.6: 2D electronic spectra in $T = 0$ ps resulting from individual Liouville pathways (2.14). The system investigated is a dimer with energies $e_1 = 14,000$ cm^{-1} and $e_1 = 16,000$ cm^{-1}, with resonance coupling $J = 200$ cm^{-1} and with parallel transition dipole moments equal in the excitonic basis. The bath is described by the EGCF (1.47) with parameters $\lambda = 250$ cm^{-1}, $\tau_c = 100$ fs and $T_B = 300$ K. The subfigures A), B), D), E), G) and H) represent pathways R_{1g}, R_{2g}, R_{4g}, R_{3g}, $R^{\dagger}_{1f}$ and $R^{\dagger}_{2f}$ respectively. In this arrangement, the rephasing trajectories are in the middle column, while the non-rephasing ones are in the left column. The subfigures C), F) and I) in the right column represent sum of the two spectra on the left. Unlike the individual pathways, they do have direct physical interpretation of total stimulated emission, ground state bleach and excited state absorption respectively.

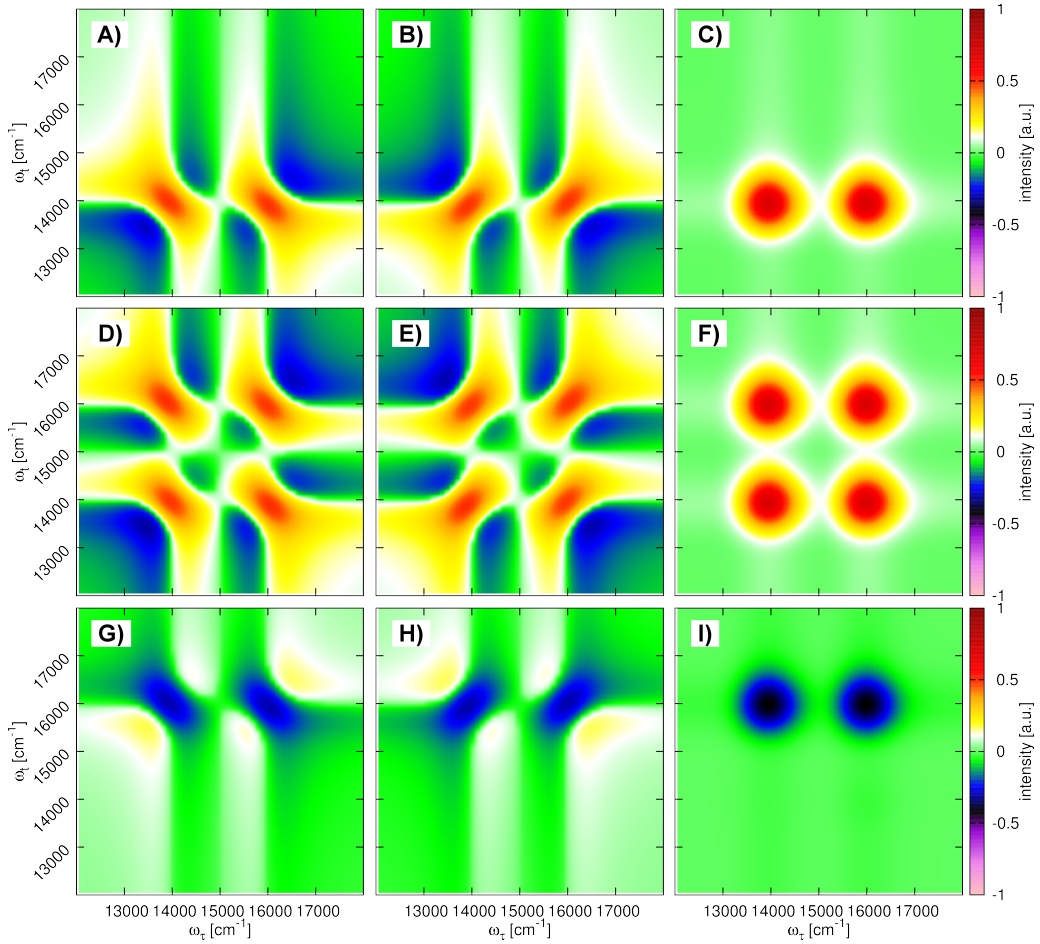

Figure 2.7: 2D electronic spectra in $T = 40$ ps resulting from individual Liouville pathways (2.14). The system investigated is a dimer with energies $e_1 = 14,000$ cm^{-1} and $e_1 = 16,000$ cm^{-1}, with resonance coupling $J = 200$ cm^{-1} and with parallel transition dipole moments equal in the excitonic basis. The bath is described by the EGCF (1.47) with parameters $\lambda = 250$ cm^{-1}, $\tau_c = 100$ fs and $T_B = 300$ K. The subfigures A), B), D), E), G) and H) represent pathways R_{1g}, R_{2g}, R_{4g}, R_{3g}, $R^{\dagger}_{1f}$ and $R^{\dagger}_{2f}$ respectively. In this arrangement, the rephasing trajectories are in the middle column, while the non-rephasing ones are in the left column. The subfigures C), F) and I) in the right column represent sum of the two spectra on the left. Unlike the individual pathways, they do have direct physical interpretation of total stimulated emission, ground state bleach and excited state absorption respectively.

CHAPTER

THREE

STUDY OF NON-SECULAR EFFECTS

In the reduced density matrix formalism, there are several general approaches that can be used to derive equations of motion of second or higher order in the system-bath coupling that describe the dissipative dynamics of open quantum systems. Direct application of the Nakajima-Zwanzig identity is one such approach developed long ago [Nak58, Zwa60]. Equations of motion resulting from direct application of this scheme are characterized by the presence of time retarded terms responsible for energy relaxation and decoherence processes. Equations of this type, derived in the Section 1.7.3, are denoted as *time non-local*. Later, an alternative approach to the derivation of the RDM equations of motion has emerged which yields *time local* equation of motion [Has77, Shi77]. Both theories express the terms responsible for the dissipative dynamics in form of an infinite series in terms of the system-bath interaction Hamiltonian, but differ in time ordering prescriptions for the cumulant expansion of the evolution operator (see Section 5.1.2). The time local equations correspond to the so-called partial time ordering prescription of the cumulant expansion, while the time non-local equations result from the so-called chronological time ordering [Muk78, Muk79]. Although the two schemes yield formally different equations of motion for the RDM, they are in fact equivalent as long as the complete summation of the corresponding infinite series is performed. When the infinite series are truncated at a finite order, the two theories yield equations that predict different RDM dynamics. This is a result of different statistical assumptions about the bath that are implicitly made in the two cases [Muk78, Muk79]. In all orders of expansion, the so-called *Markov approximation* can be used to transform the time non-local equation of motion into a certain time-local form. This has to be regarded as an additional approximation which simplifies the numerical treatment of the time non-local equations. Interestingly, in the second order the time-local equations and the time

non-local equations with the Markov approximation, derived in the Section 1.7.4, have exactly the same form [Val13].

Until recently, most experiments were not sensitive to coherence between electronic levels. This allowed a host of further approximations to simplify equations of motion. Most notably the *secular approximation* discussed in Section 1.7.5, which amounts to decoupling RDM elements oscillating on different frequencies from each other and thus limits the energy transfer phenomena to separate dynamics of population transfer and coherence dephasing [May01]. Even on very short times scale, experiments aimed at studying population dynamics (pump probe) are not sensitive enough to coherence between electronic levels to require non-secular theory, although it was suggested that measured relaxation time can be distorted by non-secular effects [Bar99]. Consequently, most of the theory developed for evaluation of experiments focuses on improving calculation of the relaxation rates [Zha98, Yan02, Jan04]. With experiments now uncovering new details about the role of electronic coherence, theoretical methods beyond rate equations for probabilities which are both accurate and numerically tractable are required. Although schemes for constructing equations of motion for the RDM beyond second order, like the hierarchical equations of motion [Tan89, Ish05, Tan09], seem feasible and promising [Ish09a, Ish09b, Hei12], second order theories might still be the only option for treatment of extended molecular systems. It was suggested previously that second order perturbation theory with respect to system-bath coupling provides a suitable framework for development of such methods [Man08]. This notion is also supported by the fact that in the special case of the so-called spin-boson model, second order time-local equation of motion already represents an exact equation of motion for the RDM [Dol08].

In this chapter based on the article [Olš10], we study the following four different second order theories: (a) full TNL-QME, Eq. (1.79), resulting from the Nakajima-Zwanzig identity or equivalently from the chronological ordering prescription in the cumulant expansion, (b) the full TL-QME, Eq. (1.84), resulting from the partial ordering prescription in the cumulant expansion, or equivalently from Markov approximation applied to TNL-QME, (c) time non-local equation with secular approximation (secular TNL-QME), and (d) time local equation with secular approximation (secular TL-QME). We discuss the applicability of these equations to the description of the energy relaxation and decoherence dynamics in small systems of molecular excitons. We emphasize the recent 2D spectroscopic experiments, the dynamics of coherence between electronic excited states and the lifetime of the electronic coherence, which is very relevant to the discussion about the coherent dynamics of the FMO pigment-protein complex and related photosynthetic systems. Note that, in this section, *full* refers to the equations

n	$\frac{\epsilon_n}{cm^{-1}}$	$\frac{d_{n,x}}{\lvert d_n \rvert}$	$\frac{d_{n,y}}{\lvert d_n \rvert}$	$\frac{d_{n,z}}{\lvert d_n \rvert}$	$\frac{\lvert d_n \rvert}{d_0}$	h_n	$\frac{\alpha_n}{grad}$
1	9850	1	0	0	0.65	0	0
2	10000	−0.94	0.34	0	2.15	10	60
3	10150	−0.94	0.34	0	0.9	10	120

Table 3.1: Parameters of the model trimer. The parameter ϵ_n represents the transition energy of n-th monomer, transition dipole moments $\boldsymbol{d}_n$ are taken relative to some value d_0. Parameters h_n and α_n are explained on Fig. 3.1.

where no secular approximation has been applied. These equations are still of second order of perturbation theory.

3.1 Calculation on a Trimer

In this chapter, we study dynamics of a model aggregate viewed via population and coherence dynamics and via 2D coherent spectrum. We define a simple model aggregate for which we calculate excited state dynamics including evolution of coherences between electronic states, linear absorption and 2D spectra at chosen population times. Calculations of linear absorption, which require only knowledge of the time evolution of optical coherences, are performed using all four methods and the results are compared. The dynamics of the optical coherences in the 2DES spectra calculations use the secular time local QME, since it is known to yield exact result at least for some models [Dol08] and since the time-nonlocal theories lead to certain artifacts when applied on optical coherences dynamics calculation. The population dynamics is calculated using all four methods we discussed in the Section 1.7, and the results are compared.

The simplest model of an aggregate that can exhibit all effects observed in Ref. [Eng07] is a trimer. The geometry of the models, together with the meaning of the parameters is presented in Fig. 3.1. In Tab. 3.1 we summarize the main parameters of the model. Parameters J, h and d_0 from Tab. 3.1 are not independent. For given h_n and $\boldsymbol{d}_n$ we could in principle calculate the value of resonance coupling J. Because we are not interested in the absolute amplitude of the absorption or 2D spectra we assume d_0 to be fixed by the values of h_n and $\boldsymbol{d}_n$ to yield the expected value of J. All three resonance couplings J between the molecules are set to $J = 200$ cm^{-1} for the calculations presented here. The values of the transition dipole moments determine the initial condition for the population dynamics. We assume that the excitation light intensity and the value of the transition dipole moment are such that the system is only weakly excited. The total population of the excited state band is normalized to 0.01. The relative values of the transition dipole moments are chosen so that the linear

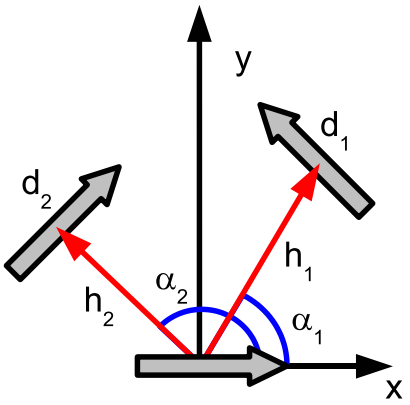

Figure 3.1: Geometry and parameters of a trimer aggregate. One monomer is chosen to be positioned at the origin of the coordinate system, with the transition dipole moment pointing along the x axis. The positions the transition dipole moments of the other two molecules in space are characterized by their distance h_2 and h_3 from the origin of coordinates and by the angles α_2 and α_3. Orientations and lengths of the dipoles are given in Tab. 3.1. In our example we assume that the aggregate is planar.

absorption spectrum (see Fig. 3.2) shows peaks of roughly the same height. Two peaks originating from the energetically lowest and the energetically highest states dominate the spectrum, the third level contributes as a shoulder to lowest energy peak.

Two parameters that influence the coupling of the model system to the bath are reorganization energy λ and correlation time τ_c. We vary these parameters in the range that can conceivably represent chlorophylls in photosynthetic complexes (see e. g. Refs. [Zig06, Cho05]).

3.2 Population Relaxation and Evolution of Coherences

First, we compare relaxation dynamics of populations of excited state of our aggregate after excitation by an ultrashort laser pulse. TL-QME was solved by standard numerical methods for ordinary differential equations provided by the Mathematica® software. For the TNL-QME we used fast Fourier transform method. Figure 3.3 presents the first 1 ps of the population dynamics after a $\delta-$pulse excitation (1.29) of the trimer from Tab. 3.1 at the temperature $T_B = 300$ K. Reorganization energy $\lambda = 120$ cm^{-1} and correlation time $\tau_c = 50$ fs are the same at all three monomers. The dynamics with the same parameters for a selected coherence element $\rho_{13}(t)$ is presented in Fig. 3.4. The overall conclusion is that all four methods yield a similar general behavior for the populations, with

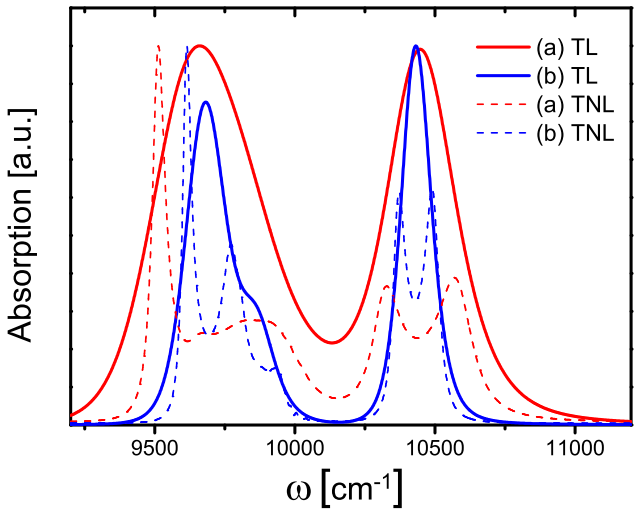

Figure 3.2: Linear absorption spectrum of the model trimer for various parameters of the system bath interaction: (a) $\lambda = 120$ cm^{-1}, $\tau_c = 50$ fs, (b) $\lambda = 30$ cm^{-1}, $\tau_c = 100$ fs, calculated by the secular TL-QME (full lines) and the secular TNL-QME (dashed lines).

some difference at the short time evolution and also slightly different long time equilibrium. Examination of the Figure 3.4 leads us to the conclusion that the methods yield two different results - a short coherence lifetime for the time local methods, and a relatively longer lifetime in case of the time non-local methods. The behavior of the coherence $\rho_{13}(t)$ represents a general tendency that we have observed for all electronic coherences over a wide range of parameters.

Let us now concentrate on short time behavior of the populations and coherences in more detail. In the short time evolution of the coherences the four methods form two distinct groups with short (TL methods) and long (TNL methods) coherence lifetime. Whether the underlying equation is secular or not seems to have only a little influence on the coherence dynamics. Fig. 3.5 shows the short time $(0 - 400$ fs) comparison of the population calculated by the four equations of motion. We can clearly see that the results can be naturally grouped according to the presence of fast oscillatory modulation of the population relaxation dynamics. In the one group we have the full TL and full TNL methods, where such oscillations clearly occur, the second group comprises the two secular methods with no oscillations present. Thus, it can be concluded that the non-secular terms in the equations of motion are the cause of these oscillations. This is also supported by comparison of the population dynamics of the full TL-QME and the full TNL-QME from Fig. 3.3 (e. g. the population of the state 1). The oscillation on the full TNL curve last longer than those of the full TL one, which reflects the longer coherence lifetime we have found for the TNL equations.

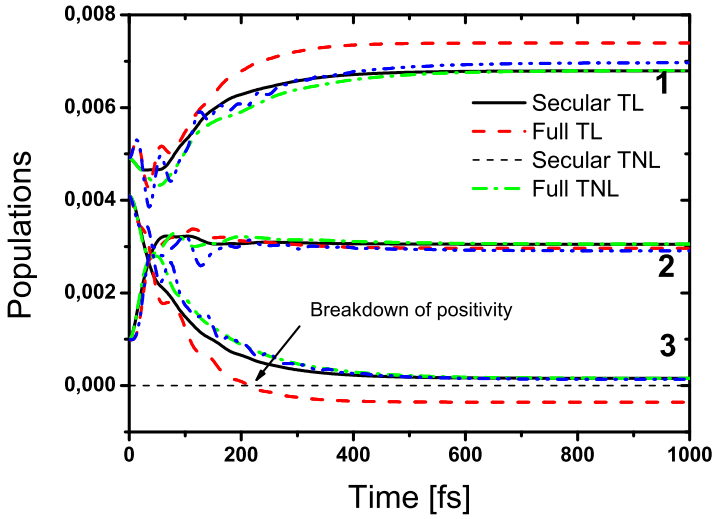

Figure 3.3: First 1000 fs of the excited state population dynamics of a trimer with parameters $\lambda = 120$ cm^{-1}, $\tau_c = 50$ fs, calculated by all four methods. For these particular parameters, the full TL-QME breaks positivity of the RDM diagonal elements after 200 fs. Its prediction for the populations of the lowest and highest levels is significantly different from the other three methods.

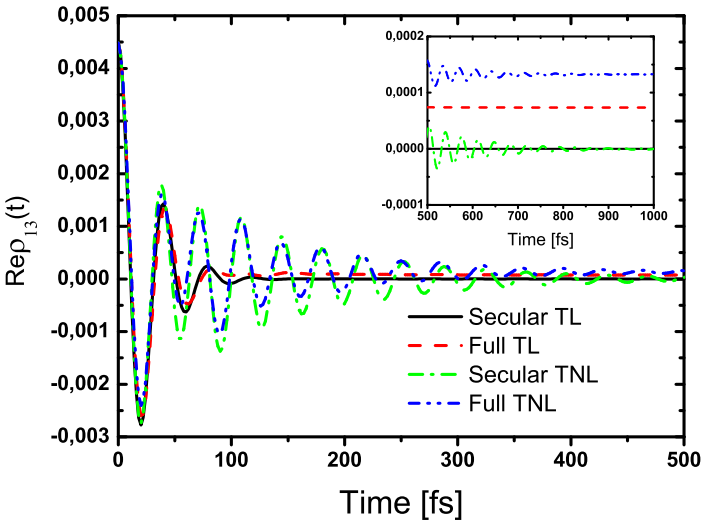

Figure 3.4: First 500 fs of the dynamics of the RDM coherence element $\rho_{13}(t)$, with parameters from Fig. 3.3, calculated by all four methods. Detail of the long time part of the time evolution is presented in the inset.

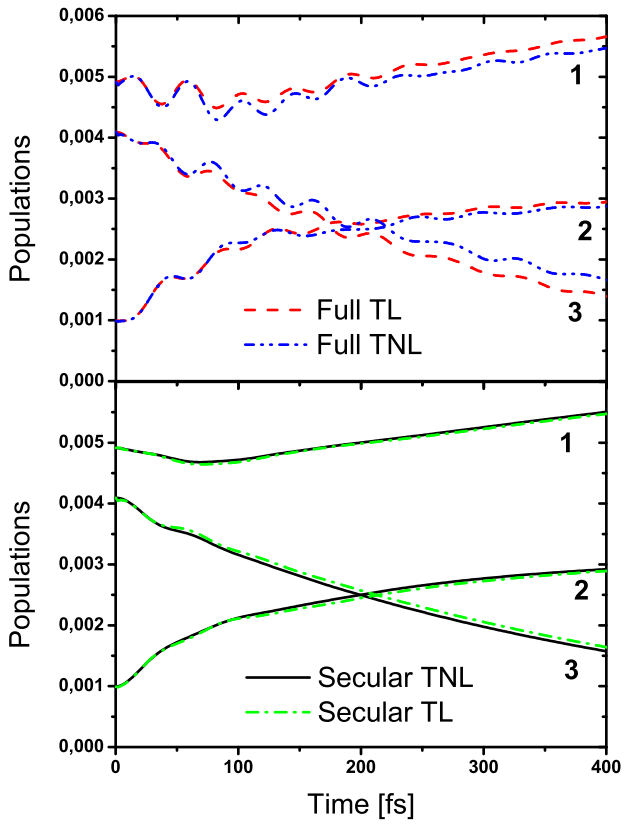

Figure 3.5: First 400 fs of the population dynamics of the trimer with parameters $\lambda = 30$ fs and $\tau_c = 100$ fs. Results of full TL-QME and TNL-QME are presented in upper subfigure (A), the secular results are found the the lower subfigure (B).

Let us now discuss the long time limit of the time evolution. As expected, the two secular theories yield the same equilibrium at long population times. This equilibrium corresponds to the canonical distribution of population among the excitonic levels at $T_B = 300$ K. In both secular TNL and secular TL cases, coherences have relaxed to zero at long times as the inset of the Fig. 3.4 demonstrates. The non-secular TNL and TL equations yield non-zero, stationary coherences at long times, and correspondingly, the long time equilibrium populations do not correspond to the canonical thermal equilibrium. Although both non-secular theories converge to results different from the canonical equilibrium (1.19), the full TNL equation yields populations that are physical at all times for the studied system parameters, i. e. they are always positive. The full TL equation on the other hand fails to keep probabilities positive at long times, and the occupation probability of the highest electronic level becomes negative after 200 fs for the parameters used on Fig. 3.3.

In light of the recent experiments on the FMO complex [Eng07] and other photosynthetic systems [Lee07, Cal09, Mer09, Col10, Har12], the conclusion that time non-local theories lead to a longer coherence lifetime than the time-local ones (i. e. also longer than the standard constant rate theories) is probably the most interesting. We have performed calculations of the RDM dynamics while varying the reorganization energy and the correlation time. The absolute values of the coherence $\rho_{13}(t)$ elements were fitted by a single exponential to estimate coherence life-time. The results are summarized in Fig. 3.6. The Fig. 3.6A shows the results for secular TL and secular TNL equations. Clearly, with growing correlation time τ_c, the full TNL equations lead to a increasing coherence lifetime. The full TL equation shows only a very weak dependence of the coherence lifetime on correlation time. Another interesting observation is that for correlation time longer than 50 fs, the dependence of the coherence lifetime on the reorganization energy λ is different for full TNL and TL methods. Time local theory, in accordance with the standard rate theories, predicts decrease of the coherence lifetime with λ. The full TNL theory predicts (within the parameter range studied here) an opposite tendency. The Fig. 3.6B shows similar conclusion for the non-secular versions of the theories, with the same difference between TL and TNL theory. The dependence of the coherence lifetime on λ in case of TNL equations is not monotonous.

3.3 Two-Dimensional Spectrum

As discussed in the Introduction, the secular TL equation of motion yields an exact result for the dephasing of an isolated optical coherence [Dol08]. One

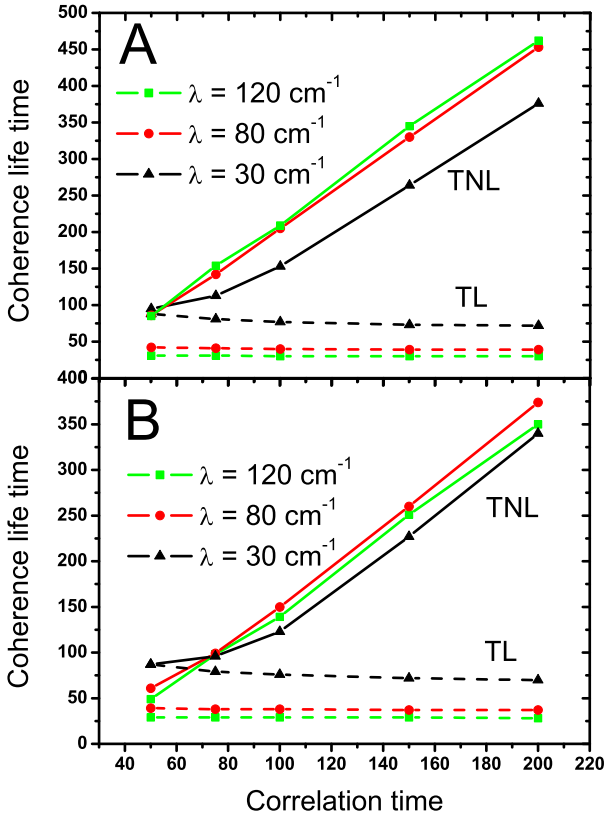

Figure 3.6: The lifetime of coherence $\rho_{13}(t)$ as obtained from fitting the coherence dynamics calculated by all four methods for various parameters λ and τ_c. The upper subfigure (A) shows the lifetimes obtained by the secular methods, while the lower subfigure (B) presents the same for non-secular methods.

can show, by comparison of the absorption spectra calculated by secular TL and TNL methods (see Fig. 3.2), that the TNL theory leads to certain artifacts (second peak) and is therefore not suitable for the description of the optical coherence evolution. Consequently, one can only hope to obtain valid results for the evolution superoperators at the first and the third time interval of the third order response functions by the TL theories. Alternative approach which we didn't chose here would be using the stochastic method introduced in Chapter 5. In Ref. [Man06b] it was shown that non-secular terms in the TL equations for optical coherences lead to temperature dependence of the positions of excitonic bands in absorption spectra. This dependence was shown to be strong when the electronic states involved are characterized by significantly different reorganization energy [Man06b, Man08]. Indeed it can be shown for homodimer that the non-secular terms are exactly zero in second order TL theory if the monomers exhibit the same reorganization energy [Man08]. We can therefore expect the non-secular effects in the optical coherences to be weak in our case, and we choose secular TL to calculate the evolution superoperators in the first and third time interval of the RF, Eq. (2.13c).

Concerning the population interval, the situation is somewhat different. As we have shown above, the non-secular TL theory leads to dynamics that breaks the positivity condition for the population probabilities at long times. At the same time, short time dynamics is very similar to the full TNL. Both theories predict population oscillations during the lifetime of the electronic coherences. The full TNL equation, however, preserves positivity, at least for the parameters studied here, and can be therefore used to calculate meaningful 2D spectra. For the same reason, both secular theories can also be successfully used to calculate 2D spectrum. As the oscillation of the populations predicted by non-secular theories are too small to be reliably observed in 2D spectrum (only a small change of the crosspeak amplitude due to the population transfer is observed after 140 fs of relaxation in 2D spectrum of Fig. 3.7) we expect only a small difference of the 2D spectrum to appear between the secular and full TNL theories. For the calculation of the representative 2D spectrum we therefore choose the secular TL and the full TNL theories. These two differ from each other mainly in the prediction of the lifetime of the electronic coherences. The observable difference in the calculated 2D spectra should therefore predominantly result from the different lifetime of the electronic coherence.

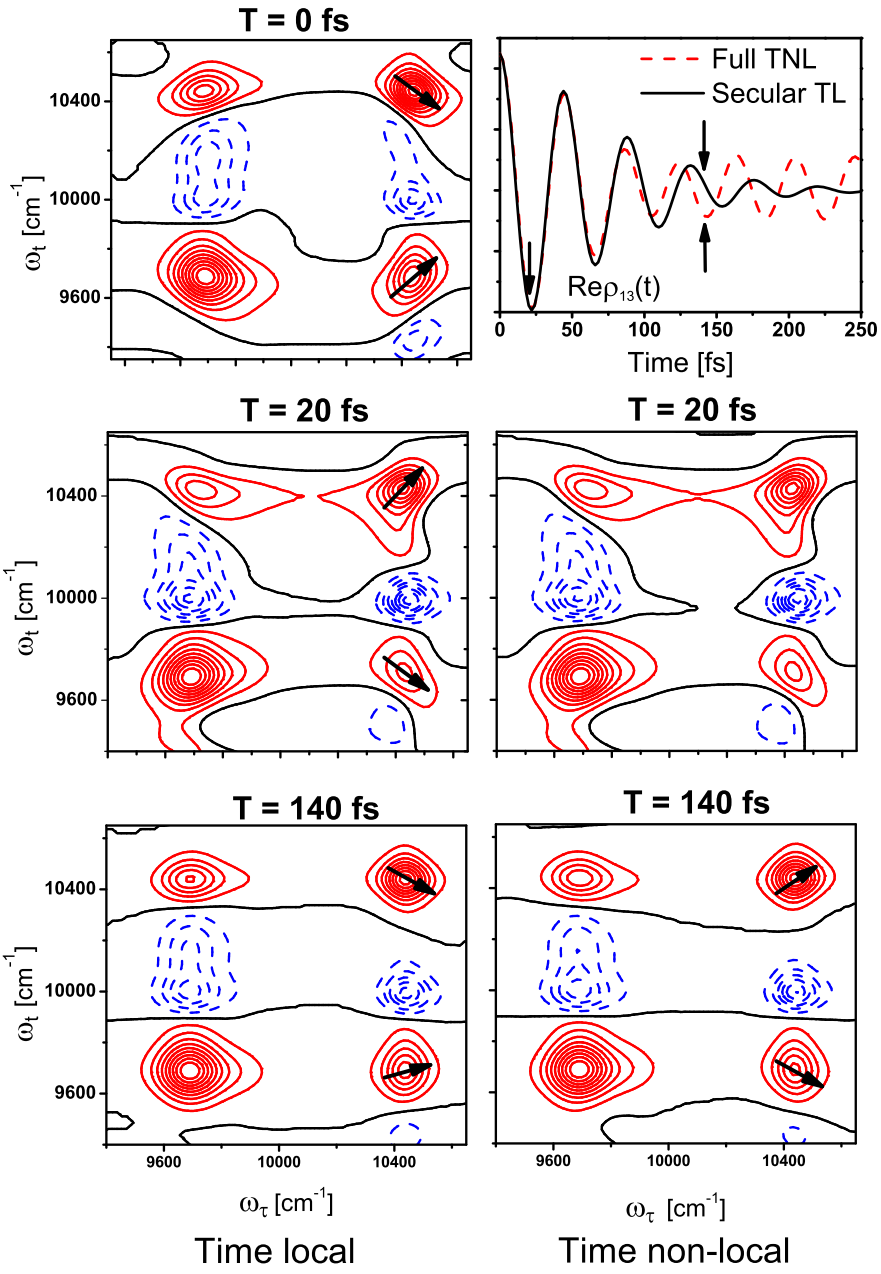

Figure 3.7: Two-dimensional coherent spectra of the trimer model at population times $T = 0$, 20 and 140 fs calculated by the secular TL method (left column) and the full TNL method (right column). The system-bath interaction parameters are $\lambda = 30$ cm^{-1} and $\tau_c = 100$ fs. The coherence element $\rho_{13}(t)$, which is mainly responsible for the oscillatory behavior of the cross-peaks, is presented in the upper right corner of the figure. The 2D spectrum at $T = 0$ fs is the same for both methods and is therefore presented only once. The population times are selected so that they represent different phases of the $\rho_{13}(t)$ element (denoted by arrows on the coherence element figure). Arrows in the 2D spectra denote the orientation of the peaks. All spectra are normalized to 1 with contour step of 10 %. Positive features are in full red line, negative features are represented by dashed blue line, and the zero contour is depicted by the full black line.

Fig. 3.7 presents 2D spectra for $\lambda = 30$ cm^{-1} and $\tau_c = 100$ fs. These parameters lead to a rather slow relaxation and consequently to narrow spectral peaks in both absorption (see Fig. 3.2) and 2D spectra. This allows us to clearly see characteristic $T-$dependent oscillations of the peaks in 2D spectrum. At $T = 0$ fs, both methods provide the same 2D spectrum, with four peaks. Two diagonal peaks arise when all three perturbations of the system by electric field occur on the same level, while two cross-peaks appear from interactions occurring on different levels. Negative peaks correspond to excited state absorption. For two molecules that are not excitonically coupled, all contributions to the cross-peaks cancel out exactly, while if two molecules are excitonically coupled non-zero cross-peaks appear. The shapes of the peaks are influenced by the phase evolution of the coherence elements of RDM during the population time T. On the upper left figure of Fig. 3.7 we have marked the elongation of the diagonal and off-diagonal peaks by arrows. The elongation can be best judged by looking at the zero contour (in black). This particular elongation is characteristic for the phase of the $\rho_{13}(t)$ element (see upper right figure of Fig. 3.7) at $T = 0$. At $T = 20$ fs the phases of the $\rho_{13}(t)$ calculated by both methods are opposite to the phase at $T = 0$. The 2D spectra calculated by the two different methods at $T = 20$ fs differ only in the precise positions of the contours. This phase of the coherence element is characterized in 2D spectrum by a different orientation of the peaks. Interestingly, at $T = 140$ fs the two methods predict $\rho_{13}(t)$ that have mutually opposite phases and as a consequence the 2D spectra at $T = 140$ fs calculated by different methods differ in the orientation of their cross-peaks. Since the secular TL theory predicts a simple dephasing of the coherence and a regular oscillation with a single frequency proportional to the energy difference between corresponding energy levels, it is in principle possible to distinguish, even experimentally, deviations from this prediction. Our conclusion is that such a deviation should be a consequence of the memory effects in the reduced system time evolution.

3.4 Validity of Secular and Markov Approximations

Several conclusions about the applicability of the secular and Markov approximations can be drawn from the above results. As pointed out in Ref. [Dol08], Markov approximation, which in the second order in system-bath coupling converts the TNL equations to the TL ones, leads accidentally to an exact result for an optical coherence element interacting with the harmonic bath. It has been also pointed out previously [Ish09b, Kub69] that in the same case, the TNL equations lead to

artifacts. When studying relaxation dynamics of the populations and electronic coherences in excitonic systems, full TL theory leads to a breakdown of the positivity of the RDM, while none of the secular theories suffer from this problem. In principle, the full TNL theory suffers from this problem, too. However, it has been found less susceptible to it here. The secular theories lead to canonical density matrix at long times, while the full TNL results in a stationary state characterized by non-zero (but constant) coherences. Such result corresponds to an additional renormalization of the electronic states by the interaction with bath, and has to be expected even at a weak coupling limit [Gev00]. It is important to note in this context that the canonical equilibrium (1.19) is to be expected for the system consisting of the molecule and the bath as a whole, not for its parts [Gev00].

For the population dynamics we are therefore forced to conclude that the full TNL theory represents the best candidate for a correct description of relaxation phenomena in the second order of the system bath interaction. It predicts similar population transfer times as other methods, it is much less sensitive to the breakdown of the positivity than its TL counterpart, and it leads to a bath renormalization of the canonical equilibrium. Most interestingly however, unlike in the TL theory, the coherence lifetime can attain wider range of values in the TNL theory, depending of the correlation time of the bath. The lifetime of the electronic coherence predicted by the non-perturbative methods, for example by the hierarchical equations of motion, is $300 - 500$ fs for various systems with parameters similar to the photosynthetic molecular aggregates [Ish09b, Zhu11, Kre12]. Comparable lifetimes can be obtained by the TNL theories with proper choice of the bath-correlation time. This is not true for the TL theories. The lifetime observed in the FMO [Eng07] is longer than a picosecond it is thus not well explained by the TNL theories. Since the publication of [Olš10], it was proposed that the picosecond lifetime can be explained by the coupling of electronic and vibrational states [Chr12, Che13a, Tiw13].

In the light of the above conclusions about the dynamics of optical coherences and the populations and coherences of the one exciton band, we suggest a hybrid approach to calculating 2D spectra, which consists of the application of the TL method on optical coherences (first and third time interval) and the full TNL method on the calculation of the RDM dynamics in the one exciton band during the population time T.

CHAPTER

FOUR

RESPONSE FUNCTION CORRELATIONS THROUGH PROJECTOR OPERATORS

For the description of the most 2D experiments, the third order semi-classical light-matter interaction response function theory is well established. Response functions of model few-level systems with pure dephasing (i. e. with no energy transfer between the levels) can even be expressed analytically in terms of the EGCF, using the second order cumulant in Magnus expansion [Muk95]. Some examples of small chromophores in solution fall in this category [Nem08, Nem10] when investigated on time scales shorter then radiative lifetime. For a Gaussian bath this analytical theory is exact, and thus knowing the EGCF of the electronic transitions enables us to determine linear (absorption) as well as non-linear spectra.

However, the construction of exact response functions for realistic energy transferring systems, such as Frenkel excitons in photosynthetic aggregates [vA00], is no longer possible. Photosynthetic complexes are relatively large, and the proper methods to simulate finite timescale stochastic fluctuations at finite temperatures [Tan06, Ish09a, Ish09b] carry a substantial numerical cost. Practical calculations thus require some type of reduced dynamics where only electronic degrees of freedom are treated explicitly. These approaches usually rely on a host of approximations that seem to work well for most spectroscopic techniques [Nov03, Nov05, vG06, Abr09] and in systems where the details of system-bath coupling are apparently less important [Zig06]. With increasing details of the excited state dynamics revealed by the 2D spectroscopy [Rea07, Rhe09, Abr10] and with increasing size of the studied systems, it becomes more and more important to keep the numerical cost of simulations low, while simultaneously account for experimentally observed quantum effects. One of the possible research directions is to extend on existing reduced density matrix (RDM) theories [Zha98, Pal09] or relax certain approximations [Olš10].

It was demonstrated that RDM master equations derived by projection operator technique reproduce exactly the linear response [Dol08]. In the case of higher order RFs, however, the same approach necessarily neglects bath correlations between the different periods of photo-induced system evolution (i. e. between the coherence time τ and the waiting time T of the FWM experiment). The failure to account for this correlation leads sometimes to a complete loss of the experimentally observed dynamics in simulated 2D spectra, such as in the case of the vibrational modulation of electronic 2D spectra [Nem08]. Because vibrational modulation leads to effects similar to those attributed to electronic coherence, developing methods that can account for its effect reliably in complex systems is of utmost importance. One possible approach to the problem is to derive equations of motion for the response as a whole, and to take the previous time evolution of the system into account explicitly [Ric10]. In this chapter, based on the article [Olš12], we take a different route in which the correlation effects are treated by a specific choice of the projection operator. Once a projector is specified, it can be used for any method of treating system bath interaction. We apply the previously suggested parametric projection operator technique [Man11] to a calculation of the second order response of a quantum system. The second order response operators can be used to determine the state of a molecular system subject to excitation by a weak light with arbitrary properties, and thus its importance goes beyond the semi-classical system light interaction theory [Man10]. Alternatively, calculation of the second order response can be viewed as a first step towards more involved calculation of the third order RFs that is required for the modeling of the third order non-linear spectra.

4.1 Theory

As discussed in the Section 1.7, one can derive master equations by the projector approach from the Nakajima-Zwanzig identity (1.70). Let us assume we have derived a master equation by applying the corresponding projector operator $\mathcal{P}$ and calculated elements of the reduced evolution superoperator $\tilde{\mathcal{U}}(t)$, Eq. (1.60). We can then assemble an approximate response function (2.14), for instance

$$\tilde{R}_{2g,kl}(t,T,\tau) = \tilde{\mathcal{U}}^{(egeg)}_{kgkg}(t)\mathcal{V}^{(R)}_{(eg)}\tilde{\mathcal{U}}^{(eeee)}_{klkl}(T)\mathcal{V}^{(L)}_{(eg)}\tilde{\mathcal{U}}^{(gege)}_{glgl}(\tau)\mathcal{V}^{(R)}_{(ge)}|g\rangle\langle g| \,. \tag{4.1}$$

It can be shown that $\tilde{R}_{2,kl}$ can also be written as

$$\begin{aligned}\tilde{R}_{2g,kl}(t,T,\tau) = \mathrm{Tr}_B\{&\mathcal{U}^{(egeg)}_{kgkg}(t)\mathcal{V}^{(R)}_{(eg)}\mathcal{P}\mathcal{U}^{(eeee)}_{klkl}(T) \\ &\times\mathcal{V}^{(L)}_{(eg)}\mathcal{P}\mathcal{U}^{(gege)}_{glgl}(\tau)\mathcal{V}^{(R)}_{(ge)}\mathcal{P}|g\rangle\langle g|w_{\mathrm{eq}}\} \,.\end{aligned} \tag{4.2}$$

However, the exact expression for $R_{2,kl}$ reads as

$$R_{2g,kl}(t,T,\tau) = \mathrm{Tr}_B\{\mathcal{U}^{(egeg)}_{kgkg}(t)\mathcal{V}^{(R)}_{(eg)}(\mathcal{P}+\mathcal{Q})\mathcal{U}^{(eeee)}_{klkl}(T) \\ \times\mathcal{V}^{(L)}_{(eg)}(\mathcal{P}+\mathcal{Q})\mathcal{U}^{(gege)}_{glgl}(\tau)\mathcal{V}^{(R)}_{(ge)}(\mathcal{P}+\mathcal{Q})|g\rangle\langle g|w_{\mathrm{eq}}\}, \qquad (4.3)$$

where we added the projector-pair $\mathcal{P}+\mathcal{Q}=1$, which equals the identity operator, to proper places in Eq. (4.3). Eqs. (4.2) and (4.3) differ by the $\mathcal{Q}$-containing terms that cannot be in general eliminated, and consequently one cannot expect master equations based on a single projector operator $\mathcal{P}$ of any type to reproduce the third order RFs. This applies also to the validity of non-perturbative schemes of calculations of non-linear response, such as those derived in Refs. [Gel05] and [Man06a]. Note that we do not claim that master equations cannot lead to exact form of $\tilde{\mathcal{U}}(t)$ in a single interval. They sometimes do, even if they are based on finite order perturbation in system-bath coupling [Dol08]. This exactness is enabled by the fact that the solution of the finite order equation contains all orders of perturbation

$$\frac{d\rho(t)}{dt} = \Lambda(t)\rho(t) \overset{\text{yields}}{\rightarrow} \rho(t) = e^{\int_0^t d\tau\,\Lambda(\tau)}\rho(0)\ . \qquad (4.4)$$

What we address here is their inability to compensate the $\mathcal{Q}$-containing terms between intervals of the RF, i. e. to take into account the effect of the bath history on the change of electronic state after the delta pulse excitation.

A general solution of this problem was proposed in Ref. [Man11]. It was argued that one cannot write down a single exact master equation for all three intervals of the RF. Rather, one has to write a different master equation for each interval. This is formally possible by introducing three different projectors: $\mathcal{P}^{AK}$, the Argyres-Kelly projector (1.63), for the first, $\mathcal{P}_\tau$ for the second and $\mathcal{P}_{\tau+T}$ for the third interval of the response [Man11]. The projectors $\mathcal{P}_\tau$ and $\mathcal{P}_{\tau+T}$ are constructed so as to cancel the $\mathcal{Q}$-containing term exactly for $J_{mn}=0$. In this limit, all RFs (2.14) can be exactly reproduced by the corresponding master equations.

In the following sections, we will treat the case of $J_{mn}\neq 0$. We present a way how to calculate the second order response operators (2.17) and their Hermite conjugates $R_{I^*}=R_I^\dagger$, $R_{II^*}=R_{II}^\dagger$ by a time-local master equation that includes the $\mathcal{Q}$-containing terms in the exact expression

$$R_{II}(t,\tau) = \mathrm{Tr}_B\{\mathcal{U}^{(eeee)}(t)\mathcal{V}^{(L)}_{(eg)}(\mathcal{P}+\mathcal{Q})\mathcal{U}^{(gege)}(\tau)(\mathcal{P}+\mathcal{Q})\mathcal{V}^{(R)}_{(ge)}|g\rangle\langle g|w_{\mathrm{eq}}\} \qquad (4.5)$$

by a proper choice of a new projector $\mathcal{P}_{\tau,II}$ so that

$$R_{II}(t,\tau) = \mathrm{Tr}_B\{\mathcal{U}^{(eeee)}(t)\mathcal{V}^{(L)}_{(eg)}\mathcal{P}_{\tau,II}\mathcal{U}^{(gege)}(\tau)\mathcal{P}^{AK}\mathcal{V}^{(R)}_{(ge)}|g\rangle\langle g|w_{\mathrm{eq}}\} \ . \tag{4.6}$$

The response operators R_I and R_{I^*} are not treated, because the non-trivial effects cannot manifest in the case of non-degenerate ground state. Their treatment is analogical to the treatment of response operators R_{II} and R_{II^*}. The projector $\mathcal{P}_{\tau,II}$ is chosen in such way that it contains the time evolution of the bath in the first interval of the response, where the relevant system dynamics is the one of an optical coherence. The projector corresponding to the pathway R_{II} and the length of the first interval τ reads according to Ref. [Man11, Olš12]

$$\mathcal{P}_{\tau,II}\bullet = \mathrm{Tr}_B\left\{\bullet\right\} U^g(\tau)w_{\mathrm{eq}} \sum_{\tilde{n}} U^{e\dagger}_{\tilde{n}}(\tau)\, K_{\tilde{n}}\, e^{g^*_{\tilde{n}\tilde{n}}(\tau)} \ . \tag{4.7}$$

This choice gives an exact description of the bath for $J_{mn} = 0$. For a non-zero coupling it corresponds to the secular approximation in the first interval equation of motion (1.84).

Instead of deriving the master equation directly for $R_{II/II^*}(t,\tau)$, we derive it for RDM excited by two ultrashort pulses according to the initial condition (1.29)

$$\rho^{(2)}_{II/II^*}(t,\tau) = R_{II/II^*}(t,\tau)|E_0|^2 \ . \tag{4.8}$$

As with the response operators (2.17), the operator of the conjugated pathway I^* and II^* is Hermite-conjugate to the operator of normal pathway I and II. We also define the total density matrices in the first and second intervals of R_{II}

$$W^{(1)}_{II}(t) = \mathcal{U}^{(gege)}(\tau)\mathcal{P}^{AK}\mathcal{V}^{(R)}_{(ge)}|g\rangle\langle g|w_{\mathrm{eq}}|E_0|^2 \ , \tag{4.9}$$

$$W^{(2)}_{II}(t) = \mathcal{U}^{(eeee)}(t)\mathcal{V}^{(L)}_{(eg)}\mathcal{P}_{\tau,II}\mathcal{U}^{(gege)}(\tau)\mathcal{P}^{AK}\mathcal{V}^{(R)}_{(ge)}|g\rangle\langle g|w_{\mathrm{eq}}|E_0|^2 \ , \tag{4.10}$$

their Hermite conjugates $W^{(1)}_{II^*}(t) = (W^{(1)}_{II}(t))^\dagger$ and $W^{(2)}_{II^*}(t) = (W^{(2)}_{II}(t))^\dagger$, and the RDM of the first interval of the RF

$$\rho^{(1)}_{II/II^*}(t) = \mathrm{Tr}_B W^{(1)}_{II/II^*}(t) \ . \tag{4.11}$$

Further on in the text, all derivations will be done for the pathway R_{II}, Eq. (2.17b), and we omit the index II. The treatment of the pathway R_{II^*} is analogical. We define an bath evolution operator for the system in the excited eigenstate $|\tilde{n}\rangle$

$$U^e_{\tilde{n}}(\tau) = \exp\left(-\frac{i}{\hbar}(T + V^e_{\tilde{n}\tilde{n}}(\{Q\}) - \langle V^e_{\tilde{n}\tilde{n}}(\{Q\}) - V_g(\{Q\})\rangle)\tau\right) \ , \tag{4.12}$$

where the potential energy bath operators $V^e_{\tilde{n}\tilde{n}}$ for the excited eigenstates $|\tilde{n}\rangle$ are defined by Eq. (1.32). By the choice of the projector (4.7) we prescribe an ansatz

$$W^{(2)}(0) = W^{(1)(I)}(\tau) \equiv \rho^{(1)(I)}(\tau) w^{(I)}_\tau, \tag{4.13}$$

and

$$w^{(I)}_\tau \equiv \sum_{\tilde{n}} K_{\tilde{n}} U^g(\tau) w_{\rm eq} U^{e\dagger}_{\tilde{n}}(\tau)\, e^{g^*_{\tilde{n}\tilde{n}}(\tau)} \ . \tag{4.14}$$

For zero resonance coupling J_{mn}, this is an exact prescription for the bath. For non-zero resonance coupling, it is an approximation comparable to the secular approximation. Projector (4.7) can be written in short as

$$\mathcal{P}_\tau \bullet = {\rm Tr}_B \left\{ \bullet \right\} w^{(I)}_\tau. \tag{4.15}$$

It is important to note that $w^{(I)}_\tau$ is not a purely bath operator, and it does not generally commute with ρ. Also the interaction picture with respect to the system Hamiltonian H_S denoted by (I) applies to it. It stands on the right hand side of ρ when evaluating R_{II}, while in R_{II^*} it would stand on the l.h.s. of ρ. This follows from the diagrams in Fig. 2.1B. The full form of $W^{(1)}(\tau)$ is

$$W^{(1)}(\tau) = \ U^g(\tau) w_{\rm eq} \sum_{\tilde{n}} U^{e\dagger}_{\tilde{n}}(\tau)\, K_{\tilde{n}} e^{i(\varepsilon_{\tilde{n}} + \langle V^e_{\tilde{n}\tilde{n}} - V_g \rangle)\tau/\hbar} \rho^{(1)}(0). \tag{4.16}$$

From now on, the upper index (2) will be omitted in text for the sake of brevity.

We can verify that the projector property $\mathcal{P}^2_\tau = \mathcal{P}_\tau$ is fulfilled

$$\begin{aligned} &\mathcal{P}_\tau \mathcal{P}_\tau \left(|\tilde{m}\rangle\langle\tilde{n}|\, w \right) \\ &\quad = |\tilde{m}\rangle\langle\tilde{n}|\, {\rm Tr}_B \left\{ U^g(\tau) w_{\rm eq}\, U^{e\dagger}_{\tilde{n}}(\tau) \right\} {\rm Tr}_B \left\{ w \right\}\, e^{2 g^*_{\tilde{n}\tilde{n}}(\tau)} \\ &\quad = |\tilde{m}\rangle\langle\tilde{n}|\, e^{-g^*_{\tilde{n}\tilde{n}}(\tau)}\, {\rm Tr}_B \left\{ w \right\}\, e^{2 g^*_{\tilde{n}\tilde{n}}(\tau)} = \mathcal{P}_\tau \left(|\tilde{m}\rangle\langle\tilde{n}|\, w \right) \ . \end{aligned} \tag{4.17}$$

Here, we used expression for the line shape function $g(t)$ in the second cumulant approximation

$$e^{-g(t)} = {\rm Tr}_B \left\{ U^{g\dagger}(t) U^e(t) w_{\rm eq} \right\} \ . \tag{4.18}$$

The action of the projector $\mathcal{P}_\tau (\equiv \mathcal{P}_{\tau,II})$ on the electronic state is asymmetric, because the projector was derived for the Liouville pathway R_{II} (see Fig. 2.1B).

Let us focus on the details of the application of the projector $\mathcal{P}_\tau$ with the

Nakajima-Zwanzig identity (1.70)

$$\begin{aligned}
&\frac{d}{dt}\mathcal{P}W^{(I)}(t) = \mathrm{NZ}_1 + \mathrm{NZ}_2 + \mathrm{NZ}_3 = \\
&\quad - \mathcal{P}\mathcal{L}^{(I)}(t) \exp\left(-i \int_{t_0}^{t} d\tau \; \mathcal{Q}\mathcal{L}^{(I)}(\tau) \right) \mathcal{Q}W^{(I)}(t_0) \\
&\quad - \mathcal{P}\mathcal{L}^{(I)}(t) \int_{0}^{t-t_0} ds \; \exp\left(-i \int_{t_0}^{s} d\tau' \; \mathcal{Q}\mathcal{L}^{(I)}(\tau') \right) \mathcal{Q}\mathcal{L}^{(I)}(t-s)\mathcal{P}W^{(I)}(t-s) \\
&\quad - i\mathcal{P}\mathcal{L}^{(I)}(t)\mathcal{P}W^{(I)}(t) \; . \qquad (4.19)
\end{aligned}$$

We use it up to the second-order in $\mathcal{L}^{(I)}$ and we set $t_0 = 0$. We write the Eq. (4.19) as sum of terms NZ_1, NZ_2 and NZ_3 for easier referencing. The term NZ_1 is the so-called initial terms that vanishes thanks to the properties of the projector (4.15) and separability of the initial condition of the first-order response function $\rho^{(1)}(0) = w_{\mathrm{eq}}|g\rangle\langle g|$. The last term NZ_3 corresponds to an effective Liouvillian, and it is usually purely electronic operator. Now, with the parametric projector it contains additional terms originating from the system-bath interaction. It is important to note that the projector $\mathcal{P}_\tau$ itself contains the system-bath interaction to all orders in the form of the exponential of the line-shape function (see Eq. (4.7)). The success of the second order master equations (of the form $\dot{\rho} = -\alpha_2\rho$, where the dot denotes the time derivative, and α_2 is some second order operator) lies in the fact that their solutions includes all orders of the perturbation ($\rho = e^{-\alpha_2 t}\rho_0$). The solution corresponds to a partial summation of the perturbative series to infinity. For some types of bath, such as the bath consisting of harmonic oscillators, this may even lead to exact master equations [Dol08]. When higher order terms are added to the right hand side of the equation motion by a procedure that does not respect the form of higher order terms dictated by the cumulant expansion, the resulting equation of motion may lead to unphysical results. Therefore, one has to take care in application of the projector $\mathcal{P}_\tau$, not to allow higher than second order contributions to appear on the right hand side of the Nakajima-Zwanzig identity (4.19). Since the difference between projectors $\mathcal{P}^{AK}$ and $\mathcal{P}_\tau$ is only in dynamics of the system-bath coupling during time τ, their difference is at least of the first order in ΔV. Since the NZ_2 with Argyres-Kelly projector is already of the second order in ΔV in all its terms, the difference caused by using projector $\mathcal{P}_\tau$ will be of higher order in ΔV. In the second order master equation, the term NZ_2 with projector $\mathcal{P}_\tau$ has to be equivalent to the form obtained with the AK projector that yields the TNL-QME (1.79). Applying the following approximation $\rho^{(I)}(t-\tau') \approx \rho^{(I)}(t)$ in the term NZ_2 we obtain it in the form the second order

relaxation term of TL-QME (1.84).

4.2 Derivation of Parametric Quantum Master Equation

In this section we will evaluate the contribution of the only new non-trivial term NZ_3 of Eq. (4.19) to the new parametric QME. Applying the definitions of its component operators from Section 1.7 we obtain

$$\mathrm{NZ}_3 = -\frac{i}{\hbar}\mathrm{Tr}_B\left\{ \left[\sum_m \Delta V_m^{(I)}(t) K_m^{(I)}(t), \rho^{(I)}(t)\, w_\tau^{(I)}\right]_- \right\} w_\tau^{(I)} \tag{4.20}$$

where

$$\rho^{(I)}(t) = \mathrm{Tr}_B\left\{\mathcal{P}_\tau W^{(I)}(t)\right\}. \tag{4.21}$$

Using Eq. (4.14) yields

$$\begin{aligned}
\mathrm{NZ}_3 = &-\frac{i}{\hbar}\sum_{m\tilde{k}} e^{g_{\tilde{k}}^*(\tau)}\mathrm{Tr}_B\Big\{\Delta V_m(t) K_m^{(I)}(t)\rho^{(I)}(t)\, w_{\mathrm{eq}} \\
&\times U^g(\tau) U_{\tilde{k}}^{e\dagger}(\tau) K_{\tilde{k}}\Big\} w_\tau^{(I)} \\
&+\frac{i}{\hbar}\sum_{m\tilde{k}} e^{g_{\tilde{k}}^*(\tau)}\mathrm{Tr}_B\Big\{\rho^{(I)}(t)\, w_{\mathrm{eq}} U^g(\tau) U_{\tilde{k}}^{e\dagger}(\tau) \\
&\times K_{\tilde{k}} \Delta V_m^{(I)}(t) K_m^{(I)}(t)\Big\} w_\tau^{(I)}\,.
\end{aligned} \tag{4.22}$$

Now we have to set $e^{g_{\tilde{k}}^*(\tau)} \approx 1$ since its contribution is of higher order in ΔV. Applying the first order expansion

$$U^g(\tau) U_{\tilde{n}}^{e\dagger}(\tau) \approx 1 + \frac{i}{\hbar}\int_0^\tau d\tau'\, \Delta V_{\tilde{n}\tilde{n}}^e(-\tau'), \tag{4.23}$$

yields

$$
\begin{aligned}
\mathrm{NZ}_3 = \frac{1}{\hbar^2}\int_0^\tau d\tau' \Bigg[\sum_{m\tilde{k}} K_m^{(I)}(t)\rho^{(I)}(t)K_{\tilde{k}} - \rho^{(I)}(t)K_{\tilde{k}}K_m^{(I)}(t) \Bigg] \\
\times \mathrm{Tr}_B \left\{ \Delta V_{\tilde{k}}^{(I)}(-\tau')\Delta V_m^{(I)}(t)\, w_{\mathrm{eq}} \right\} w_\tau^{(I)} \\
= \sum_{m\tilde{k}} \left(K_m^{(I)}(t)\rho^{(I)}(t)K_{\tilde{k}} - \rho^{(I)}(t)K_{\tilde{k}}K_m^{(I)}(t) \right) \\
\times \left(\dot{g}^*_{m\tilde{k}}(t+\tau) - \dot{g}^*_{m\tilde{k}}(t) \right) w_\tau^{(I)}.
\end{aligned} \tag{4.24}
$$

By putting the Eq. (4.24) together with the TNL-QME (1.78), originating from term NZ_2, and by tracing over bath DOF we obtain the parametric quantum master equation [Olš12]

$$
\begin{aligned}
\frac{d}{dt}\rho^{(I)}(t) = &- \frac{1}{\hbar^2}\sum_{i,j}\int_0^{t-t_0} ds \\
&\Big(C_{ji}(s)[K_j^{(I)}(t), K_i^{(I)}(t-s)\rho^{(I)}(t-s)]_- \\
&- C_{ij}(-s)[K_j^{(I)}(t), \rho^{(I)}(t-s)K_i^{(I)}(t-s)]_- \Big) \\
&+ \sum_{m\tilde{k}} \left(K_m^{(I)}(t)\rho^{(I)}(t)K_{\tilde{k}} - \rho^{(I)}(t)K_{\tilde{k}}K_m^{(I)}(t) \right) \left(\dot{g}^*_{m\tilde{k}}(t+\tau) - \dot{g}^*_{m\tilde{k}}(t) \right)
\end{aligned} \tag{4.25}
$$

in the interaction picture. The first three lines of Eq. (4.25) correspond to the standard TNL-QME, Eq. (1.78), while the last line represent the τ-dependent contribution which the standard TNL-QME does not predict.

Let us investigate the τ-dependent term only. First, we turn to Schrödinger picture by substituting $\rho^{(I)}(t) = U_S^\dagger(t)\rho(t)U_S(t)$. We denote the new τ-dependent term of the parametric QME by $\mathcal{D}(t;\tau)$

$$
\begin{aligned}
&\mathcal{D}(t;\tau)\rho(t) = \\
&\qquad \sum_{m\tilde{k}} \left(K_m\rho(t)K_{\tilde{k}}^{(I)}(-t) - \rho K_{\tilde{k}}^{(I)}(-t)K_m \right) \left(\dot{g}^*_{m\tilde{k}}(t+\tau) - \dot{g}^*_{m\tilde{k}}(t) \right)
\end{aligned} \tag{4.26}
$$

It can be easily verified that the new term preserves the trace of $\rho(t)$, because $\mathrm{Tr}\left(K_m\rho(t)K_{\tilde{k}}^{(I)}(-t) - \rho K_{\tilde{k}}^{(I)}(-t)K_m \right) = 0$. From the inspection of the term $\dot{g}^*_{m\tilde{k}}(t+\tau) - \dot{g}^*_{m\tilde{k}}(t)$ we can conclude that the effect of the parameter τ is transient. If EGCF tends to zero on a time scale given by some bath correlation time, this term also tends to zero. The dynamics at long times is therefore not affected by the delay between the two excitation interactions. In the next part we study the

effect of the τ-dependent term numerically for a heterodimer. Since the new term (4.26) is time-local, it can be added in its present form also to the TL-QME (1.88) and yield

$$\frac{d}{dt}\rho_{ab}(t) = \sum_{cd} -i\mathcal{L}_{abcd}\rho_{cd}(t) + \mathcal{R}_{abcd}\rho_{cd}(t) + \mathcal{D}_{abcd}(t,\tau)\rho_{cd}(t) \ . \tag{4.27}$$

4.3 Numerical Results and Discussion

In this section, we study the dynamics of the elements of the response functions, Eqs. (2.17). The RDM $\rho(t;\tau)$ for which we derived Eqs. (4.25) and (4.27) corresponds the response function R_{II} (see Eq. (4.8) for the case of $E_0 = 1$). We compare the dynamics in two cases. In the first case, the evolution operator $\mathcal{U}^{(eeee)}(T)$ appearing in Eqs. (2.17) is calculated by standard time dependent TL-QME derived using the AK projector, Eq. (1.63), with $w_0 = w_{\rm eq}$. In the second case, it is calculated using Eq. (4.27). We use the relation $\rho_{II^*,ij}(t) = \rho^*_{II,ji}(t)$ between the RDMs from different Liouville pathways.

The most simple system which exhibits τ-dependent correction to the standard TL-QME is a molecular heterodimer. In general, it is characterized by orientation and magnitude of its transition dipole moments, the excited state energies ε_1, ε_2 of the component molecules, their resonance coupling J and the properties of the bath. We denote the difference of the excited state energies by $\Delta \equiv \varepsilon_1 - \varepsilon_2$, and we set the magnitudes of the transition dipole moments to unity. The initial condition is assumed in a form $\rho^{(1)}(0) = |g\rangle\langle g|$. The evolution during the first interval of the response follows Eq. (1.84). For the calculations presented on Figs. 4.1, 4.2 and 4.3, we choose the anti-parallel orientation of the transition dipole moments, while for the calculation shown on Figs. 4.4 and 4.5, we choose the parallel orientation. The temperature is set to $T = 300$ K in all calculations.

First, let us investigate the sensitivity of the excited state dynamics to the interplay of the delay τ and the phase of the bath vibrations. Fig. 4.1 shows the dynamics of the electronic coherence between the excited states $|e_1\rangle$ and $|e_2\rangle$ in presence of the bath represented by a single-mode general Brownian oscillator, EGCF (1.49), with parameters $\lambda = 50$ cm^{-1}, $\gamma = 1$ ps^{-1}, $\Omega_{\rm Bath} = 100$ ps^{-1} and $\Delta = 100$ cm^{-1}. Both calculations show that the standard TL-QME calculation of $\mathcal{U}^{(eeee)}(T)$ is insensitive to the phase of bath vibrational mode during the time evolution in the first interval. The parametric TL-QME, Eq. (4.27), shows a distinct sensitivity to this phase. In the calculation on the Fig. 4.1, the vibration of the bath is much faster than the period (333 fs) of the electronic coherence. The two theories give the same result for $\tau = 0$ fs, then they start to deviate and after one period of bath oscillator, at $\tau = 60$ fs, they coincide again. Initial phase

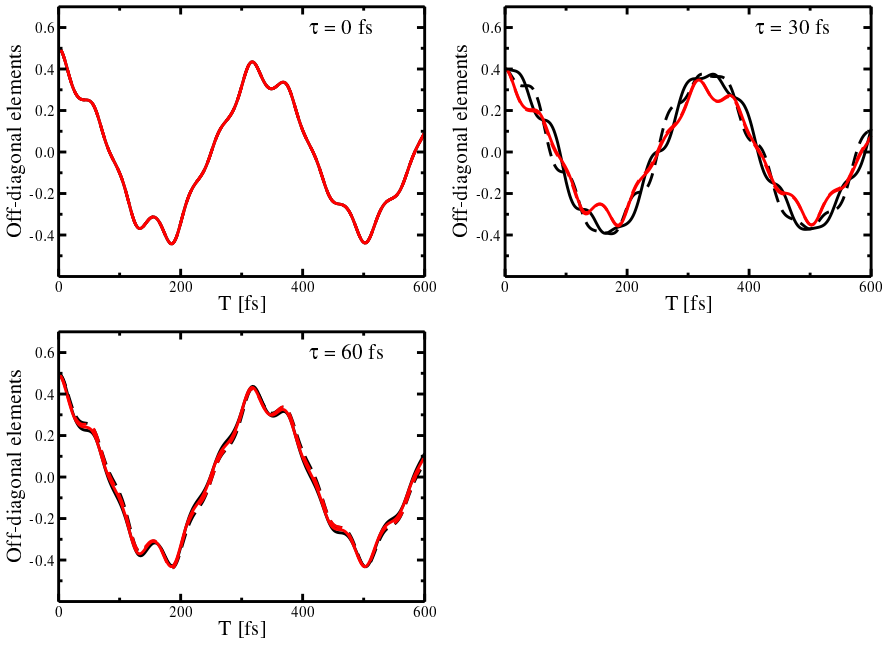

Figure 4.1: The time evolution of the real parts of R^*_{II} and R_{II} for a heterodimer with energy gap $\Delta = 100$ cm^{-1}, interacting with a bath represented by a general Brownian oscillator with parameters $\lambda = 50$ cm^{-1}, $\gamma = 1$ ps^{-1}and $\Omega_{\text{Bath}} = 100$ ps^{-1}. Red lines, the matrix element 12 of R^*_{II} according to standard TL-QME (dashed) and the corresponding parametric TL-QME (full). Black lines, the matrix element 12 of R_{II} according to standard TL-QME (dashed) and the corresponding parametric TL-QME (full).

of $\rho_{II^*,12}$ and $\rho_{II,12}$ is in general different at $T = 0$ fs because of their different time evolution in the first interval (they are not simply complex conjugates of each other). In the Fig. 4.2, we calculated the same system, but we used bath with parameters $\lambda = 5$ cm^{-1}, $\gamma = 1$ ps^{-1}, $\Omega_{\text{Bath}} = 19$ ps^{-1}. The frequency is now resonant with the frequency of the electronic coherence, which makes the effect more significant. The two theories give the same result for $\tau = 0$ fs, and at $\tau = 360$ fs, which is approximately one period of the bath vibration mode. Unlike in Fig. 4.1, the initial phase of $\rho_{II^*,12}$ and $\rho_{II,12}$ differs significantly in $T = 0$ fs because of their different time evolution in τ.

In both the cases studied above, the time evolution of the off-diagonal elements of the second order response operator is slightly modulated by the time evolution of the vibrational DOF. The phase of the oscillations seems to be mostly unaffected.

Figs. 4.3 and 4.4 demonstrate the influence of the resonance coupling on the population and electronic coherence dynamics in the homodimer. As above, we perform calculation according to standard TL-QME and the parametric TL-QME. This time, we choose the overdamped Brownian oscillator with fixed $\tau = 60$ fs and $\Delta = 100$ cm^{-1}, reorganization energy $\lambda = 120$ cm^{-1} and correlation time $\tau_c = \Lambda^{-1} = 50$ fs to represent the bath, and we change the resonance coupling. We

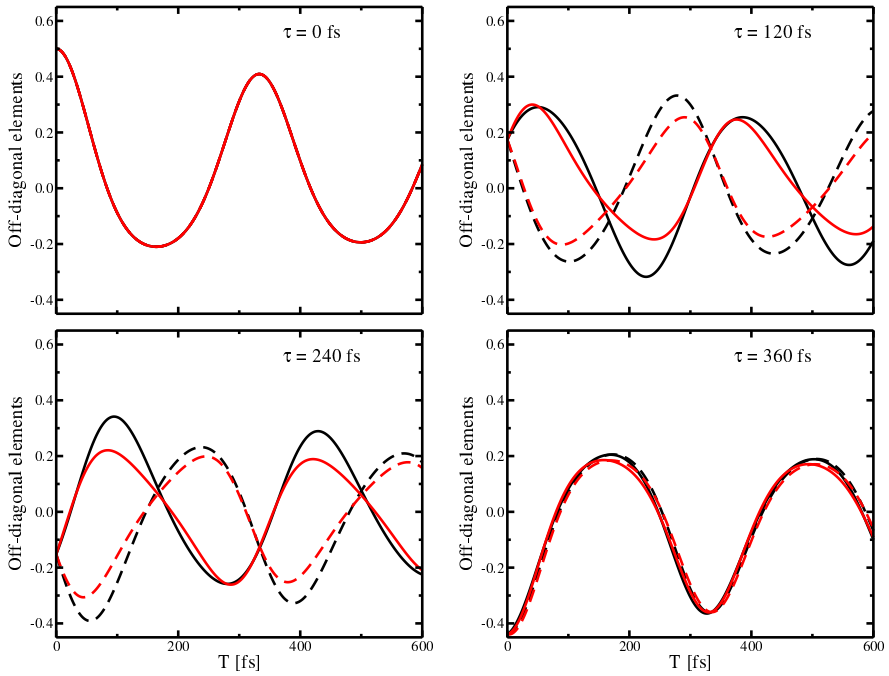

Figure 4.2: The time evolution of the real parts of R^*_{II} and R_{II} for a heterodimer with energy gap $\Delta = 100$ cm^{-1}, interacting with a bath represented by a general Brownian oscillator with parameters$\lambda = 5$ cm^{-1}, $\gamma = 1$ ps^{-1} and $\Omega_{\text{Bath}} = 19$ ps^{-1}. Red lines, the matrix element 12 of R^*_{II} according to standard TL-QME (dashed) and the corresponding parametric TL-QME (full). Black lines, the matrix element 12 of R_{II} according to standard TL-QME (dashed) and the corresponding parametric TL-QME (full).

calculate both diagonal and off-diagonal elements ("populations" and "coherences") of the operators $\rho_{II^*/II}$. For $J = 0$ cm^{-1}, there is no population dynamics. By increasing the coupling, the difference between the theories in the diagonal elements increases. In the Fig. 4.3, the dipole moments of the molecules are anti-parallel, while in Fig. 4.4 they are parallel.

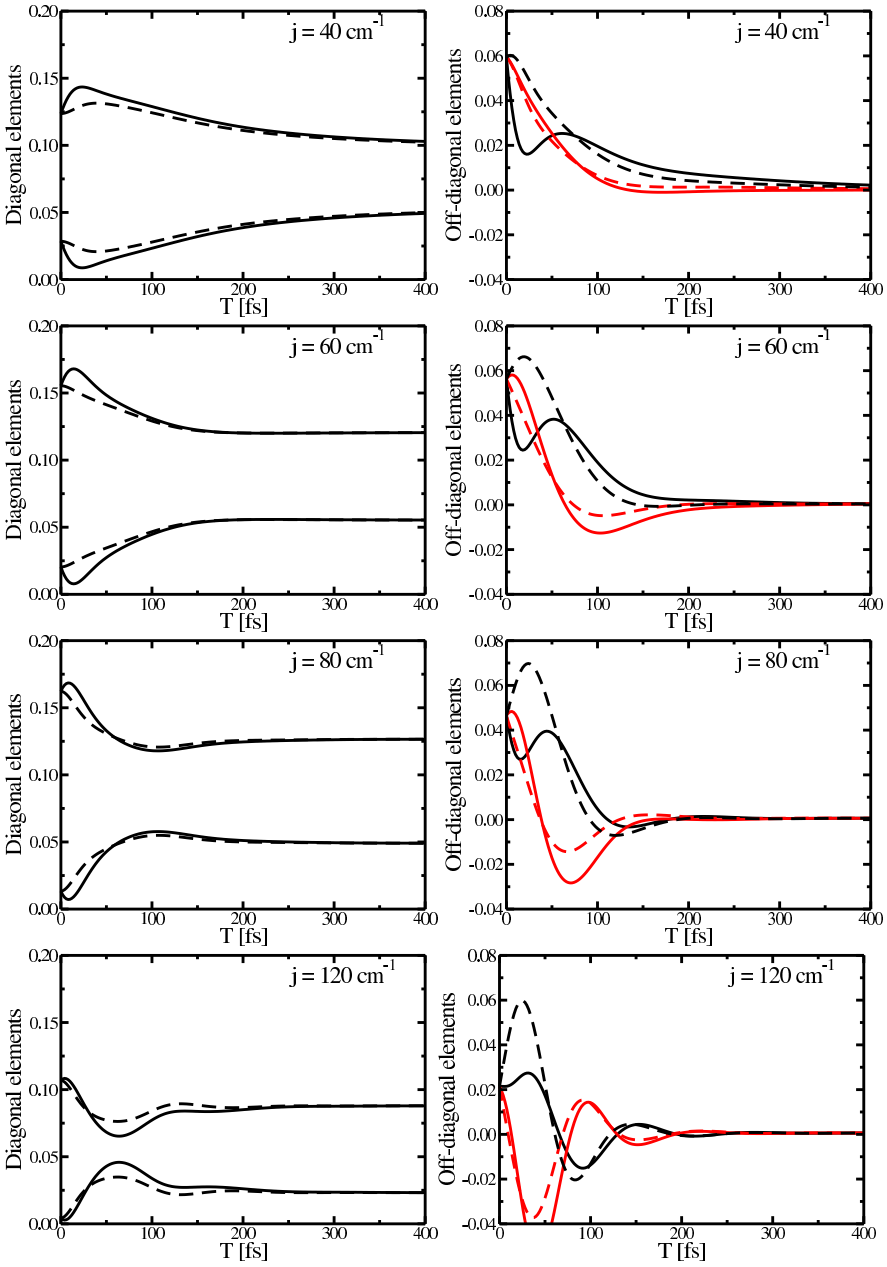

Figure 4.3: The time evolution of the real parts of R^*_{II} and R_{II} and their dependency on the resonance coupling J for a heterodimer with energy gap $\Delta = 100$ cm^{-1} and an anti-parallel arrangement of the transition dipole moments, interacting with a bath represented by an overdamped Brownian oscillator with reorganization energy $\lambda = 120$ cm^{-1} and correlation time $\tau_c = \Lambda^{-1} = 50$ fs. The delay between the two pulses is fixed to $\tau = 60$ fs. Black lines, the matrix elements 11, 22 (left column) and 12 (right column) of R_{II} according to standard TL-QME (dashed) and the corresponding parametric TL-QME (full). Red lines, the matrix element 12 (right column) of R^*_{II} according to standard TL-QME (dashed) and the corresponding parametric TL-QME (full).

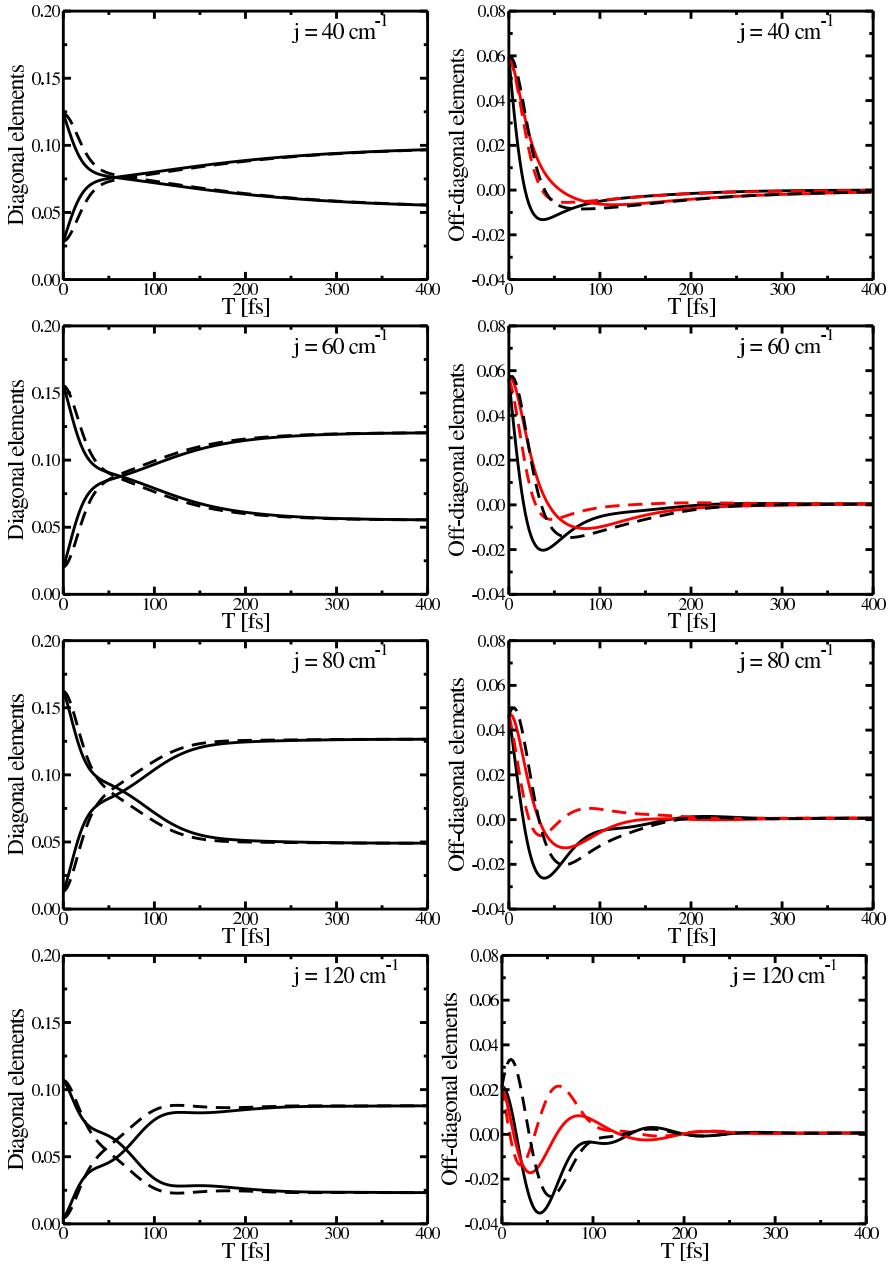

Figure 4.4: The same as Fig. 4.3 but for a heterodimer with parallel transition dipole moment arrangement.

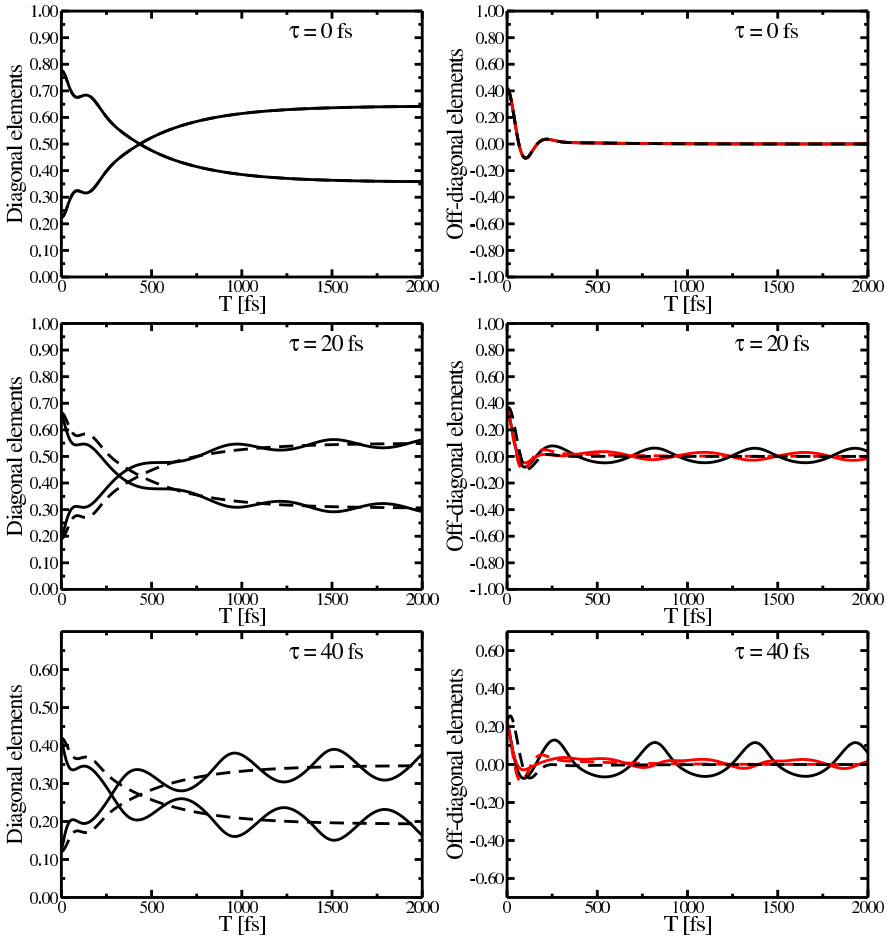

Figure 4.5: The time evolution of the real parts of R^*_{II} and R_{II} a heterodimer with energy gap $\Delta = 100$ cm^{-1}, resonance coupling $J = 33.1$ cm^{-1} and a parallel arrangement of the transition dipole moments, interacting with a bath represented by one overdamped Brownian oscillator with parameters $\Lambda^{-1} = 100$ fs and $\lambda_{\text{overdamped}} = 12$ cm^{-1} and an undamped vibration with reorganization energy $\lambda_{\text{harmonic}} = 30$ cm^{-1} and frequency $\Omega_{\text{Bath}} = 60$ cm^{-1}. Black lines, the matrix elements 11, 22 (left column) and 12 (right column) of R_{II} according to standard TL-QME (dashed) and the corresponding parametric TL-QME (full). Red lines, the matrix element 12 (right column) of R^*_{II} according to standard TL-QME (dashed) and the corresponding parametric TL-QME (full).

Let us now investigate a molecular dimer coupled to overdamped harmonic bath with EGCF (1.47) and to a single harmonic mode with frequency Ω_{Bath} described by EGCF (1.41). The harmonic mode is assumed to continue oscillating even long after thermalization in the overdamped part of the bath has taken place. Therefore, the τ-dependent term of Eq. (4.26) changes the system dynamics also at long times. The time dependence of the density operator elements for different τ is shown in Fig. 4.5. Parameters of the overdamped bath are $\Lambda^{-1} = 100$ fs and $\lambda_{\text{overdamped}} = 12$ cm^{-1} and of the harmonic mode $\lambda_{\text{harmonic}} = 30$ cm^{-1}, $\Omega_{\text{Bath}} = 60$ cm^{-1}. The dimer is characterized by $\Delta = 100$ cm^{-1}, $J = 33.1$ cm^{-1} and the parallel electronic transition dipole moments of the molecules. We can notice

that the interaction of the vibrational mode with the electronic DOF induces oscillations in both the diagonal and off-diagonal elements of the density operator. The amplitude of the oscillations increases with increasing τ. Since the EGCF of the harmonic mode, Eq. (1.41), is periodic, we expect the relative amplitude of the oscillations to decrease again for sufficiently long τ, and to become zero for $\tau = 2\pi/\Omega_{\mathrm{Bath}}$. However, in such long τ the second order response would be almost zero due to the decay of the optical coherence in the first interval. Fig. 4.5 suggests that the phase of the oscillation does not change linearly with τ. To understand this behavior, we can study a simple equation of the form

$$\dot{\rho}(t) = -\alpha(\rho(t) - \rho_0) + (f(t+\tau) - f(t))\rho(t), \tag{4.28}$$

which describes exponential decay to a limiting value ρ_0 with the rate constant α and a modulation by the function

$$f(t) = \int_0^t d\tau \; A\cos(\omega\tau). \tag{4.29}$$

Eq. (4.29) represents a first integral of the EGCF of an undamped vibrational mode, Eq. (1.41). The solution of Eq. (4.29) with the parameters $\alpha = 0.01$, $A = 10^{-4}$, $\omega^{-1} = 60$ and $\rho_0 = 0.6$ is shown in Fig. 4.6. We can see that the oscillation phase and period of the oscillations is indeed not proportional to τ, and the amplitude increases with τ similarly to Fig. 4.5. The behavior is therefore a direct consequence of the parametric term in the parametric QME.

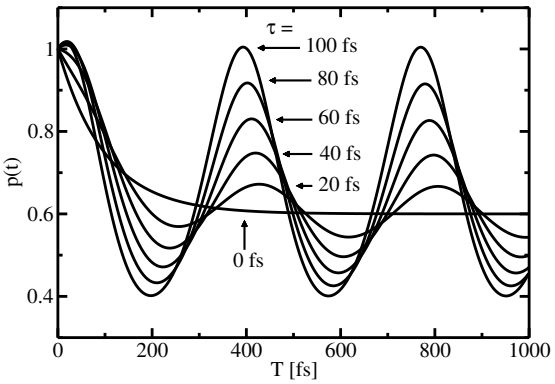

Figure 4.6: The time evolution of "population" according to model Eq. (4.28). The curves are solutions for τ increasing from 0 fs to 100 fs with step of 20 fs.

The overall picture arising from the numerical simulations is the following: Except for special cases, such as the molecular homodimer, the excited state dynamics of an open quantum system, as it is observed by the non-linear spectroscopy, indeed depends on the delay τ between the FWM scheme. The 2D

spectroscopy therefore observes a certain averaged dynamics. The effects seem to be rather small in most cases, but they might be observable by an advanced implementation of 2D spectroscopy. They are especially pronounced in the case of the intramolecular vibrational modes, which have frequency similar to the electronic energy gap between excitonic levels. Both the dynamics of electronic level populations and electronic coherences are affected. In order to identify these effects in the experimental data, the theory has to be extended to include also the third interval of the third order non-linear response. The corresponding projection operator $\mathcal{P}_{T+\tau}$ which now depends on the duration of both the coherence and the population intervals τ and T, respectively, has been already proposed an tested for $J_{mn} = 0$ in Ref. [Man11]. The formulation of the theory for the third interval of the response of a multilevel excitonic system in a similar manner as performed here for the second interval will be the subject of our future work.

CHAPTER

FIVE

STOCHASTIC UNRAVELING OF RESONANCE COUPLING BY CUMULANT EXPANSION

The hierarchical equations of motion method [Tan89, Ish05, Tan09] became very popular recently for calculation of excited state dynamics in photosynthetic systems as it combines feasibility with accuracy [Ish09c, Ish09a, Ish09b, Hei12, Kre12] and even promises efficient implementation on modern parallel computers [Kre11]. The only drawback of the method is that the calculations become more difficult with decreasing temperature [Ish09c].

In this section, another method which provides an exact solution to the reduced density matrix problem for Gaussian bath is proposed. The method is based on a stochastic unraveling of the equation of motion for the reduced density matrix in the resonance coupling. The leading idea is to cover the resonance coupling term in Hamiltonian by stochastic unraveling rather than doing it with the system-bath coupling as it is usual in ordinary stochastic methods. The evolution of the system's state is modeled by an ensemble of trajectories in the space of the projectors on the states in the system's Hilbert space. This projector space is known in the theory of non-linear spectroscopy as the *Liouville space* (see Ref. [Muk95]). Each trajectory from the ensemble can be assigned a sequence of resonance coupling-free evolution operators that remains after the unraveling. The resulting expression is related to the high order non-linear response functions, and it can be evaluated analytically. The properly weighted sum over trajectories gives an exact result for the system's reduced dynamics.

The proposed method offers an advantage over the existing exact methods in systems with strong system-bath coupling and comparatively weak resonance coupling since the strong coupling to the bath does not increase the computational cost. It can be also very well used in systems with complicated spectral densities, which is a challenging task for the HEOM method.

We apply our method to the case of a heterodimer, motivated by the works on an interaction between charge transfer (CT) states and the excitons in photosynthetic reaction center [Ren04, Man06b]. In the absorption spectrum of this system, one can observe a large blue shift of the lowest energy band with increasing temperature [Hub98]. Previous works used either the local basis [Ren04] or the excitonic basis [Man06b] as a starting point of their theory. It was concluded that the large reorganization energy of the CT state is the reason for the temperature dependent shift of the absorption band. It can be shown that the necessary condition for the band shift is the difference in the energy-gap correlation function of the two involved types of states, the excitonic and the CT states. It can be even shown that in second order theories the non-secular terms, and correspondingly the shift, vanishes when the reorganization energies in the dimer are the same [Man08]. We therefore concentrate on a dimer in which the one dipole forbidden local state is characterized by a large reorganization energy and a zero transition dipole moment (playing thus a role of the CT state), and the second state is optically allowed, characterized by a moderate reorganization energy (playing a role of an excitonic state). Due to the resonance interaction between these two excited states, we observe two peaks in the absorption spectra, which shift as function of the system parameters and various approximations discussed.

5.1 Theory

5.1.1 Basic Principle

Let us introduce a different separation of the total Hamiltonian H, Eq. (1.9), in this section. We define

$$\begin{aligned} H_J = &\sum_{m=1}^{N_e}\sum_{n=1}^{N_e} J_{nm}(|e_m\rangle\langle e_n| + |e_n\rangle\langle e_m|)(1-\delta_{mn}) \\ &+ \sum_{m=1}^{N_f}\sum_{n=1}^{N_f} J^f_{nm}(|f_m\rangle\langle f_n| + |f_n\rangle\langle f_m|)(1-\delta_{mn}) \,, \end{aligned} \tag{5.1}$$

$$H_0 = H - H_J \tag{5.2}$$

the corresponding Liouville superoperators $\mathcal{L}_J$ and $\mathcal{L}_0$, evolutions operators $U_J(t)$ and $U_0(t)$, and superoperators $\mathcal{U}_J(t)$ and $\mathcal{U}_0(t)$. We will start with the closed system, whose evolution superoperator is a solution of the Liouville equation

$$\frac{d}{dt}\mathcal{U}(t) = i(\mathcal{L}_0 + \mathcal{L}_J)\mathcal{U}(t) \,. \tag{5.3}$$

The reason for separation of $\mathcal{L}$ into $\mathcal{L}_0$ and $\mathcal{L}_J$ is that for the case $\mathcal{L}_J = 0$, we can solve the problem with the bath exactly via the cumulant expansion. Provided there is initially no entanglement between the system and the bath, we can write $\mathcal{U}(t)$ as a time-ordered exponential using time-dependent perturbation theory

$$\mathcal{U}(t) = \mathcal{U}_0(t)\Bigg[1 - i\int_0^t d\tau\ \mathcal{L}_J^{(I)}(\tau) + \\ + i^2\int_0^t d\tau \int_0^\tau d\tau'\ \mathcal{L}_J^{(I)}(\tau)\mathcal{L}_J^{(I)}(\tau')\dots\Bigg] \tag{5.4}$$

The interaction picture is taken with respect to the $\mathcal{U}_0(t)$, i. e. $\mathcal{L}_J^{(I)}(t) \equiv \mathcal{U}_0^\dagger(t)\mathcal{L}_J\mathcal{U}_0(t)$.

The proposed stochastic scheme is the following: We generate trajectories, where system exhibits random jumps between projectors on electronic states on Liouville space of electronic states. The jumps are generated in such way that they reconstruct the action of electronic J-coupling, i. e. of $\mathcal{L}_J$. Between the jumps, the system evolves according to $\mathcal{U}_0(t)$. We introduce a time discretization of the time axis into time intervals Δt. The model is exact in the limit $\Delta t \to \infty$. In every time step Δt, there is a probability $J_{ij}\,\Delta t/\hbar$ of the jump between states $|e_i\rangle\langle e_k| \to |e_j\rangle\langle e_k|$ and the same probability of the jump $|e_k\rangle\langle e_i| \to |e_k\rangle\langle e_j|$. In addition to the time evolution according to $\mathcal{U}_0(t)$, the trajectory weighting factor is multiplied by a complex number φ_c, which we will call "coherent factor" (CF) further on in the text. The coherent factor assures the correct stochastic unraveling. For each jump between bra-states, the trajectory gets a factor of $+i$, while for a jump between ket-states, it gets a factor of $-i$. Hence

$$\varphi_\mathrm{c} = i^{N_\mathrm{bra}}(-i)^{N_\mathrm{ket}}\ , \tag{5.5}$$

where N_bra and N_ket are the numbers of the jumps between bra-states and ket-states in the given trajectory, respectively.

If we introduce jump superoperators as

$$\mathcal{J}_{\mathrm{bra},i\to j}\bullet = |e_j\rangle\langle e_i|\bullet, \tag{5.6a}$$

$$\mathcal{J}_{\mathrm{ket},i\to j}\bullet = \bullet|e_i\rangle\langle e_j|, \tag{5.6b}$$

we can describe a trajectory with N jumps in times $t_1, \dots, t_N$ by a sequence of jumps $\mathcal{J}_{\tilde{1}}, \mathcal{J}_{\tilde{2}}, \dots, \mathcal{J}_{\tilde{N}}$, where every index $\tilde{k}$ should be replaced by "details" of the k^th jump, i. e. it should specify if it is a jump in bra or ket vector, and it should state between which of the states the jump occurs. The total evolution

superoperator can be then written as

$$\mathcal{U}(t) = \frac{1}{N_{\mathrm{tr}}} \sum_{n=1}^{N_{\mathrm{tr}}} \varphi_{\mathrm{c},n}\, \mathcal{U}_0(t - t_{N_n}) \mathcal{J}_{\tilde{N}_n,n} \mathcal{U}_0(t_{N_n} - t_{N_n-1}) \\ \times \ldots \mathcal{J}_{\tilde{2},n} \mathcal{U}_0(t_2 - t_1) \mathcal{J}_{\tilde{1},n} \mathcal{U}_0(t_1 - t_0). \tag{5.7}$$

The index n numbers the trajectories, and N_{tr} is number of trajectories.

To show that Eq. (5.7) gives correct result for evolution superoperator, we will investigate the individual terms of the expansion, Eq. (5.4). We can see that the term "$\mathcal{U}_0(t)1$" is covered by trajectories with no jumps, which have the probability

$$p_0 = Z^{t/\Delta t}, \tag{5.8}$$

where Z is the probability that no jump occurs in time interval Δt. If the trajectory starts in a projector $|i_0\rangle\langle j_0|$, Z reads as

$$Z = 1 - \left(\sum_{n \neq i_0} J_{i_0 n} + \sum_{m \neq j_0} J_{m j_0} \right) \Delta t/\hbar. \tag{5.9}$$

The term

$$-i\mathcal{U}_0(t) \int_0^t d\tau\ \mathcal{L}_J^{(I)}(\tau) = -i\mathcal{U}_0(t) \int_0^t d\tau\ \mathcal{U}_0^\dagger(\tau) \mathcal{L}_J \mathcal{U}_0(\tau) \\ \approx -i\mathcal{U}_0(t) \sum_{n=1}^{t/\Delta t} \mathcal{U}_0^\dagger(n\Delta t) \mathcal{L}_J \mathcal{U}_0(n\Delta t) \tag{5.10}$$

of Eq. (5.4) is represented by trajectories with one jump at time $\tau = n\Delta t$, which constitute the individual terms of the sum in Eq. (5.10). A trajectory with one jump evolves according to the evolution superoperator $\mathcal{U}_0(t) = \mathcal{U}_0^{i'j}(t) \mathcal{U}_0^{i'j\dagger}(\tau) \mathcal{U}_0^{ij}(\tau)$, which corresponds to the time evolution in ij-th projector on electronic states for time τ, the action of $\mathcal{L}_J$ which transfers the projector $i'j$ into the projector ij and a time evolution in this projector for time $t - \tau$. The factor "$-i$" is included in the φ_{c}. The probability of such a trajectory with time of the jump τ is given by

$$p_{i'j,ij} = J_{ii'}\, \Delta t/\hbar\ Z^{t/\Delta t - 1}\ . \tag{5.11}$$

It yields the correct ratio

$$\frac{p_{i'j,ij}}{p_0} = \mathcal{L}_J^{i'j,ij} Z^{-1} \approx \mathcal{L}_J^{i'j,ij}\ . \tag{5.12}$$

The Liouvillian $\mathcal{L}_J$ is hence not explicitly present in the sum over trajectories, but

it is included by proportion of trajectories with particular number of jumps, as

$$\frac{1}{\hbar}\mathcal{L}_J = \sum_{i,j} J_{ij}\left(\mathcal{J}_{\mathrm{bra},i\to j} - \mathcal{J}_{\mathrm{ket},i\to j}\right) \ .$$

There is also a trajectory with a jump between the projectors ij and ij' for each trajectory with a jump from ij to $i'j$. It comes from the second term of the commutator, Eq. (1.54). The trajectory gets additional minus sign, and the CF is therefore i, see Eq. (5.5). One easily verifies that trajectories with multiple jumps reconstruct the higher order terms of the expansion, Eq. (5.4).

5.1.2 Bath Influence

For the case of a closed system, the superoperators $\mathcal{U}_0(t)$ in Eq. (5.7) are obtained explicitly. For open systems, we perform a trace over bath DOF and the cumulant expansion, and we get complex factors in terms of the lineshape functions, Eq. (1.34). The reduced evolution superoperator can then be written as

$$\begin{aligned}\mathrm{Tr}_B\,\mathcal{U}(t) = \frac{1}{N_{\mathrm{traj.}}}\sum_{n=1}^{N_{\mathrm{traj.}}} C_n\varphi_{\mathrm{c},n}\,\mathcal{U}_S(t-t_{N_n})\times \\ \mathcal{J}_{\tilde{N}_n,n}\mathcal{U}_S(t_{N_n}-t_{N_n-1})\ldots\mathcal{J}_{\tilde{1},n}\mathcal{U}_S(t_1-t_0)\ . \end{aligned} \tag{5.13}$$

The factor

$$C_n = \mathrm{Tr}_B\left\{\mathcal{U}_B^{\tilde{N}_n}(t_{N_n}-t_{N_n-1})\ldots\mathcal{U}_B^{\tilde{1}}(t_1-t_0)w_{\mathrm{eq}}\right\} \tag{5.14}$$

can be evaluated analytically using second order cumulant expansion in a manner similar to the evaluation of non-linear response functions (see e. g. [Muk95]).

Let us illustrate the procedure on the case with two jumps, one on the bra-side, $\langle g| \to \langle e_i|$, in time t_0 and the other on the ket-side, $|g\rangle \to |e_j\rangle$, in time t_1. The factor (5.14) then yields

$$C = \mathrm{Tr}_B\{U_j^e(t-t_1)U^g(t_1-t_0)w_{\mathrm{eq}}U_i^{e\dagger}(t-t_0)\} \tag{5.15}$$

in the Hilbert-space representation. By proper rearranging of the terms, one can distribute the bath evolution operators into pairs $U_n^e(t)U^{g\dagger}(t)$, $U_n^{e\dagger}(t)U^g(t)$, $U^g(t)U_n^{e\dagger}(t)$ or $U^{g\dagger}(t)U_n^e(t)$ and obtain

$$C = \mathrm{Tr}_B\{U^g(t-t_0)U_i^{e\dagger}(t-t_0)U_j^e(t-t_1)U^{g\dagger}(t-t_1)w_{\mathrm{eq}}\}\ . \tag{5.16}$$

This can always be done provided the bath density matrix is stationary and commutes with the operator $U^g(t)$. This is satisfied for the canonical equilibrium

w_{eq}. One can write evolution equation for the pairs

$$\frac{d}{dt}U_n^e(t)U^{g\dagger}(t) = -\frac{i}{\hbar}U_n^e(t)U^{g\dagger}(t)\Delta V_n(-t)\ , \tag{5.17a}$$

$$\frac{d}{dt}U_n^{e\dagger}(t)U^{g}(t) = \frac{i}{\hbar}U_n^{e\dagger}(t)U^{g}(t)\Delta V_n(t)\ , \tag{5.17b}$$

$$\frac{d}{dt}U^{g}(t)U_n^{e\dagger}(t) = \frac{i}{\hbar}\Delta V_n(-t)U^{g}(t)U_n^{e\dagger}(t)\ , \tag{5.17c}$$

$$\frac{d}{dt}U^{g\dagger}(t)U_n^{e}(t) = -\frac{i}{\hbar}\Delta V_n(t)U^{g\dagger}(t)U_n^{e}(t) \tag{5.17d}$$

with use of their definitions (1.22c) and (1.22d). The procedure that leads to the analytical solution dictates to evaluate all terms of Eq. (5.16) to the second order in the system-bath interaction, which can be done using expansions

$$U_n^e(t)U^{g\dagger}(t) = 1 - \frac{i}{\hbar}\int_0^t d\tau\ \Delta V_n(-\tau) - \frac{1}{\hbar^2}\int_0^t d\tau \int_0^\tau d\tau'\ \Delta V_n(-\tau')\Delta V_n(-\tau)\ , \tag{5.18a}$$

$$U_n^{e\dagger}(t)U^{g}(t) = 1 + \frac{i}{\hbar}\int_0^t d\tau\ \Delta V_n(\tau) - \frac{1}{\hbar^2}\int_0^t d\tau \int_0^\tau d\tau'\ \Delta V_n(\tau')\Delta V_n(\tau)\ , \tag{5.18b}$$

$$U^{g}(t)U_n^{e\dagger}(t) = 1 + \frac{i}{\hbar}\int_0^t d\tau\ \Delta V_n(-\tau) - \frac{1}{\hbar^2}\int_0^t d\tau \int_0^\tau d\tau'\ \Delta V_n(-\tau)\Delta V_n(-\tau')\ , \tag{5.18c}$$

$$U^{g\dagger}(t)U_n^{e}(t) = 1 - \frac{i}{\hbar}\int_0^t d\tau\ \Delta V_n(\tau) - \frac{1}{\hbar^2}\int_0^t d\tau \int_0^\tau d\tau'\ \Delta V_n(\tau)\Delta V_n(\tau')\ . \tag{5.18d}$$

The alone-standing first-order terms vanish after the trace over the bath DOF, because their mean value is zero, $\mathrm{Tr}_B \Delta V_i\, w_{\mathrm{eq}} = 0$. The pairs of the first-order terms that enter as cross-terms between different $U^g U^e$-pairs do not vanish and they have an influence on the total response-function. One can collect and evaluate

all the second-order terms that originate directly from Eqs. (5.18)

$$\frac{1}{\hbar^2}\int_0^t d\tau \int_0^\tau d\tau' \ \mathrm{Tr}_B \Delta V_n(-\tau')\Delta V_n(-\tau) w_{\mathrm{eq}} = g_{nn}(t) \ , \tag{5.19a}$$

$$\frac{1}{\hbar^2}\int_0^t d\tau \int_0^\tau d\tau' \ \mathrm{Tr}_B \Delta V_n(\tau')\Delta V_n(\tau) w_{\mathrm{eq}} = g_{nn}(-t) \ , \tag{5.19b}$$

$$\frac{1}{\hbar^2}\int_0^t d\tau \int_0^\tau d\tau' \ \mathrm{Tr}_B \Delta V_n(-\tau)\Delta V_n(-\tau') w_{\mathrm{eq}} = g_{nn}(-t) \ , \tag{5.19c}$$

$$\frac{1}{\hbar^2}\int_0^t d\tau \int_0^\tau d\tau' \ \mathrm{Tr}_B \Delta V_n(\tau)\Delta V_n(\tau') w_{\mathrm{eq}} = g_{nn}(t) \ . \tag{5.19d}$$

Similarly, one can collect the ones that originate from the first order terms of different $U^g U^e$-pairs

$$\frac{1}{\hbar^2}\int_0^{t_1} d\tau \int_0^{t_2} d\tau' \ \langle \Delta V_m(\tau)\Delta V_n(\tau')\rangle = \\ \delta_{mn}[g_{mm}(t_1) + g_{mm}(-t_2) - g_{mm}(t_1 - t_2)] \ , \tag{5.20a}$$

$$\frac{1}{\hbar^2}\int_0^{t_1} d\tau \int_0^{t_2} d\tau' \ \langle \Delta V_m(\tau)\Delta V_n(-\tau')\rangle = \\ \delta_{mn}[-g_{mm}(t_1) - g_{mm}(t_2) + g_{mm}(t_1 + t_2)] \ , \tag{5.20b}$$

$$\frac{1}{\hbar^2}\int_0^{t_1} d\tau \int_0^{t_2} d\tau' \ \langle \Delta V_m(-\tau)\Delta V_n(\tau')\rangle = \\ \delta_{mn}[-g_{mm}(-t_1) - g_{mm}(-t_2) + g_{mm}(-t_1 - t_2)] \ , \tag{5.20c}$$

$$\frac{1}{\hbar^2}\int_0^{t_1} d\tau \int_0^{t_2} d\tau' \ \langle \Delta V_m(-\tau)\Delta V_n(-\tau')\rangle = \\ \delta_{mn}[g_{mm}(-t_1) + g_{mm}(t_2) - g_{mm}(-t_1 + t_2)] \ . \tag{5.20d}$$

Here, we assumed that the bath operators on different sites are completely uncorrelated. After this procedure, the Eq. (5.16) is written as a sum of lineshape functions

$$C = [-g_{ii}(t_0 - t) - g_{jj}(t - t_1)](1 - \delta_{ij}) - \delta_{ij} g_{ii}(t_0 - t_1) \ . \tag{5.21}$$

The last step is application of the Magnus cumulant expansion. The function (5.15) is trace over product of operator exponentials. We assume ansatz in which

it can be written as an exponential of the lineshape functions. If (some) function $f(x)$ can be written as an expansion

$$f(x) = a_0 + a_1 x + a_2 x^2 + \dots \tag{5.22}$$

or as an expansion

$$f(x) = \exp\left(A_0 + A_1 x + A_2 x^2 + \dots\right) , \tag{5.23}$$

there is a unique correspondence between the coefficients a_i and A_i. We use this correspondence to obtain exponential from the second-order expression (5.21). If only second-order terms are present, trivially $A_2 = a_2$ and Eq. (5.21) yields

$$C = \exp\left([-g_{ii}(t_0 - t) - g_{jj}(t - t_1)](1 - \delta_{ij}) - \delta_{ij} g_{ii}(t_0 - t_1)\right) . \tag{5.24}$$

Intuitively, it can be understood as a proper resummation of the perturbation series that fixes its asymptotic behavior. For Gaussian processes for which only the second-order correlation functions are non-zero, this procedure leads to an exact result [Muk78].

5.1.3 Some Numerical Considerations

We described the basic principle of the method in the previous section, and we showed that it is equivalent to the time evolution via the expansion, Eq. (5.4). The sum over trajectories gives the evolution superoperator $\mathcal{U}(t)$ in some fixed time t. $\mathcal{U}(t)$ is, however, calculated up to a normalization constant, which depends linearly on the number of trajectories and according to Eq. (5.8) also on time. We would like to generate trajectories to a maximum time $t_{\max}$, and use them to evaluate $\mathcal{U}(t)$ for all times $t < t_{\max}$ in such a way that the trajectories are not generated for each time independently. One possibility is simply to use scaling of the normalization, Eq. (5.8), for times $t < t_{\max}$ of every trajectory. However, for technical reasons, we use a different way. We include the trajectory in summation only at times t for which $t_{\mathrm{LJ}} < t < t_{\max}$, where t_{LJ} is the time of the last jump in the trajectory, and we ignore the trajectory in evaluation of the times $t < t_{LJ}$. This also leads to the correct result, because the ratio of the trajectories that have a jump in the interval $t_{\mathrm{LJ}} < t < t_{\max}$ to the total number of trajectories is proportional to the scaling of normalization factor Eq. (5.8) with time

$$\frac{p_{\text{has jumps in } (t_{\mathrm{LJ}}, t_{\max})}}{p_{\text{all}}} = Z^{(t_{\max} - t_{\mathrm{LJ}})/\Delta t}. \tag{5.25}$$

Ignoring trajectories at $t < t_{LJ}$ times thus provides the correct normalization.

5.1.4 Connection to the Feynman-Vernon Influence Functional

The connection can be drawn between the described method and the well-known Feynman-Vernon influence functional [Fey63, Gra88]. Similarly to Eq. (5) in Ref. [Mak95], the path integral for the time evolution of a reduced density matrix can be written in the time-discretised form on a Hilbert space of a finite dimension

$$\begin{aligned}\rho(s'',s';t) = &\sum_{s_0^+}\sum_{s_1^+}\cdots\sum_{s_{N-1}^+}\sum_{s_0^-}\sum_{s_1^-}\cdots\sum_{s_{N-1}^-}\\ &\langle s''|e^{-iH_{SJ}\Delta t/\hbar}|s_{N-1}^+\rangle\ldots\langle s_1^+|e^{-iH_{SJ}\Delta t/\hbar}|s_0^+\rangle\\ &\times\langle s_0^+|\rho_S(0)|s_0^-\rangle\times\\ &\langle s_0^-|e^{iH_{SJ}\Delta t/\hbar}|s_1^-\rangle\ldots\langle s_{N-1}^-|e^{iH_{SJ}\Delta t/\hbar}|s'\rangle\\ &I(s_0^+,\ldots,s_{N-1}^+,s'',s_0^-,\ldots,s_{N-1}^-,s';t)\ .\end{aligned}\tag{5.26}$$

Here $H_{SJ}=H_S+H_J$, $\rho_S(0)$ is the initial system reduced density matrix and s_i^+, s_i^-, s', s'' number states from the system's Hilbert space. The sums run through the whole Hilbert space of the system. The time is discretized into N steps of size Δt. The influence functional has a form

$$\begin{aligned}&I(s_0^+,\ldots,s_{N-1}^+,s'',s_0^-,\ldots,s_{N-1}^-,s';t)\\ &\quad=\mathrm{Tr}_B[e^{-i\langle s''|H_{BSB}|s''\rangle\Delta t/2\hbar}e^{-i\langle s_{N-1}^+|H_{BSB}|s_{N-1}^+\rangle\Delta t/\hbar}\\ &\qquad\times\ldots e^{-i\langle s_0^+|H_{BSB}|s_0^+\rangle\Delta t/2\hbar}w_{\mathrm{eq}}e^{i\langle s_0^-|H_{BSB}|s_0^-\rangle\Delta t/2\hbar}\\ &\qquad\times\ldots e^{i\langle s_{N-1}^-|H_{BSB}|s_{N-1}^-\rangle\Delta t/\hbar}e^{i\langle s'|H_{BSB}|s'\rangle\Delta t/2\hbar}]\ ,\end{aligned}\tag{5.27}$$

where $H_{BSB}=H_B+H_{S-B}$.

Our method, to which we will refer as to stochastic unraveling of resonance coupling (SURC) method in the rest of this work, relies on an approximation of the expression $e^{-iH_{SJ}\Delta t/\hbar}$ in the Eq. (5.26) using the Trotter expansion $e^{-i(H_S+H_J)\Delta t/\hbar}\approx e^{-iH_S\Delta t/\hbar}e^{-iH_J\Delta t/\hbar}$. This expression after further approximation yields

$$e^{-iH_{SJ}\Delta t/\hbar}\approx e^{-iH_S\Delta t/\hbar}\sum_{rs}\left(\delta_{rs}-\frac{i}{\hbar}J_{rs}\Delta t\right)|r\rangle\langle s|\ .\tag{5.28}$$

If the path integral was to be performed without any importance sampling at this point, at each timestep, we would have trajectories that jump between the states $|r\rangle$ and $|s\rangle$ and gain factor $iJ_{rs}\Delta t/\hbar$ and those that stay in the same state $|r\rangle=|s\rangle$ and gain factor "1". Trajectories with too many jumps, however, tend to cancel each other. The SURC can thus be viewed as an importance

sampling in which we prefer the trajectories with less jumps by factor $J_{rs}\Delta t/\hbar$, and we increase correspondingly the phase change if the jump occurs. This allows us to trivially perform most of the summations in Eq. (5.26), because terms $\langle s_i^-|e^{iH_S J\Delta t/\hbar}|s_{i+1}^-\rangle \approx \langle s_i^-|e^{iH_S\Delta t/\hbar}|s_{i+1}^-\rangle\delta_{s_i^- s_{i+1}^-}$ for most of the cases. Luckily, our influence functional has a particularly simple form: If there is a sequence of consecutive states $|s_i\rangle$, $|s_{i+1}\rangle$,..., $|s_n\rangle$, for which $|s_i\rangle = |s_{i+1}\rangle = \cdots = |s_n\rangle$, all factors with indices between $(i+1)$ and $(n-1)$ can be expressed as one factor in terms of the lineshape functions and the states can be excluded from the expression for the influence functional.

5.2 Numerical Results

In this section, we study the dynamics of optical coherences of the density matrix of a molecular dimer in order to test the precision and the numerical stability of our method. We will demonstrate how the SURC works for a simple system with no bath, i. e. the case

$$T = V_g = V_n^e(\{Q\}) = V_n^f(\{Q\}) = 0 \tag{5.29}$$

of the total Hamiltonian (1.9), and for an exactly solvable system with a simple model of bath. We also calculate absorption spectra of a model dimer with full harmonic bath and compare the results obtained by this method with those obtained with the full and secular TL-QME (1.84) and with the HEOM.

First, we demonstrate that the method correctly reproduces coherent quantum dynamics. We set the same excitation energies for both molecules $\epsilon_1 = \epsilon_2 = 10^4$ cm^{-1} and a non-zero resonance coupling $J = 50$ cm^{-1}. The bath is not present, Eq. (5.29), and the dynamics can therefore be solved exactly. We calculate the element $\mathcal{U}_{e_1g,e_1g}(t)$ of the evolution superoperator, and we compare the exact dynamics with the dynamics obtained by SURC. The results are presented in Fig. 5.1. We present the results of three runs of SURC, each of them performed with 10^8 trajectories. SURC dynamics is very close to the exact one. At longer times, SURC runs start to differ from the exact solution and the convergence gets worse. The numerical noise does not allow calculation to times longer than approximately $\hbar/(2\pi J)$.

To show that the SURC method is exact also for an open system with harmonic bath, we calculate element $\mathcal{U}_{e_1g,e_1g}(t)$ of the evolution superoperator for a molecular dimer with simple bath that allows exact solution of the model. It is represented by a single undamped harmonic oscillator, EGCF (1.41) for each molecule. In the SURC calculation, harmonic oscillators are treated implicitly by EGCF, Eq. (1.41).

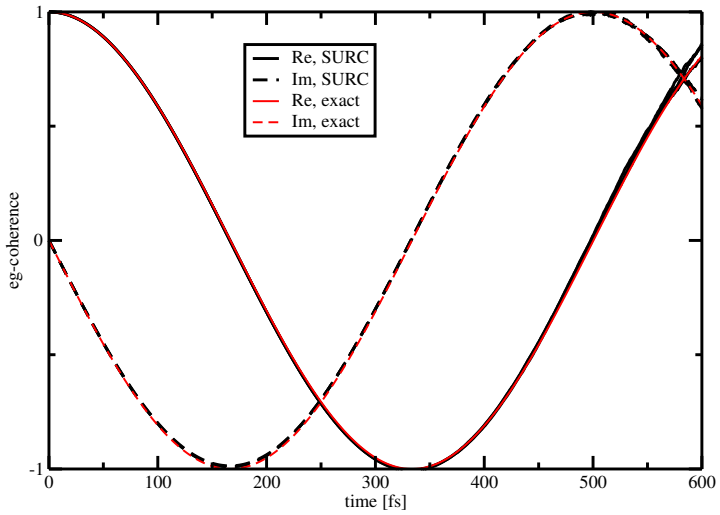

Figure 5.1: "Optical coherence" element $\mathcal{U}_{e_1g,e_1g}(t)$ of the evolution superoperator of a molecular homodimer in no contact with bath. The site and resonance interaction energies are $\epsilon_1 = \epsilon_2 = 10^4$ cm^{-1}, $J = 50$ cm^{-1}, and the frequency 10^4 cm^{-1} is subtracted from the plot. The red lines correspond to the explicit exact solution of the dynamics, black lines represent the dynamics calculated by SURC using 10^8 trajectories. Full lines correspond to the real part and dashed lines to the imaginary part.

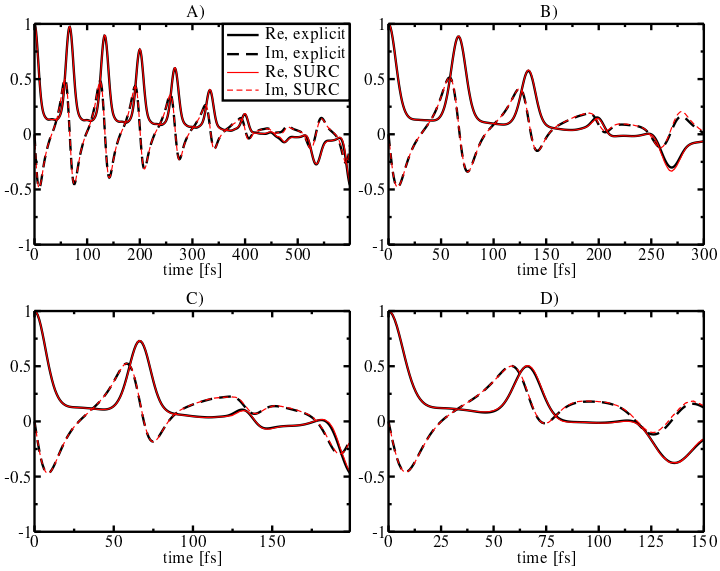

Figure 5.2: "Optical coherence" element $\mathcal{U}_{e_1g,e_1g}(t)$ of the evolution superoperator of a molecular homodimer coupled with one harmonic oscillator per site. The site energies and the reorganization energies are $\epsilon_1 = \epsilon_2 = 10^4$ cm^{-1}, $\lambda_1 = \lambda_2 = 500$ cm^{-1}, the oscillator frequencies are $\omega_1 = \omega_2 = 500$ cm^{-1}, and the frequency 10^4 cm^{-1} is subtracted from the plot. The resonance interaction energy J has values of 50 cm^{-1}, 100 cm^{-1}, 150 cm^{-1}, 200 cm^{-1} in plots A), B), C) and D). The red lines correspond to the explicit exact solution of the dynamics, black lines represent dynamics by SURC using 10^8 trajectories. Full lines correspond to the real part and dashed lines to the imaginary part. Temperature of the initial condition is $T = 100$ K.

This calculation is compared in Fig. 5.2 with the exact explicit solution. The calculated system is a homodimer with parameters $\epsilon_1 = \epsilon_2 = 10^4$ cm^{-1}, $\lambda_1 = \lambda_2 =$ 500 cm^{-1}, $\omega_1 = \omega_2 = 500$ cm^{-1} and the temperature of initial condition, Eq. (1.73), equal to 100 K. We performed four calculations for values of $J = 50$ cm^{-1}, 100 cm^{-1}, 150 cm^{-1} and 200 cm^{-1}. We can see that the correspondence of the exact solution with the SURC solution is very good. The time up to which we can calculate is inversely proportional to J.

Let us now compare the absorption spectra calculated by SURC with other frequently used theories. We use a dimer with parameters $\epsilon_1 = 9600$ cm^{-1}, $\epsilon_2 =$ 10000 cm^{-1}, $\lambda_1 = 100$ cm^{-1}, $\lambda_2 = 1000$ cm^{-1}, $\tau_{c,1} = \tau_{c,2} = 100$ fs. The big difference in reorganization energies is typical in situations where the molecules have very different surroundings (e. g. protein envelope and water) or for systems with both excitonic and charge transfer states, as discussed in the Introduction. Only the site 1 has non-zero transition dipole moment, since the site 2 represents a CT state. The length of the dipole moment is arbitrary since it only changes normalization of the spectra. The Fig. 5.3 shows absorption spectra in three cases: $J = 0$ cm^{-1}, 100 cm^{-1} and 300 cm^{-1}. For $J = 0$ cm^{-1}, this is a problem of non-interacting monomers which is exactly solvable [Dol08, Man11], and all theories give the same result. With a gradual increase of J, we see an increase of the excitonic splitting, noticeable as a shift of the higher of the peaks (lower transition frequency) to the red. The results of full TL-QME and SURC calculations are similar, while the secular approximation gives an exaggerated peak splitting. The HEOM, which is considered an exact theory in this regime of parameters, is in very good agreement with the SURC method. The Fig. 5.5A plots the positions of the lower frequency peak for the four theories and quantifies the difference in its shift with J. Already here, we can conclude that the full TL-QME captures the decrease of the excitonic splitting with respect to the excitonic basis surprisingly well.

In Fig. 5.4 we plot the temperature depentdence of the absorption spectra for the same model dimer. Here, we can notice that the SURC is in nearly perfect match with the HEOM, and that the full TL-QME also captures the right tendency. We can notice a shift of the lower frequency peak to higher frequencies with increasing temperature. This demonstrates an increasing dynamic localization by the bath with increasing temperature. The secular TL-QME gives opposite peak shift with respect to the other theories. This shift is caused by the slight temperature dependent changes in the lines shape, because the transition frequencies remain the same for all temperatures in the secular TL description. For lower temperatures, we can notice a difference between the SURC and full TL-QME in the width of the wider peak. With increasing temperature, these two theories also increasingly differ in the lower frequency peak position, as is shown

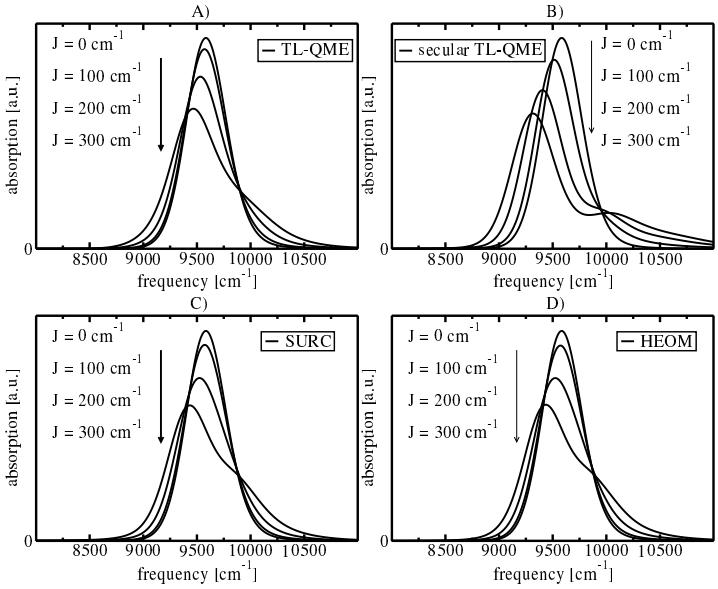

Figure 5.3: Absorption spectra of a molecular homodimer coupled to an overdamped harmonic bath, EGCF (1.47), calculated by A) full TL-QME, B) secular TL-QME, C) SURC and D) HEOM. The parameters are $\epsilon_1 = 9600$ cm^{-1}, $\epsilon_2 = 10000$ cm^{-1}, $\lambda_1 = 100$ cm^{-1}, $\lambda_2 = 1000$ cm^{-1}, $\tau_{c,1} = \tau_{c,2} = 100$ fs and $T = 300$ K. Absorption spectra are calculated for $J = 0$ cm^{-1}, $J = 100$ cm^{-1}, $J = 200$ cm^{-1} and $J = 300$ cm^{-1}.

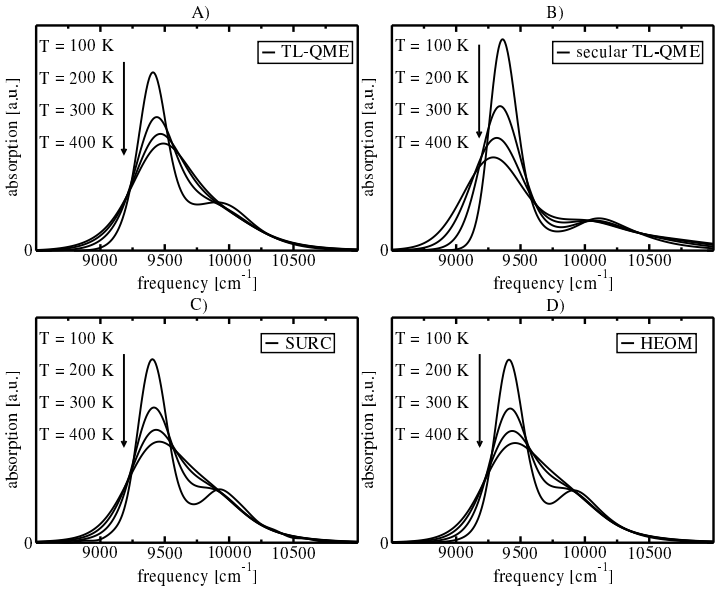

Figure 5.4: Temperature dependence of the absorption spectra of a molecular homodimer coupled to an overdamped harmonic bath, EGCF (1.47), calculated by A) full TL-QME, B) secular TL-QME, C) SURC theory and D) HEOM. The parameters are $\epsilon_1 = 9600$ cm^{-1}, $\epsilon_2 = 10000$ cm^{-1}, $\lambda_1 = 100$ cm^{-1}, $\lambda_2 = 1000$ cm^{-1}, $J = 300$ cm^{-1} and $\tau_{c,1} = \tau_{c,2} = 100$ fs. Absorption spectra are calculated for temperatures ranging from 100 K to 400 K. Figure D) shows the change of the left peak frequency with temperature for all three aforementioned theories.

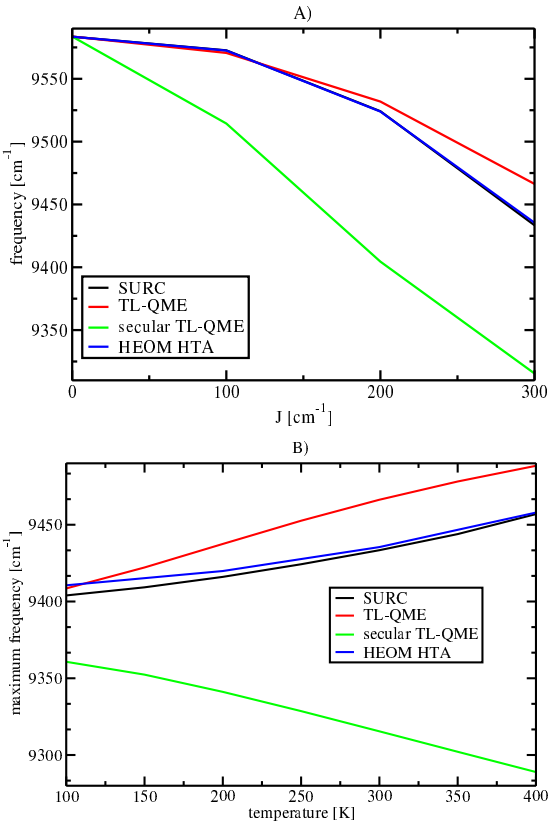

Figure 5.5: Positions of the maxima of the lower frequency peak of the spectra for A) resonance coupling dependence (Fig. 5.3) and B) temperature dependence (Fig. 5.4).

on Fig. 5.5B. The nearly perfect match of SURC and HEOM gets worse at lower temperatures, which is caused by employing the high-temperature approximation (HTA) [Ish09c] of Eq. (1.47) in the HEOM case:

$$C_{mn}^{\mathrm{HTA}}(t) = \frac{2\lambda}{\beta}\frac{(3\Lambda^2 - \nu_1^2)e^{-\Lambda t} - 2\Lambda\delta(t)}{\Lambda^2 - \nu_1^2}\delta_{mn} - i\hbar\lambda\Lambda\delta_{mn}e^{-\Lambda t}\,, \tag{5.30}$$

which requires $\hbar\beta\Lambda < 1$. The HTA extends the range of validity of HEOM towards lower temperatures while at the same time it preserves an exponential time-decay the correlation function. This is essential for constructing the reduced hierarchy in a computationally efficient manner and ties HEOM to specific forms of the spectral density. Arbitrary spectral densities and lower temperatures are readily implemented in SURC using the exact EGCF, whereas the treatment by HEOM requires a decomposition of the spectral density into shifted peaks [Tan94, Kre12].

In its present form, the SURC is limited to short time evolution due to the dynamic sign problem. For the cases discussed here, the HEOM implementation on massively parallel graphics processing units (GPU-HEOM) [Kre13] exceeds the SURC implementation in speed. However, the SURC is also massively parallelizable. Moreover, it has minimal memory requirements independent of the system size and its computational cost does not increase with the complexity of the EGCF used. For example, the treatment of spectral densities with n shifted peaks by HEOM [Tan94, Kre12] can be a challenging task in some cases since the HEOM computational cost grows as $\frac{1}{2nN}\frac{(2nN+k)!}{k!(2nN-1)!}$ both in memory and CPU time, where N is the number of sites and k is the Hierarchy depth required for convergence. The SURC may therefore offer advantage over the HEOM for larger systems with more involved spectral densities, or serve as a good check of convergence for HEOM.

CONCLUSION

In this thesis, we have focused on the problems of relaxation, energy transfer and decoherence in the photosynthetic molecular aggregates. Motivated by the fast progress in the ultrafast non-linear spectroscopy, we followed a research program that aims to improve the description of the photo-induced dynamics of molecular aggregates. Generally, there is a lack of theories able to correctly describe the relaxation, energy transfer and decoherence induced by the coupling of the molecular aggregate to the phonon bath on the sub-picosecond timescales probed by the non-linear spectroscopic experiments. This makes this area of research very interesting. We have centered the discussion around three related problems: Firstly, we studied effects of the Markov and the secular approximations on the coherence lifetime and energy transfer in the time local and non-local theories of second-order in the system-bath coupling. Secondly, we have improved the description of the bath correlations between the intervals of the second-order photo-induced response function that were treated by construction of a new quantum master equation derived in the formalism of parametric projection operators. And thirdly, we developed the new stochastic method based on the unraveling of the resonance-coupling by the cumulant expansion.

Summary of Work Done

The first part of the work highlights the importance of the non-secular effects to the question whether the energy transfer in the photosynthetic systems can be enhanced by the presence of the quantum coherence. Such enhancement would be essentially a non-secular effect. The discussion started together with the surprising discovery of the long coherence lifetime in the FMO complex [Eng07]. Now, certain part of the scientific community accepts the enhancement of the energy transfer efficiency by the quantum coherence as an established fact [Bal11, Ved11], although no positive evidence to support such claims is available [Man13a]. Our results indicate that the non-secular effects seem rather small, which agrees with the results

of other authors [Pan11]. Further, our results indicate that among the models of second-order in the system-bath coupling, (and within the range of parameters we investigated), the time local equations predict too short lifetime of the electronic coherence in comparison to the lifetime of oscillations in experiments measured on most photosynthetic molecular aggregates [Lee07, Cal09, Mer09, Col10, Har12] as well as in comparison to the results of the hierarchical equations of motion [Ish09b, Zhu11, Kre12]. The time non-local equations predict wider range for the coherence lifetime depending on the bath correlation time and they are thus consistent with the results both of the hierarchical equations of motion and the experimental data. They also grant stability with respect to the breakdown of positivity typical for the time-local equations. The lifetime observed in the FMO complex [Eng07] is longer than a picosecond and it is thus not well explained by the TNL model we investigated, nor by the non-perturbative theories.

In the second part, we followed the result of [Man12] that the third and the second order response of a multilevel system cannot be completely evaluated by propagating reduced density matrix by the equations of motion derived using a single projection operator. Such treatment would inevitably neglect correlations between the time evolution of the bath during the neighboring intervals of the non-linear response function. We presented the parametric projector quantum master equation that approximately accounts for these correlations in the second interval of the second-order response function. We showed that in the absence of the resonance coupling the method yields an agreement with the result obtained by the second order cumulant method. We confirmed by numerical simulations that for different delays τ between the excitation pulses, distinct dynamics of both excited state populations and electronic coherence occurs, in the presence of environmental degrees of freedom with finite bath correlation time and in the presence of intra-molecular vibrations. The two-dimensional Fourier transformed spectroscopy sees in these cases some averaged dynamics.

The aforementioned investigation of the non-secular effects is also an important source of motivation for the third research topic presented in this thesis. We proposed a method using a stochastic unraveling of the resonance coupling (SURC) by the cumulant expansion. The method is massively parallelizable, allows the use of arbitrary energy-gap correlation function, and it is exact for Gaussian harmonic baths, which we tested by comparing it with exactly solvable model of a dimer with single vibrational coordinate on both sites. The method was used to evaluate the optical coherence dynamics in a model dimer, where one site represents a normal electronic state and the other represents a charge-transfer state with large reorganization energy and zero transition dipole moment. Unlike in the systems investigated in the first part of the thesis, the non-secular effects play an important

part here and the effect is clearly visible already in the dimer absorption spectrum. We should stress here that in this case, the non-secular effects are not connected to the energy transfer, but only to the mixing of the optical coherences. Detailed and precise method is required to describe these non-secular effects properly. We investigated the dependence of absorption spectrum of the dimer on temperature and resonance coupling. Comparison with full time-local quantum master equation leads us to a conclusion that despite the well-known problems of the time-local approach, such as the positivity breaking under some parameters, it describes the non-secular effects between the optical coherences rather well for the used range of parameters. On the other hand the failure of the secular theory clearly shows the importance of the non-secular effects in the system. The match with the hierarchical equations of motion is very good, which also serves as a good benchmark of both theories.

Outlook

The fact that neither the TNL second-order quantum master equations nor the hierarchical equations of motion predict the correct lifetime of oscillations in the 2DES of the FMO probably indicates that the observed oscillations are either not entirely caused by the electronic coherence or that the FMO complex is very special in some other way. (For example by presence of strong bath correlations between different chromophores [Pan10].) Although the atomistic simulations do not indicate any spatial correlations between the baths of the Chlorophyll molecules [Olb11], other explanations exist as well. It was proposed that although the purely vibrational origin of the coherence was excluded in the original article [Eng07], the superposition of the electronic and vibrational states can correctly explain the effect [Chr12, Che13a, Tiw13]. The electronic states enhance the intensity of the resonant vibrational states that provide the prolonged lifetime typical for the coherence between the vibrational DOF. The increase of the energy transfer hypothesis still remains an ungrounded speculation.

The proposed approach using parametric projection quantum master equation for description of the bath correlations between the intervals of the second-order response function has some remarkable properties. While other theories, such as the hierarchical equations of motion, are able to describe these bath-correlation effects as well, they are usually numerically very costly. Some molecular aggregates relevant in the primary processes of photosynthesis, such as the FMO, already present great challenge for them [Hei12]. The proposed approach offers a possibility of calculations at very low numerical cost, which could allow calculations for bigger systems. Also, the extension of the method to the third-order response function

necessary for the calculation of the 2DES experiments, presents very promising area for further research. Such approach presents certain challenges: While in the first interval of the response function, the optical coherences mix only due to the non-secular effects and they mostly remain in single Liouville pathway, in its second interval, the populations are significantly transferred due to relaxation. Therefore, the populations do not stay within single Liouville pathway approximations used in derivation of the parametric QME for the second interval of the response will probably not be well-satisfied.

The SURC method is very promising as well. It can be easily used with a bath specified by an arbitrary energy gap correlation function, which is, for example, numerically very costly for the hierarchical equations of motion. It has almost no memory requirements and allows massive parallelization. In principle, it can be also extended to allow the description of the laser-pulse excitations and therefore the calculation of the third-order response function, the core object probed by the non-linear spectroscopy. However, there is currently an important difficulty arising from the so-called dynamic sign problem, a numerical instability caused by the summation of many complex-valued factors with different phases, which prevents useful calculation in times longer that few hundreds of femtoseconds. There is a hope that this instability could be lifted by performing the unraveling not in the site basis, but for example in the excitonic basis, where no additional stochastic jumps will be required after the thermalization is reached. The limited amount of jumps would significantly improve the dynamic sign problem, which makes further development of the SURC method promising area for the future work.

BIBLIOGRAPHY

[Abr06] D. Abramavičius and S. Mukamel, *J. Chem. Phys.* **124**, 034113, (2006).

[Abr09] D. Abramavičius, B. Palmieri, D. V. Voronine, F. Šanda, and S. Mukamel, *Chem. Rev.* **109**, 2350, (2009).

[Abr10] D. Abramavičius and S. Mukamel, *J. Chem. Phys.* **133**, 064510, (2010).

[Aha93] Y. Aharonov, L. Davidovich, and N. Zagury, *Phys. Rev. A* **48**, 1687–1690, (1993).

[Arg64] P. N. Argyres and P. L. Kelley, *Phys. Rev. A* **134**, 98, (1964).

[Bal11] P. Ball, *Nature* **474**, 272–274, (2011).

[Bar99] I. Barvík, V. Čápek, and P. Heřman, *J. Lumin.* **83-84**, 105, (1999).

[Bla02] R. E. Blankenship, *Molecular Mechanism of Photosynthesis.* Blackwell Science, Oxford, (2002).

[Bri04a] T. Brixner, T. Mančal, I. V. Stiopkin, and G. R. Fleming, *J. Chem. Phys.* **121**, 4221, (2004).

[Bri04b] T. Brixner, I. V. Stiopkin, and G. R. Fleming, *Opt. Lett.* **29**, 884, (2004).

[Bru12] P. Brumer and M. Shapiro, *Proc. Natl. Acad. Sci. U. S. A.* **109**, 19575–19578, (2012).

[Cal09] T. R. Calhoun, N. S. Ginsberg, G. S. Schlau-Cohen, Y.-C. Cheng, M. Ballottari, R. Bassi, and G. R. Fleming, *J. Phys. Chem. B* **113**, 16291, (2009).

[Car12] J. R. Caram, N. H. C. Lewis, A. F. Fidler, and G. S. Engel, *J. Chem. Phys.* **136**, 104505, (2012).

[Che13a] A. Chenu, N. Christensson, H. F. Kauffmann, and T. Mančal, *Scientific Reports* **3**, 2029, (2013).

[Che13b] A. Chenu, P. Malý, and T. Mančal, *ArXiv* 1306.1693, (2013).

[Cho05] M. H. Cho, H. M. Vaswani, T. Brixner, J. Stenger, and G. R. Fleming, *J. Phys. Chem. B* **109**, 10542, (2005).

[Chr12] N. Christensson, H. F. Kauffmann, T. Pullerits, and T. Mančal, *J. Phys. Chem. B* **116**, 7449, (2012).

[Col09] E. Collini and G. D. Scholes, *Science* **323**, 369, (2009).

[Col10] E. Collini, C. Y. Wong, K. E. Wilk, P. M. G. Curmi, P. Brumer, and G. D. Scholes, *Nature* **463**, 644, (2010).

[Cow04] M. L. Cowan, J. P. Ogilvie, and R. J. D. Miller, *Chem. Phys. Lett.* **386**, 184, (2004).

[Dal92] J. Dalibard, Y. Castin, and K. Molmer, *Phys. Rev. Lett.* **68**, 580–583, (1992).

[Dol08] R. Doll, D. Zueco, M. Wubs, S. Kohler, and P. Hanggi, *Chem. Phys.* **347**, 243, (2008).

[Dre03] J. Dreyer, A. M. Moran, and S. Mukamel, *Bull. Korean Chem. Soc.* **24**, 1091–1096, (2003).

[Eng07] G. S. Engel, T. R. Calhoun, E. L. Read, T.-K. Ahn, T. Mančal, Y.-C. Cheng, R. E. Blankenship, and G. R. Fleming, *Nature* **446**, 782, (2007).

[Fai00] B. Fain, *Irreversibilities in Quantum Mechanics*. Kluwer Academic Publishers, Dordrecht, (2000).

[Fas12] F. Fassioli, A. Olaya-Castro, and G. D. Scholes, *J. Phys. Chem. Lett.* **3**, 3136–3142, (2012).

[Fey63] R. P. Feynman and F. L. Vernon, *Annals of Physics* **24**, 118–173, (1963).

[Foe48] T. Foerster, *Annalen der Physik* **2**, 55–75, (1948).

[Gel05] M. F. Gelin, D. Egorova, and W. Domcke, *J. Chem. Phys.* **123**, 164112, (2005).

[Gev00] E. Geva, E. Rosenman, and D. Tannor, *J. Chem. Phys.* **113**, 1380, (2000).

[Gra88] H. Grabert, P. Schramm, and G. L. Ingold, *Phys. Rep.-Rev. Sec. Phys. Lett.* **168**, 115–207, (1988).

[Gre98] W. Greiner, *Quantum Mechanics: Special Chapters.* Springer-Verlag, Berlin Heidelberg New York, (1998).

[Har12] E. Harel and G. S. Engel, *Proc. Natl. Acad. Sci. U. S. A.* **109**, 706, (2012).

[Has77] N. Hashitsume, F. Shibata, and M. Shingu, *J. Stat. Phys.* **17**, 155–169, (1977).

[Hei12] B. Hein, C. Kreisbeck, T. Kramer, and M. Rodríguez, *New J. Phys.* **14**, 023018, (2012).

[Hub59] J. Hubbard, *Phys. Rev. Lett.* **3**, 77–78, (1959).

[Hub98] H. Huber, M. Meyer, H. Scheer, W. Zinth, and J.Wachtveitl, *Photosynthesis Research* **55**, 153, (1998).

[Huo10] P. Huo, S. Bonella, L. Chen, and D. F. Coker, *Chem. Phys.* **370**, 87–97, (2010).

[Ish05] A. Ishizaki and Y. Tanimura, *J. Phys. Soc. Jpn.* **74**, 3131–3134, (2005).

[Ish08] A. Ishizaki and Y. Tanimura, *Chem. Phys.* **347**, 185, (2008).

[Ish09a] A. Ishizaki and G. R. Fleming, *J. Chem. Phys.* **130**, 234110, (2009).

[Ish09b] A. Ishizaki and G. R. Fleming, *J. Chem. Phys.* **130**, 234111, (2009).

[Ish09c] A. Ishizaki and G. R. Fleming, *Proc. Natl. Acad. Sci. U. S. A.* **106**, 17255, (2009).

[Ish10] A. Ishizaki and G. R. Fleming, *New Journal of Physics* **12**, 055004, (2010).

[Ish11] A. Ishizaki and G. R. Fleming, *J. Phys. Chem. B* **115**, 6227–6233, (2011).

[Jan04] S. Jang, M. D. Newton, and R. J. Silbey, *Phys. Rev. Lett.* **92**, 218301, (2004).

[Jon03] D. M. Jonas, *Annu. Rev. Phys. Chem.* **54**, 425, (2003).

[Ken82] V. M. Kenkre and P. Reineker, *Exciton Dynamics in Molecular Crystals and Aggregates.* Springer, (1982).

[Kje06] P. Kjellberg, B. Bruggemann, and T. Pullerits, *Physical Review B* **74**, 024303, (2006).

[Kre11] C. Kreisbeck, T. Kramer, M. Rodriguez, and B. Hein, *J. Chem. Theory Comput.* **7**, 2166, (2011).

[Kre12] C. Kreisbeck and T. Kramer, *J. Phys. Chem. Lett.* **3**, 2828, (2012).

[Kre13] C. Kreisbeck and T. Kramer. Exciton dynamics lab for light-harvesting complexes (gpu-heom), (2013). electronic tool at nanohub.org.

[Kub69] R. Kubo, *Adv. Chem. Phys.* **15**, 11, (1969).

[Lac05] D. Lacroix, *Phys. Rev. A* **72**, 013805, (2005).

[Lee07] H. Lee, Y.-C. Cheng, and G. Fleming, *Science* **316**, 1462–1465, (2007).

[Mak95] N. Makri and D. E. Makarov, *J. Chem. Phys.* **102**, 4600–4610, (1995).

[Man06a] T. Mančal, A. V. Pisliakov, and G. R. Fleming, *J. Chem. Phys.* **124**, 234504, (2006).

[Man06b] T. Mančal, L. Valkunas, and G. R. Fleming, *Chem. Phys. Lett.* **432**, 301, (2006).

[Man08] T. Mančal, L. Valkunas, E. L. Read, G. S. Engel, T. R. Calhoun, and G. R. Fleming, *Spectroscopy* **22**, 199, (2008).

[Man10] T. Mančal and L. Valkunas, *New Journal of Physics* **12**, 065044, (2010).

[Man11] T. Mančal and F. Šanda, *ArXiv* 1011.3803v1, (2011).

[Man12] T. Mančal and F. Šanda, *Chem. Phys. Lett.* **530**, 140–144, (2012).

[Man13a] T. Mančal, *J. Phys. Chem. B* **117**, 11282–11291, (2013).

[Man13b] T. Mančal. *Quantum Effects in Biology*, chapter Principles of Multi-Dimensional Electronic Spectroscopy. Cambridge University Press, (2013). To be published.

[May01] V. May and O. Kühn, *Charge and Energy Transfer Dynamics in Molecular Systems*. Wiley-VCH, Berlin, (2001).

[Mei97] T. Meier, V. Chernyak, and S. Mukamel, *J. Chem. Phys.* **107**, 8759, (1997).

[Mer09] I. P. Mercer, Y. C. El-Taha, N. Kajumba, J. P. Marangos, J. W. G. Tisch, M. Gabrielsen, R. J. Cogdell, E. Springate, and E. Turcu, *Phys. Rev. Lett.* **102**, 057402, (2009).

[Mo05] Y. Mo, R.-X. Xu, P. Cui, and Y. Yan, *J. Chem. Phys.* **122**, 084115, (2005).

[Moh08] M. Mohseni, P. Rebentrost, S. Lloyd, and A. Aspuru-Guzik, *J. Chem. Phys.* **129**, 174106, (2008).

[Muk78] S. Mukamel, I. Oppenheim, and J. Ross, *Phys. Rev. A* **17**, 1988–1998, (1978).

[Muk79] S. Mukamel, *Chem. Phys.* **37**, 33–47, (1979).

[Muk95] S. Mukamel, *Principles of nonlinear spectroscopy.* Oxford University Press, Oxford, (1995).

[Nak58] S. Nakajima, *Progress Of Theoretical Physics* **20**, 948–959, (1958).

[Nem08] A. Nemeth, F. Milota, T. Mančal, V. Lukeš, H. F. Kauffmann, and J. Sperling, *Chem. Phys. Lett.* **459**, 94, (2008).

[Nem10] A. Nemeth, F. Milota, T. Mančal, V. Lukeš, J. Hauer, H. F. Kauffmann, and J. Sperling, *J. Chem. Phys.* **132**, 184514, (2010).

[Nov03] V. Novoderezhkin, M. Wendling, and R. v Grondelle, *J. Phys. Chem. B* **107**, 11534, (2003).

[Nov05] V. I. Novoderezhkin, M. A. Palacios, H. v Amerongen, and R. v Grondelle, *J. Phys. Chem. B* **109**, 10493, (2005).

[Olb11] C. Olbrich, J. Strümpfer, K. Schulten, and U. Kleinekathöfer, *J. Phys. Chem. B* **115**, 758–764, (2011).

[Olš10] J. Olšina and T. Mančal, *J. Mol. Model.* **16**, 1765–1778, (2010).

[Olš11] J. Olšina, F. Šanda, L. Valkunas, and T. Mančal. Towards understanding the role of coherent dynamics in natural light harvesting. In *Ultrafast Phenomena XVII* 604–606. Oxford University Press, (2011).

[Olš12] J. Olšina and T. Mančal, *Chem. Phys.* **404**, 103–115, (2012).

[Olš13] J. Olšina, T. Kramer, C. Kreisbeck, and T. Mančal, *ArXiv* 1309.0749v1, (2013).

[Pal09] B. Palmieri, D. Abramavičius, and S. Mukamel, *J. Chem. Phys.* **130**, 204512, (2009).

[Pan10] G. Panitchayangkoon, D. Hayes, K. A. Fransted, J. R. Caram, E. Harel, J. Wen, R. E. Blankenship, and G. S. Engel, *Proc. Natl. Acad. Sci. U. S. A.* **107**, 12766–12770, (2010).

[Pan11] G. Panitchayangkoon, D. V. Voronine, D. Abramavičius, J. R. Caram, N. H. C. Lewis, S. Mukamel, and G. S. Engel, *Proc. Natl. Acad. Sci. U. S. A.* **108**, 20908–20912, (2011).

[Pis06] A. V. Pisliakov, T. Mančal, and G. R. Fleming, *J. Chem. Phys.* **124**, 234505, (2006).

[Rea07] E. L. Read, G. S. Engel, T. R. Calhoun, T. Mančal, T. K. Ahn, R. E. Blankenship, and G. R. Fleming, *Proc. Natl. Acad. Sci. U. S. A.* **104**, 14203, (2007).

[Red65] A. G. Redfield, *Advances in Magnetic Resonance* **1**, 1, (1965).

[Ren04] T. Renger, *Phys. Rev. Lett.* **93**, 188101, (2004).

[Rhe09] H. Rhee, Y.-G. June, J.-S. Lee, K.-K. Lee, J.-H. Ha, Z. H. Kim, S.-J. Jeon, and M. Cho, *Nature* **548**, 310, (2009).

[Ric10] M. Richter and A. Knorr, *Annals of Physics* **325**, 711–747, (2010).

[Sch07] M. Schröder, M. Schreiber, and U. Kleinekathöfer, *J. Chem. Phys.* **126**, 114102, (2007).

[Sha04] J. Shao, *J. Chem. Phys.* **120**, 5053–5056, (2004).

[Sha06] J. Shao, *Chem. Phys.* **322**, 187–192, (2006).

[Shi77] F. Shibata, Y. Takahashi, and N. Hashitsume, *J. Stat. Phys.* **17**, 4, (1977).

[Shi03] Q. Shi and E. Geva, *J. Chem. Phys.* **119**, 12063–12076, (2003).

[Sto02] J. T. Stockburger and H. Grabert, *Phys. Rev. Lett.* **88**, 170407, (2002).

[Tan89] Y. Tanimura and R. Kubo, *J. Phys. Soc. Jpn.* **58**, 101–114, (1989).

[Tan94] Y. Tanimura and S. Mukamel, *J. Phys. Soc. Jpn.* **63**, 66–77, (1994).

[Tan06] Y. Tanimura, *J. Phys. Soc. Jpn.* **75**, 082001, (2006).

[Tan09] M. Tanaka and Y. Tanimura, *J. Phys. Soc. Jpn.* **78**, 073802, (2009).

[Tiw13] V. Tiwari, W. K. Peters, and D. M. Jonas, *Proc. Natl. Acad. Sci. U. S. A.* **110**, 1203–1208, (2013).

[vA00] H. v Amerongen, L. Valkunas, and R. v Grondelle, *Photosynthetic Excitons.* World Scientific, Singapore, (2000).

[Val13] L. Valkunas, D. Abramavičius, and T. Mančal, *Molecular Excitation Dynamics and Relaxation: Quantum Theory and Spectroscopy*. WILEY-VCH, (2013).

[Ved11] V. Vedral, *Sci. Am.* **304**, 20, (2011).

[vG06] R. v Grondelle and V. I. Novoderezhkin, *Phys. Chem. Chem. Phys.* **8**, 793, (2006).

[Wu10] J. Wu, F. Liu, Y. Shen, J. Cao, and R. J. Silbey, *New J. Phys.* **12**, 105012, (2010).

[Xu05] R.-X. Xu, P. Cui, X.-Q. Li, Y. Mo, and Y. Yan, *J. Chem. Phys.* **122**, 041103, (2005).

[Yan02] M. Yang and G. R. Fleming, *Chem. Phys.* **275**, 355, (2002).

[Zha98] W. M. Zhang, T. Meier, V. Chernyak, and S. Mukamel, *J. Chem. Phys.* **108**, 7763, (1998).

[Zho05] Y. Zhou, Y. Yan, and J. Shao, *Europhys. Lett.* **72**, 334–340, (2005).

[Zhu11] J. Zhu and S. Kais, *J. Phys. Chem. B* **115**, 1531–1537, (2011).

[Zig06] D. Zigmantas, E. L. Read, T. Mančal, T. Brixner, A. T. Gardiner, R. J. Cogdell, and G. R. Fleming, *Proc. Natl. Acad. Sci. U. S. A.* **103**, 12672, (2006).

[Zwa60] R. Zwanzig, *J. Chem. Phys.* **33**, 1338, (1960).

LIST OF ABBREVIATIONS

2D	Two-dimensional
2DES	Two-dimensional electronic spectrum
AK	Argyres-Kelly (projector), Eq. (1.63)
CF	Coherent factor, Eq. (5.5)
CT	Charge transfer
DOF	Degree of freedom
EGCF	Energy-gap correlation function
ESA	Excited state absorption
FMO	Fenna-Matthews-Olson photosynthetic pigment-protein complex
FWM	Four-wave mixing
GSB	Ground-state bleach
GSM	Ground-state manifold
HEOM	Hierarchical equations of motion
HTA	High Temperature Approximation, Eq. (5.30)
OQS	Open quantum system
RDM	Reduced density matrix
RF	Response function
SBC	System-bath coupling
SE	Stimulated emission

SURC	Stochastic unraveling by resonance coupling
QME	Quantum Master Equation
TL	Time-local
TNL	Time-nonlocal